Modelling of Carbon Nanotubes and Carbon Nanotube-Reinforced Polymers with Applications to Composite Structures

Justin Wuite

Submitted in fulfilment of the academic requirements for the degree of Master of Science in Engineering in the School of Mechanical Engineering

All work for this dissertation was completed at the University of Kwazulu-Natal, Howard College Campus

Durban, South Africa
January 2005

Abstract

Owing to their exceptional mechanical and physical properties, carbon nanotubes seem to hold a great promise as an ideal structural reinforcing material for composites of high-strength and low-density. However for the development and ultimate implementation of nanotube-reinforced composite materials, predictive models of nanotube reinforcement need to be developed. Due to the size, which is at the molecular level, and the geometry of carbon nanotubes, traditional composite modelling approaches need to be modified when modelling nanotube-reinforced composites. The focus of this research is to develop models of the elastic behaviour of single-walled carbon nanotubes and their composites.

A structural mechanics approach to modelling the deformation of carbon nanotubes at the molecular level is first investigated. Fundamental to the proposed concept is the notion that a carbon nanotube is a geometrical frame-like structure and the bonds between neighbouring atoms act as load-bearing members. The sectional property parameters of these beams are established by a linkage between structural mechanics and molecular mechanics.

Secondly, the stiffening effect of carbon nanotubes is investigated using micromechanical methods. The effects of the orientation and agglomeration of carbon nanotubes are also examined theoretically. The results obtained from these models are compared to theoretical and experimental results available in the literature. The effective elastic properties of nanotube-reinforced polymers determined from the micromechanics analysis are then used in the analysis of a nanotube-reinforced polymer used in a weight-critical structural application.

Preface

The author declares this dissertation to be his own unaided work except where due acknowledgement is made to others. This dissertation is being submitted for the degree of Master of Science in Engineering to the University of Kwazulu-Natal, Howard College Campus, and has not been submitted previously for any other degree or examination.

Acknowledgements

The author wishes first and foremost to thank Professor Sarp Adali for his guidance and advice. He would also like to thank his fellow postgraduate students for all the encouragement, assistance and advice.

The author gratefully acknowledges the National Research Foundation (NRF), for the scholarships awarded him for this study.

Contents

List of Figures

List of Tables

Chapter 1

Introduction

Since the discovery of multi-wall carbon nanotubes in the early 1990s (Iijima et al. 1991), and subsequent synthesis of single-wall carbon nanotubes, a wide range of research activities have gone into carbon nanotube structures and their applications. This is due to the unusual properties expected of carbon nanotubes. These outstanding physical properties are due to the near-perfect microstructure of the nanotubes, which at the atomic scale can be thought of as a hexagonal sheet of carbon atoms rolled into a cylinder closed at either end with caps containing pentagonal rings.

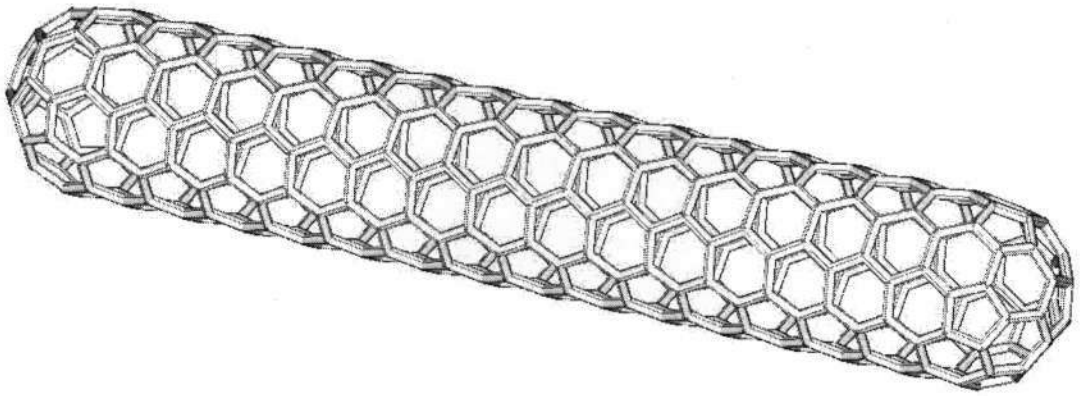

Figure 1-1 Representation of the structure of a carbon nanotube

Many researchers have reported properties that exceed those of any previously existing materials. It has been suggested that carbon nanotubes have a density half that of aluminium, have tensile strengths twenty times that of high strength steel alloys, have current carrying capacities 1000 times that of copper, and transmit heat twice as well as pure diamond (Collins *et al.* 2000). As a result of their small size and extraordinary mechanical, electrical and thermal properties, a wide range of applications have been proposed for carbon nanotubes. Applications proposed are in the fields of material reinforcement, field emission panel displays, chemical sensing, drug delivery and nanoelectronics.

The main focus of this dissertation is the use of carbon nanotubes as a filler phase to provide structural reinforcement to a host polymer. Conventional carbon fibre-reinforced polymer composites have been produced for many years, and are now widely used in applications ranging from sports equipment to military aircraft. The high stiffness and high strength of carbon fibres are owed to the strong covalent bonds between in planar carbon atoms in the graphene sheets, which form the fibres. However, the mechanical properties of carbon fibres still fall well short of the in-planar properties of graphite due to structural imperfections. Carbon nanotubes on the other hand have a near perfect microstructure resulting in unmatched strength and stiffness making them ultimate filler materials for structural reinforcement. Numerical simulations on nanotubes have predicted tensile moduli on the order of 1 TPa and elastic strains of 5%. Despite the difficulties associated with manipulating objects on the size scale of carbon nanotubes, experimental measurements have been carried out on them verifying the mechanical properties predicted.

The combination of high stiffness and high strength of carbon nanotubes allows for the addition of a low volume fraction of nanotubes to match traditional composite properties. Alternately, the addition of a higher volume fraction of nanotubes may result in a composite with stiffness and strength ratios unachievable with traditional composites. Both scenarios suggest substantial weight savings for weight-critical applications. As a result of their high modulus-to-weight and strength-to-weight ratios, NASA predicts that single-walled nanotube composites will reduce spacecraft weight by 50% or more.

The potential benefits of carbon nanotube-reinforced polymers (NRP) are not only structural but also include an increase in the working temperature range, the thermal stability and the electrical conductivity of the composite. This multifunctionality suggests that the materials may be designed to meet both mechanical and secondary material property specifications. Another benefit offered by NRPs over traditional composites is the small size of the nanotubes. Their nanoscale size has an advantage in the processing and manufacturing of the composites as it allows more flexibility in the shape of the product and the production rate. The nanoscale size also allows for reinforcement in the out of plane direction of a composite shell.

For the full potential benefits predicted for nanotube-reinforced polymers (NRPs) to be realised, a number of critical issues in the production of NRPs need to be overcome first. Some of these critical issues are outlined below:

- The current high cost and low production rate of carbon nanotubes: At the moment, the price of the raw nanotube material is several orders of magnitude higher than the cost of high strength carbon fibres used in composite applications. However, more cost-effective and higher yielding production methods are currently being developed. The quality and form of the nanotubes produced are also important factors to be considered in the production of nanotubes.

- The nanotube-polymer interface: To achieve the excellent structural properties predicted for NRPs, there has to be suitable bonding between the nanotubes and the polymer matrix to allow for sufficient load transfer at the nanotube-polymer interface. Several studies have demonstrated a good load transfer between nanotubes and a polymer however more research is required in this area.

- Dispersion of the nanotubes within the polymer: The van der Waals force that exists between nanotubes make them difficult to disperse in a polymer thus effective dispersion techniques need to be developed to provide uniform material properties.

- Orientation of the nanotubes within the polymer: It is also desirable to be able to control the nanotube orientations within the composite thus tailoring the material properties. Methods have been developed to orient free standing and as-grown nanotubes while progress has been made in the use of magnetism to align nanotubes within a polymer.

- Nanotube form and geometry: Nanotubes occur in various forms (single-walled nanotubes, multi-walled nanotubes and nanoropes), diameters and lengths. Thus the relationship between the nanotube form and its mechanical properties need to be determined.

Due to the size and structure of nanotubes being at an atomic level, traditional methods of composite modelling are not qualified to model nanotube-reinforced composites. To allow for the interpretation of experimental results and the design of NRP composites structures, accurate models of NRP behaviour are needed. Molecular dynamics simulations have been performed on carbon nanotubes and their composites at an atomistic level but these methods are very computationally expensive and can only simulate finite systems of a few hundred atoms. Thus molecular dynamics simulations are not suitable for the modelling of NRPs.

They do however give useful insight into subjects such as: elastic properties of nanotubes, fracture behaviour of nanotubes, forces between nanotubes, and the nanotube-polymer interface. The use of continuum methods to describe the behaviour of NRP has also been explored. However, careful consideration needs to be taken when using continuum methods to determine the behaviour of materials at an atomic scale.

In this dissertation, a continuum method linking molecular structures of nanotubes to their macroscopic responses through energy equivalence is presented. This method allows for the static analysis of nanotubes at an atomistic level. Traditional micromechanics and composite models are also extended to address specific features characteristic of NRP materials. The effects of nanotube alignment and agglomeration on the effective moduli of NRPs were quantitavely determined. Micromechanical results are then used to describe the behaviour of a NRP in a structural application.

Chapter 2

Background

2.1 Structure of carbon nanotubes

The outstanding properties predicted for carbon nanotubes are the result of their atomic structure which can be visualized as graphene sheets that have been rolled into cylinders. Graphene sheets are two-dimensional arrangements of carbon atoms in a hexagonal array. Each carbon atom is bonded to three neighbouring atoms through sp^2 hybridized orbitals at 120° to each other. The sp^2 orbitals form strong, covalent σ bonds between the carbon atoms in the graphene plane, while the remaining π orbitals normal to the graphene plane form weak van der Waals bonds between neighbouring graphene planes. The cylinders forming carbon nanotubes are typically closed at each end by hemispherical caps, the curvature of which is created by the addition of pentagons to the hexagonal lattice. Properties of carbon nanotubes depend on the atomic arrangement, the diameter, the length and the nanostructure of the nanotube.

Due to the hexagonal symmetry of the carbon atoms in the graphitic sheet, different isomers are possible depending on how the graphene sheet is rolled. The angle at which the graphene sheet is rolled is termed the nanotube chirality, which is defined by the chiral vector C_h and the chiral angle θ as shown in figure 2-1.

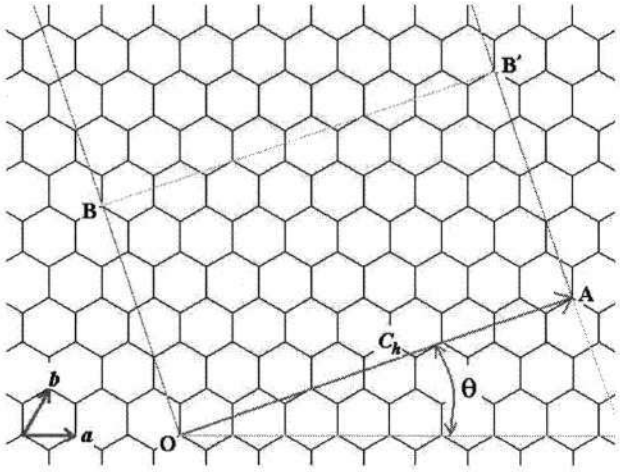

Figure 2-1 Unit cell and chiral vector for a (6,3) carbon nanotube.

The chiral vector is defined as a line connected from two crystallographically equivalent sites O and A on a two-dimensional graphene structure and may be described by the following equation:

$$C_h = n\boldsymbol{a} + m\boldsymbol{b} \tag{2.1}$$

where $\boldsymbol{a}$ and $\boldsymbol{b}$ are unit vectors on the hexagonal lattice and n and m are integers.
Based on simple geometry, the chiral angle θ and the diameter d_t of the nanotube can be given as:

$$\theta = \tan^{-1}\left(\frac{3n}{2m+n}\right). \tag{2.2}$$

$$d_t = \frac{3}{\pi} a_{c-c}\sqrt{m^2 + mn + n^2}\,, \tag{2.3}$$

where $a_{c\text{-}c}$ is the distance between neighbouring carbon atoms in a graphene sheet (approximately 0.142 nm). Three major categories of nanotube can also be defined based on the chiral angle as follows:

$\theta = 0,$	"Zigzag"
$0 < \theta < 30,$	"Chiral"
$\theta = 30,$	"Arm Chair"

The chirality has significant implications on certain material properties in particular electrical resistivity and fracture behaviour. However, other properties, and in particular the stiffness, have been found to be relatively independent of the chirality.

Carbon nanotubes can further be classified into three broad categories: single-walled nanotubes (SWNT), multi-walled nanotubes (MWNT), and Nanotube ropes. SWNTs consist of a single graphite layer wrapped into a cylindrical sheet. Typical diameters for SWNTs are on the order of 1nm, while the lengths are often in the order of μm. The diameter and length of the SWNTs are typically dependant on the particular fabrication technique used to produce the nanotubes.

MWNTs are composed of concentric SWNTs coupled together through van der Waals forces resulting in a Russian doll-like structure. The interlayer spacing between the individual shells is approximately 0.34 nm, which is close to the interlayer separation of graphite, 0.335 nm. The diameter and number of shells is again dependant on the particular fabrication technique used to produce the nanotubes. Figure 2-2 shows a transmission electron microscopy (TEM) image of a MWNT.

Due to the wan der Waal forces between nanotubes, most synthesized nanotubes are either randomly agglomerated MWCNTs or bundles of closest-packed SWCNTs. The SWNTs have a narrow diameter distribution as synthesized, and are consequently typically tightly and efficiently packed in bundles. Bundles of SWNTs, called nanoropes, can be seen in figure 2-3.

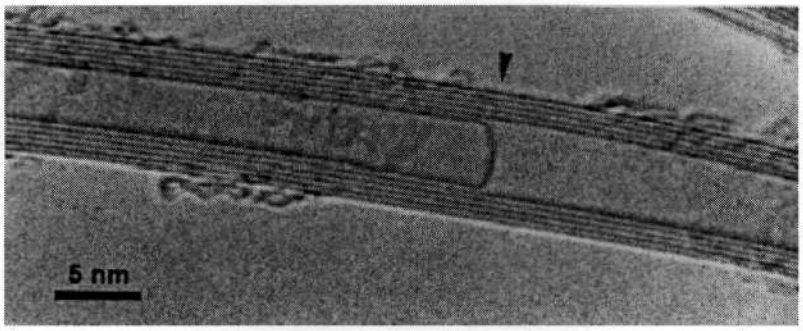

Figure 2-2 High resolution transmission electron microscopy (TEM) image of a MWNT with an internal cap highlighted by the arrow. (Harris 1999).

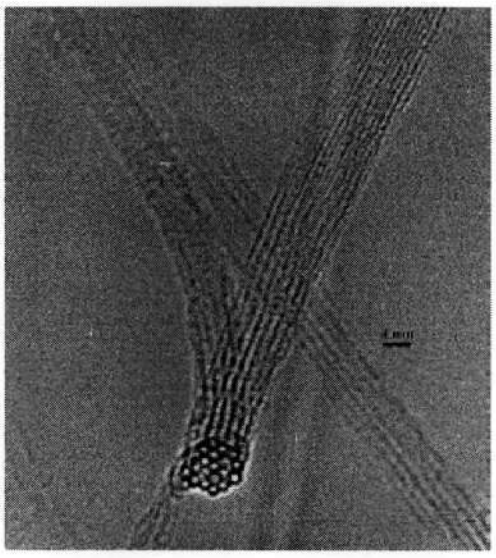

Figure 2-3 High resolution TEM image of a SWCNT bundle. (Journet *et al.* 1997).

2.2 Methods of nanotube fabrication

Since the discovery of carbon nanotubes, a variety of techniques have been developed for producing them. The manufacturing processes of the nanotubes include direct-current arc discharge, laser ablation, gas-phase catalytic growth from carbon dioxide, chemical vapor-growth deposition from hydrocarbons, and the self-assembly of single crystals of single-walled nanotubes. Some of the issues relating to the methods of nanotube fabrication, for the application of nanotube-reinforced polymer composites, are the purity of the nanotubes they produce, the number of structural defects in the nanotubes, the orientation of the nanotubes, and the ability to scale-up the method for mass production. While an in-depth discussion of nanotube fabrication techniques is beyond the scope of this dissertation, a summary of production techniques is given below.

2.2.1 Direct-current arc discharge

Nanotubes were first discovered using the direct-current arc discharge method, which uses two high-purity graphite rods brought together under a helium atmosphere depicted in figure 2-4. A voltage is applied between the rods until a stable arc is achieved. As the anode is consumed, the gap between the rods needs to be maintained by adjusting the position of the anode. Material deposits on the cathode to form a build-up consisting of an outside shell of fused material and a softer fibrous core. The core contains a tangled, poorly ordered mat of multi-walled nanotubes and impurities in the form of amorphous carbon and non-tubular fullerenes. To separate the tubes subsequent purification steps are required. Doping the electrodes with a small amount of metallic catalyst particles produces single-walled nanotubes. The limiting factor of this technique is the low production yields, making the technique unable to satisfy the high production rate needed for nanotube-reinforced composite applications.

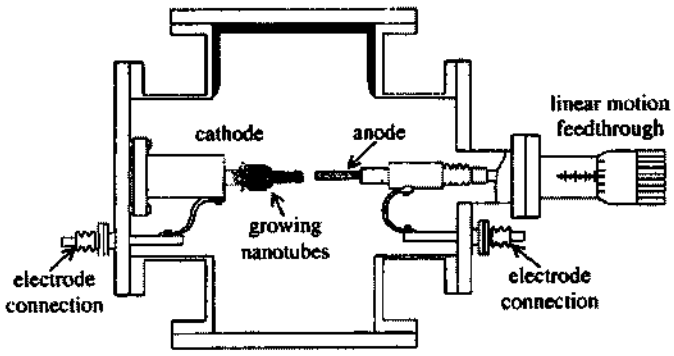

Figure 2-4 Schematic of the arc-discharge technique (Saito *et al.* 1996).

2.2.2 Laser ablation

The laser ablation technique uses a laser to vaporize a small graphite target held in a controlled atmosphere oven at temperatures near 1200°C. A tangled mat of nanotubes is then collected on a water-cooled target. Although tangled, individual tubes may be made several hundred microns in length. The graphite target is doped with cobalt and nickel catalyst to produce SWNTs and increase the yield. Impurities in the form of catalyst particles, amorphous carbon, and non-tubular fullerenes are also produced. Thus subsequent purification steps are required to separate the tubes. An improved method has been developed by using cobalt coat silica plate to align the growth of nanotubes (Terrones *et al.* 1997). The method offers control of overall length (≈50 μm) and uniformity of diameter of the nanotubes (30-50 nm). Laser ablation however faces the same low production rates as arc discharge making it unsuitable for our application. A schematic of the laser ablation process is shown in figure 2-5.

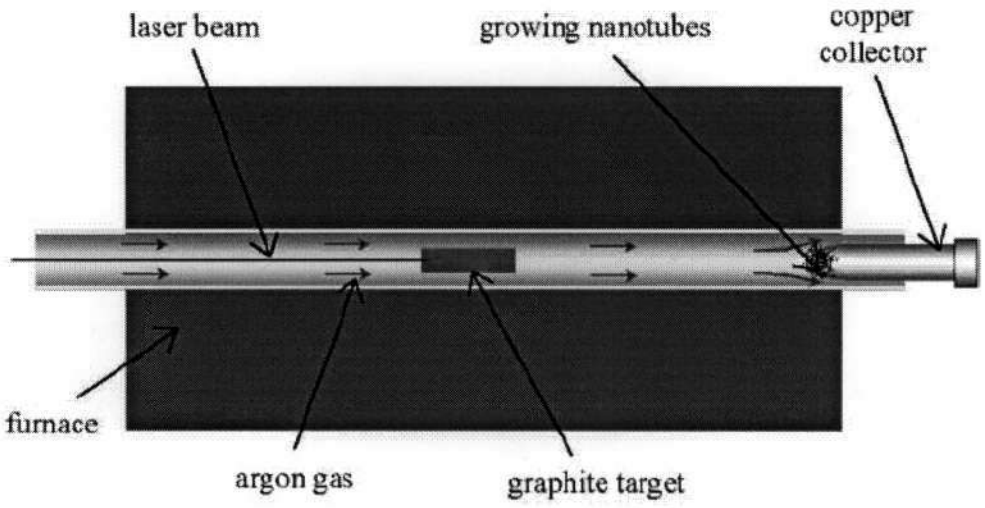

Figure 2-5 Schematic of the laser ablation process (Collins *et al.* 2000).

2.2.3 Gas-phase Techniques

In gas-phase techniques, nanotubes are formed by the decomposition of a carbon-containing gas. The gas-phase techniques have been recognized as a means of mass-producing nanotubes due to the techniques being amenable to continuous processes, the carbon source can be continuously replaced by flowing gas.

The gas-phase growth of single-walled carbon nanotubes with carbon monoxide as the carbon source has been refined to produce large quantities of single-walled carbon nanotubes

with remarkable purity. The highest yields of single-walled nanotubes occur at the highest accessible temperature and pressure (1200°C, 10 atm). The technology has been commercialized by Carbon Nanotechnologies Inc for the large-scale production high-purity single-walled nanotubes.

Other gas-phase techniques utilize hydrocarbon gases as the carbon source for production of both single and multi-walled carbon nanotubes via chemical vapor deposition (CVD). Hydrocarbons pyrolize readily on surfaces heated above 600-700°C. As a consequence, nanotubes grown from hydrocarbons can have substantial amorphous carbon deposits on the surface of the tubes and will require further purification steps. The lower processing temperature does however enable the growth of nanotubes on a wide variety of substrates, including glass. Carbon nanotubes grown with CVD techniques are shown in figure 2-6.

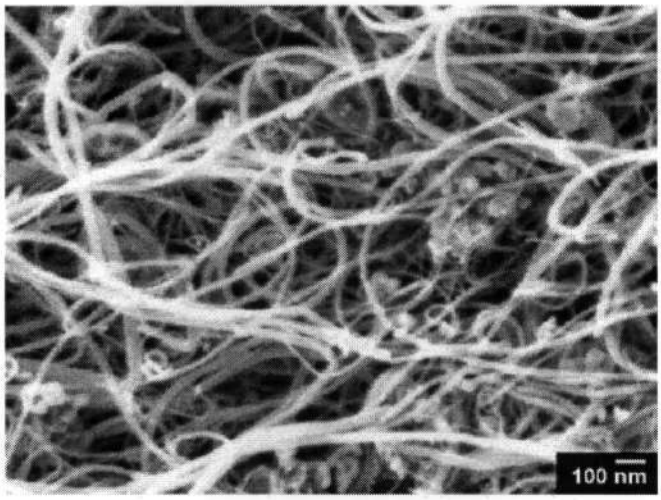

Figure 2-6 Micrograph showing tangled, spaghetti-like carbon nanotubes grown with conventional CVD techniques (Thostenson *et al.* 2001).

The synthesis of well-aligned, straight carbon nanotubes on a variety of substrates has been accomplished by the use of plasma enhanced chemical vapor deposition (PECVD). The substrate is coated with a layer of nickel catalyst and high-purity ammonia is used as the catalytic gas with acetylene being used as the carbon source. A direct-current power generates the required plasma, and a deeply carbonized tungsten filament assists the dissociation of the reactive gasses and supplies heat to the substrate. Control of the nanotube length and graphitization is accomplished by changing the growth time and temperature respectively, and application of the DC plasma results in tube growth in the direction of the plasma. The diameter of the nanotubes is controlled by the thickness of the catalyst layer.

The control over the alignment and diameter of nanotubes produced using PECVD can be seen in figure 2-7.

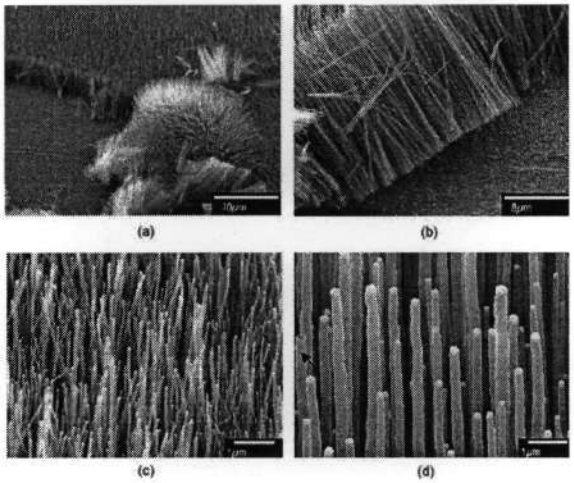

Figure 2-7 SEM micrographs showing (a,b) the straightness and (c,d) control over nanotube diameter of MWNTs grown via PECVD (Ren *et al.* 1998).

Microwave plasma enhanced chemical vapor deposition (MPECVD) is used to grow nanotubes in a direction directly normal to the surface of the substrate. An alternating microwave frequency source is used to excite the plasma imposing the self bias on the surface of the substrate resulting in nanotube growth normal to the surface of the substrate. The growth rate under plasma enhancement was shown to 40 times faster than the growth rate under thermal CVD. Figure 2-8 shown the alignment and structure of nanotubes grown using MPECVD.

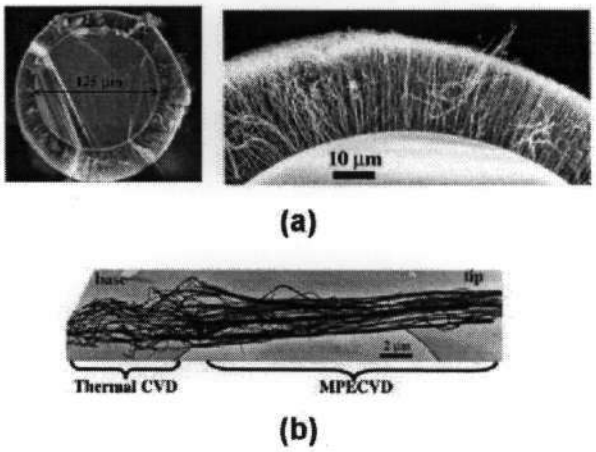

Figure 2-8 SEM micrographs showing (a) nanotubes aligned normal to the surface of a glass fibre and (b) the influence of MPECVD on the structure of the nanotubes (Bower *et al.* 2000).

2.2.4 Self-assembly of single crystals of SWNTs

The method of self-assembly of single crystals of single-walled nanotubes recently developed by Schlittler *et al.* (2001) enables the production of nanotubes in an ordered array with identical diameter, chirility and straight with a high purity. A mixture of C_{60} and Ni is evaporated through a nanostencil mask with an array of 300 nm diameter holes, which is accurately positioned a few microns above a surface and able to move with sub-nanometer precision during the evaporation process. The selection of substrate materials is crucial since the substrate should be able to constrain the C_{60} and Ni at an original 300 nm diameter evaporation area during diffusion process at high temperature. Latest studies found that the use of molybdenum substrate could provide an excellent result either in the form of a grid for transmission electron microscope (TEM) investigation or as a solid film sputtered onto a silicon wafer. The presence of the magnetic field controls the growth direction of the nanotubes.'

Method	**Arc discharge (carbon arc)**	**Chemical vapor deposition (CVD)**	**Laser ablation (vaporization)**	**High pressure CO conversion (HiPCO)**
Summary	Graphite evaporated by a plasma via high currents	Decomposition of a carbon-based gas	Graphite blasted with intense laser pulses	Metal catalysts nucleate SWNTs **at** high pressure and temperature
Yield	30%	20 to ~100 %	Up to 70%	95% purity
Strength	SWNT and MWNTs with few structural defects	Easiest to scale to industrial production	Produces SWNTs; diameter control via reaction temperature	Excellent structural integrity for a CVD process
Weakness	Tubes tend to be short and highly entangled	Typically MWNTs with a high density of defects	More expensive than the other methods	Production rates still relatively low

Table 2-1 Summary of the common methods used for carbon nanotube production.

2.3 Mechanical properties of carbon nanotubes

A large amount of the interest in using carbon nanotubes as a structural reinforcing material is due to the high stiffness and strength predicted due to the graphitic lattice structure of the nanotube. The strong covalent bonds between atoms in a graphene sheet give graphite an in-planar elastic modulus of 1.025 TPa and the tensile strength of 0.8 TPa.

Analysis of the mechanical properties of carbon nanotubes has been pursued extensively both theoretically and experimentally. Theoretical modelling can be categorised into two categories; atomistic modelling using finite sample simulation and continuum mechanics methods. Atomistic modelling methods require huge computational tasks thus limiting practical applications of these methods to systems containing a small number of atoms confined to relatively short-lived phenomena. With the diameters of nanotubes only being several times larger than the length of the bond between carbon atoms, the applicability of continuum methods to describe the mechanical behaviour of nanotubes is unclear.

Despite the difficulties associated with manipulating objects of such a small size, experimental measurements have been performed on nanotubes verifying their outstanding properties. In this section, we review the theoretical methods used to determine the mechanical properties of nanotubes and compare them to experimental results.

2.3.1 Computer simulation methods

Numerical computer simulations of a finite sample system to determine material properties have become more common recently because the increased computation power available. The three main simulation methods used are: atomistic molecular dynamics, tight binding methods and *ab inito* methods.

In classical molecular dynamics simulation, the dynamic evolution of the system is governed by Newton's classical equation of motion, which is derived from the classical Hamiltonian of the system. The atomic forces are derived as analytical derivatives of the interaction energy functions and are used to construct Newton's classical equations of motion which are second-order ordinary differential equations. A molecular dynamics code implements an algorithm to find a numerical solution of a set of coupled first-order ordinary differential equations given by the Hamiltonian formulation of Newton's second law. The equations of motion are numerically integrated forward in finite steps using a predictor-corrector method.

The quantum molecular dynamics approach computes the forces between atoms at each time step via quantum mechanical calculations within the Born-Oppenheimer approximation. The dynamic motions for ionic positions are still governed by Newtonian or Hamiltonian mechanics and described by molecular dynamics. Tight-binding molecular dynamics is a computationally efficient quantum molecular dynamics approach that provides good accuracy for structural and mechanical characteristics.

The *ab inito* or first principles methods directly solve the complex many-body Schrödinger equation using numerical algorithms, providing an accurate description of quantum mechanical behaviour. Current *ab inito* methods are based on a rigorous mathematical foundation of the density-functional theory. This is derived from the fact that the ground state total electronic energy is a functional of the density of the system.

For the computation of the mechanical properties of nanotubes, all three methods have been used in a complimentary manner. *Ab inito* methods have a high accuracy but are computationally expensive and are only able to simulate systems of hundreds of atoms. On the other hand, molecular dynamics methods are more computationally efficient, capable of simulating systems with thousands of atoms but are less accurate. Tight-binding methods lie between the other two methods in the computation required and the accuracy achieved.

2.3.2 Elastic properties

It is expected that the modulus, strength and stiffness of carbon nanotubes should be comparable to the in-plane values of graphite which are well understood. However the elastic energies of the in-plane bonds are affected by the nanotube curvature. Nanotubes of smaller diameter are affected more heavily than nanotubes of larger diameter.

The earliest theoretical prediction of Young's modulus was performed using an empirical Keating Hamiltonian with parameters determined from first principles (Overney *et al.* 1993). The structural rigidity of (5,5) nanotubes consisting of 100, 200 and 400 atoms were studied. Although Overney *et al.* did not give explicit values of Young's modulus, Treacy *et al.* (1996) suggested that the results imply a Young's modulus of 1500-5000GPa. The earliest energetics analysis of carbon nanotubes was performed by Tibbets *et al.* (1984) using continuum elastic theory. The strain energy was determined to be inversely proportional to the square of nanotube radius. Robertson *et al.* (1992) found similar results using both Tersoff and Tersoff-Brenner potentials.

Initial computational studies performed by Yakobson *et al.* (1996) used a Tersoff-Brenner potential in a molecular dynamics simulation and compared the results to the continuum shell model. The value of Young's modulus was fitted at 5.5TPa which is very high due to a very small shell thickness which was fitted at 0.066nm. Lu (1997) used an empirical model in his molecular dynamics simulation to determine the elastic properties of single-walled and multi-walled nanotubes in a simulated tensile test. Young's moduli of ~1TPa and shear moduli of ~0.5TPa were reported. Factors such as nanotube chirality, radius and number of walls had little effect on these values.

Hernandez *et al.* (1998) used a better description for interatomic forces in a non-orthogonal tight-binding method to derive the energy per-surface rather than per-volume. The surface Young's modulus was determined to be 0.42 TPa-nm which translates to a Young's modulus of 1.2TPa when a thickness of 0.34 nm is assumed. This value, which is slightly higher than that of graphite, was found to be slightly dependant on nanotube diameter. The high curvature of small diameter nanotubes tended to decrease the Young's modulus.

Using the ab inito density functional theory with pseudopotentials, Sanchez-Portal *et al.* (1999) studied the stiffness of single walled nanotubes, multi-walled nanotubes and single-walled nanotube ropes. The stiffness of single walled nanotubes was found to be close to that of the in-plane stiffness of graphite. A summary of the calculated results of Young's modulus from atomistic computational simulation methods is given in table 2-2

Method	Molecular dynamics Tersoff-Brenner field (Yakobson *et al.*1996)	Emperical Force Constant Model (Lu 1997)	Non-orthogonal tight binding (Hernandez *et al.* 1998)	Ab inito density functional theory (Sanchez-Portal *et al.* 1999)
Wall Thickness	0.06 nm	0.34 nm	0.34 nm	0.34 nm
Young's modulus	SWCNT: 5.5 TPa	SWCNT: 0.97 TPa	SWCNT: 1.2 TPa	SWCNT rope: 0.8 TPa; MWCNT: 0.95 TPa

Table 2-2 Summary of the theoretical Young's modulus of carbon nanotubes calculated in different molecular computer simulation studies

Popov *et al.* (2000a) studied the elastic properties of triangular crystal lattices formed by single-walled nanotubes by using analytical expressions based on a force-constant lattice dynamics model. Various elastic constants of nanotube crystals were calculated, showing that the elastic modulus, Poisson's ratio and bulk modulus clearly exhibit strong dependence on nanotube radius.

The first continuum mechanics approach for modelling of carbon nanotubes was performed by Tersoff (1992), who conducted simple calculations of the energies of fullerenes based on the deformation of a planar graphite sheet, treated as an elastic continuum. Tersoff concluded that the elastic properties of the graphite sheet could be used to predict the elastic strain energy of fullerenes and nanotubes.

Ru (2000a,b) used the continuum elastic shell model to study the effect of van der Waal forces on the axial buckling of double-walled nanotubes. Continuum shell models can be used to analyze the static or dynamic mechanical properties of nanotubes, however these models neglect the detailed characteristics of nanotube chirality and the forces acting on individual atoms.

By linking molecular structures of nanotubes to their macroscopic responses through energy equivalence, two continuum-based models for predicting elastic properties of nanotubes have recently been proposed by Odegard *et al.* (2002) and Li *et al.* (2003). These methods will be discussed in further detail in chapter 3. In another recent development by Zhang *et al.* (2002), a continuum theory for modelling carbon nanotubes is established by directly incorporating inter-atomic potentials into a continuum-level constitutive relation on the basis of the Cauchy-Born rule. These three models are shown to give good predictions when compared with more detailed molecular dynamics models and existing experimental results.

2.3.3 Strength of nanotubes

The strength of a material is closely related to the distribution of defects within the material and thus it has been hypothesised that the strength of carbon nanotubes may be significantly higher than that of bulk materials due to their near-perfect microstructure. For this reason, the strength of carbon nanotubes is heavily dependant on the synthesis method used as this determines the quality of the nanotubes in terms of defects. The strength of a carbon nanotube is also dependant on its length as the longer a nanotube is, the more likely it is to have the critical concentration of defects somewhere along its length.

Theoretical predictions of carbon nanotube strength have been studied extensively using molecular dynamics simulation emphasising the roles of defects, loading rate, and temperature. Simulations of nanotubes in tensile loading performed by Yakobson *et al* (2001) reported fracture strains of 30% and strengths of 150 GPa. A resistance of the nanotubes to break completely in half at very high strain was also demonstrated, with the two separated parts being connected by a chain of atoms. Belytschko *et al.* (2002) also studied the fracture of nanotubes using molecular dynamics simulations showing a moderate dependence of fracture strength on chirility. Fracture strains of 15.8% to 18.7% and fracture strengths of 93.5 GPa to 112GPa were reported.

Quantum molecular dynamics simulations of plastic yielding in carbon nanotubes have uncovered a bond rotation effect under high strains where the hexagonal lattice structure rearranges into pentagons and hexagons to lower the energy of the structure. This bond rotation is referred to as the *Stone-Wales bond-rotation*. The effects of temperature and strain rate have also been investigated on nanotubes however these simulations are limited by the small time scale molecular dynamics methods can address. These effects are not dealt with in detail in this dissertation as they are not of importance for our investigation.

Most synthesized nanotubes are either MWNTs or bundles of closest-packed SWNTs. Thus the strength due to interlayer sliding in MWNTs and the strength due to bonding between nanotubes in single-walled nanotube agglomerations is of great significance. Simulations on MWNTs attached by the outermost shell and then loaded in tension have shown that most of the load is carried in the outermost shell indicating a weak inter-shell interaction. When the outermost shell breaks, negligible load is transferred to the inner layers. This "sword in sheath" mechanism is reversible but limits the potential of multi-walled nanotubes in structural applications. Theoretical estimates of the load transfer between SWNTs have shown that in order for the full SWNT rope to participate in load bearing up to the breaking strength of SWNTs, the contact length between the nanotubes needs to be in the order of 10 to 120 microns. This is much longer than the length of SWNTs produced to date, which have mean lengths in the order of a few hundred nanometres.

2.3.4 Experimental methods

The extremely small dimensions of carbon nanotubes have posed great difficulties in experimentally determining the mechanical properties. General observations using transmission electron microscopy (TEM) were first used to provide insights into the stiffness

and strength of nanotubes. Transmission electron microscopy has also been used in a quantitative capacity and recently, the ability to measure the response of individual nanotubes to forces placed on them has been realised through scanning probe microscopy.

It should be pointed out that concepts such as Young's modulus and elastic constants belong to the framework of continuum elasticity; an estimate of these material parameters for nanotubes implies the continuum assumption. Since each individual SWNT only involves a single layer of rolled graphene sheet, the thickness t will not make any sense until it is given based on the continuum assumption. In the below-mentioned experiments, it is assumed that the thickness of the Nanotube is close to the interlayer distance in graphite, i.e. 0.34 nm.

2.3.4.1 Experimental observations using TEM: qualitative

Bent and buckled nanotubes are commonly observed in TEM images of carbon nanotubes, however completely fractured nanotubes are really observed. This is testament to the high breaking strain of nanotubes as samples for transmission electron microscopy are frequently prepared by grinding the material under a solvent in a pestle and mortar. As shown in figure 2-9, TEM images of buckled nanotubes have been compared to images produced by atomistic simulations of nanotubes in buckling showing close resemblance, indicating the accuracy of the atomistic simulations.

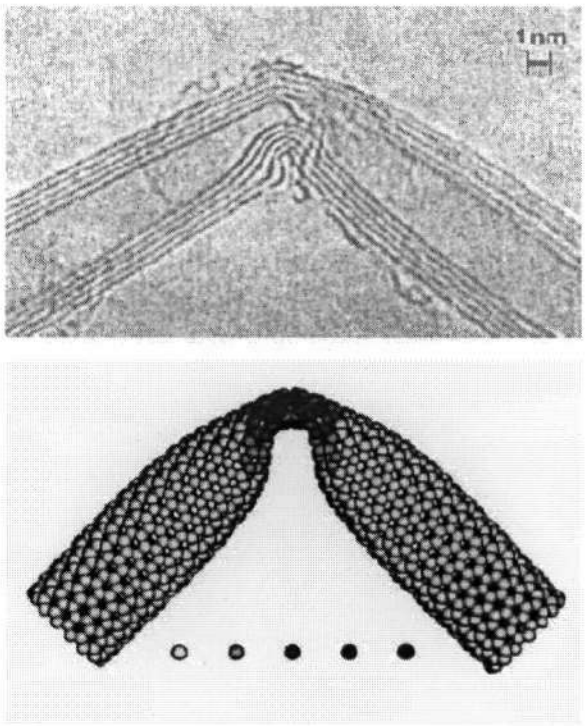

Figure 2-9 TEM micrograph and computer simulation of nanotube buckling (Yu *et al.* 2001)

2.3.4.2 Experimental observations using TEM: quantitative

Quantitative measurements of the mechanical properties of nanotubes have been carried out by measuring the mechanical resonance of nanotubes in TEM images. Treacy *et al.* (1996) deposited clusters of multi-walled nanotubes on TEM grids such that isolated nanotubes were naturally cantilevered. The amplitudes of the thermal vibrations of the cantilevered nanotubes were measured from recorded TEM images by measuring the blurred spread at the tip positions of the free ends. The mean-square amplitude as a function of temperature was used to determine the Young's modulus of the nanotubes if the are considered to act as a cantilevered beam. The Young's moduli measured ranged from 410 GPa to 4150 GPa, with an average of 1800 GPa. The large spread in values is due to uncertainties in determining the exact amplitude of the blurred tip. Krishnan *et al.* (1998) used a similar method to measure the Young's modulus of single-walled nanotubes obtaining an average Young's modulus of 1.25 TPa. Poncharal *et al.* (1999) induced mechanical resonance in cantilevered multi-walled nanotubes using electric field excitation. The bending modulus of the multi-walled nanotubes was again calculated from the measured resonance frequency and nanotube geometry. Scanning electron microscopy (SEM) images of electric field induced resonance of an individual MWNT are shown in figure 2-10.

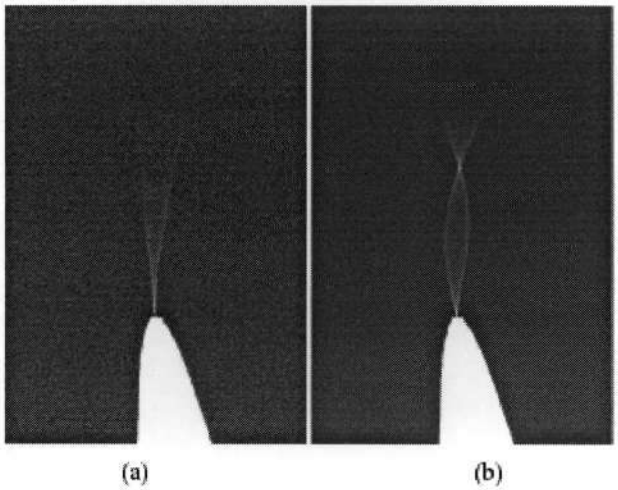

Figure 2-10 Scanning electron microscopy (SEM) images of electric field induced resonance of an individual MWCNT (a) at its fundamental resonance frequency and (b) at its second order harmonic (Poncharal *et al.* 1999)

2.3.4.3 Experimental observations using AFM

Atomic force microscopy (AFM) has enabled the manipulation of individual nanotubes directly providing techniques to study the bending and buckling of nanotubes. Wong *et al.* (1997) measured the bending modulus of multi-walled nanotubes using an atomic force microscope. Nanotubes deposited on a low friction MoS_2 surface were pinned down at one end by depositing square pads of SiO through a mask. Lateral force was applied to the free end of the nanotubes at the different points along the length of the multi-walled nanotube. The lateral force versus deflection was recorded and a Young's modulus of ~1.28 TPa was measured using a beam mechanics model and taking friction into account. An abrupt change in the force-deflection curve was noticed at deflections larger than 10°. This abrupt change in the force-deflection curve was attributed to elastic buckling of the kind observed in TEM studies. An overview of the approach used is illustrated in figure 2-11.

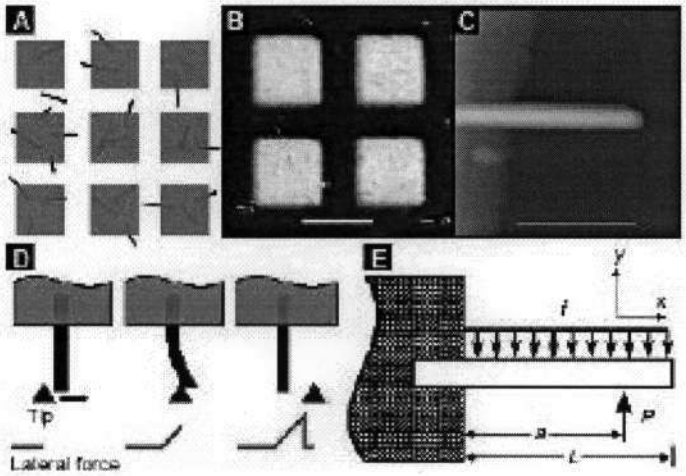

Figure 2-11 Overview of one approach used to probe mechanical properties of nanotubes: (a) Nanotubes deposited on cleaved MoS_2 substrate, then pinned by a deposition of a grid of square SiO pads. (b) Optical micrograph of sample, showing SiO pads. (c) AFM image of nanotube tip protruding from SiO pad. (d) Schematic of beam bending with AFM tip. (e) Schematic of pinned beam with a free end. (Wong et al. 1997)

Falvo *et al.* (1997) used a nanomanipulator and contact mode AFM to manually bend multi-walled nanotubes. The strong friction force between the nanotubes and the surface was sufficient to pin the nanotubes in a strained position for imaging. It was found that the nanotubes could be bent repeatedly through large angles sustaining strains of 16% without obvious fracturing (See Figure 2-12). Another technique of measuring the vertical deflection versus applied force was used by Salvetat *et al.* (1999a,b) to determine the mechanical

properties of multi-walled nanotubes and single-walled nanotube ropes. Nanotubes were dispersed onto a nanoporous membrane and an atomic force microscopy tip was positioned in the midpoint of the nanotube. A value of ~1 TPa was fit for multi-walled nanotubes grown by arc discharge, whereas nanotubes grown by the catalytic discharge of hydrocarbons had moduli an order of magnitude lower.

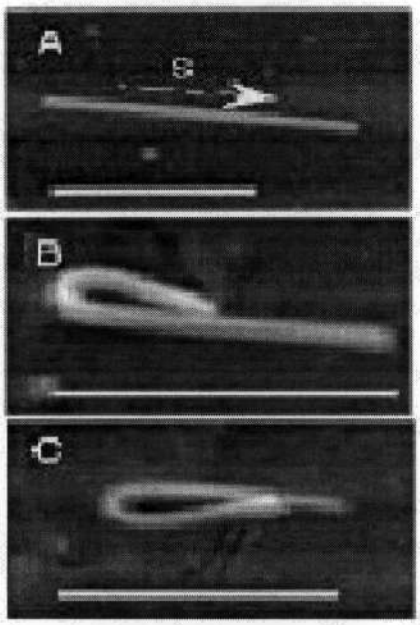

Figure 2-12 Bending and buckling of MWNTs: (a) Original straight MWNT, (b) the MWNT is bent upwards all the way back onto itself, (c) the same MWNT is bent all the way back onto itself in the opposite direction (Falvo *et al.* 1997)

The axial tensile loading of individual multi-walled nanotubes was realized by Yu *et al.* (2000a,b) using a new testing stage based on a nanomanipulation tool operating inside a scanning electron microscope. The nanomanipulation stage allowed for the positioning and clamping of individual multi-walled nanotubes or single-walled nanotube ropes between two AFM probes as can be seen in figure 2-13. A tensile load was applied to the nanotubes by displacing one of the AFM rigid probes and the applied force was determined by measuring the cantilever deflection of the other, compliant probe. Stress versus strain curves and breaking stress of the nanotubes were obtained indicating Young's moduli values in the range of 270 GPa to 950 GPa for multi-walled nanotubes and from 320 GPa to 1470 GPa (mean: 1002 GPa) for single-walled nanotube ropes. The same apparatus has been used by Yu *et al.* (2000c) to measure the shear strength between shells of multi-walled nanotubes by measuring the friction between the inner layers and the outer layers after the outer layer has broken in a "sword in sheath" mechanism. The load transferred between the outermost shell

and the neighbouring shell was found to be very low with values of shear strength for the two multi-walled nanotubes measured being 0.08MPa and 0.3MPa respectively.

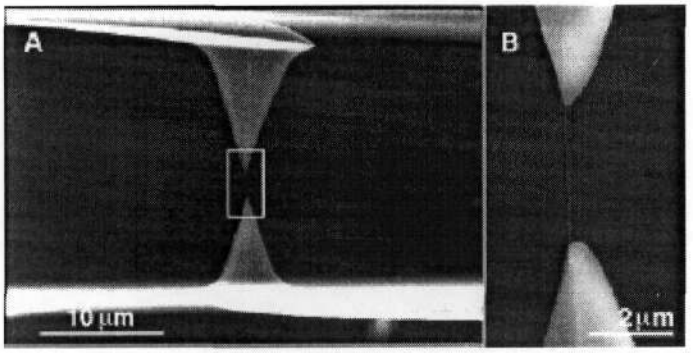

Figure 2-13 Tensile loading of individual MWCNTs. (A) An SEM image of a MWCNT attached between two AFM tips . (B) Large magnification image of the indicated region in (A) showing the MWCNT between the AFM tips. (Yu *et al.* 2000b).

Method	**Type of NT**	**Young's Modulus**
Amplitude of thermal vibration within TEM (Treacy *et al.* 1996)	Arc-discharge MWCNT	0.41 TPa to 4.15 TPa (mean: 1.8)
Amplitude of thermal vibration within a TEM (Krishnan et al.1998)	Laser ablated SWNTs	1.3 -0.4/+0.6 TPa (mean:1.25 TPa)
Electromechanical deflection and resonance within a TEM (Poncharal *et al.*1999)	Carbon arc MWNTs	~ 1 TPa for 3 nm diameter, decreasing to < 0.1 for larger diameter
Beam-bending via AFM (Wong *et al.* 1997)	Arc discharge MWCNT	1.28 TPa
Beam-bending via AFM (Salvetat *et al.* 1999)	CVD and arc-discharge MWNTs	0.81-0.16/+0.41 TPa
Beam-bending via AFM (Salvetat *et al.* 1999)	CVD MWNTs	0.1 to 0.5 TPa
Nanostressing stage within a SEM (Yu *et al.* 2000b)	Arc-discharge MWNTs	0.27 to 0.95 TPa (outer shell)
Nanostressing stage within a SEM (Yu *et al.* 2000a)	Laser ablated SWNT bundles	0.32 to 1.470 TPa (mean 1.002 TPa)

Table 2-3 Experimental values of the Young's modulus of carbon nanotubes.

2.4 Carbon nanotube-reinforced polymers

Carbon fibres have been produced for many years and are now widely used for structural reinforcement of polymer composite materials in applications ranging from sports equipment to military aircraft. The very high strength and stiffness of carbon fibres is owed to the strong atomic bonds between in-planar carbon atoms of graphitic carbon. However, their properties still fall far below the theoretical maxima of in-planar graphite owing to structural imperfections.

The near-perfect structure of carbon nanotubes has prompted much speculation of their use as the ultimate filler phase for the structural reinforcement of polymer composite materials. The high strength and stiffness of carbon nanotubes has been demonstrated theoretically and verified experimentally. In addition to their outstanding mechanical properties, carbon nanotubes have also demonstrated exceptional electrical and thermal properties suggesting that carbon nanotube-reinforced composite materials (NRPs) may meet secondary material property specifications as well as structural specifications.

Despite the potential benefits nanotube have to offer as a reinforcing material in polymer composites, critical issues must be overcome for their full benefits to be realised. Some of the critical issues concerning the uses of nanotubes in polymer composites are: the high-cost of nanotubes; interfacial bonding between the nanotubes and the polymer matrix; dispersion and orientation of the nanotubes within the polymer; and differences between nanotube forms. These issues related to the fabrication of nanotube-reinforced polymers (NRPs) are discussed in more detail below.

For the implementation of NRPs in structural applications, accurate models of NRP behaviour are need. Due to the structure of nanotubes being at an atomic scale, traditional methods of modelling composite materials can not be used to predict NRP behaviour. Thus new methods need to be developed for the accurate modelling of the mechanical behaviour of these materials.

2.4.1 Fabrication of nanotube-reinforced polymers

In recent years, nanotubes have been used in composites with a variety of matrix resins, including polyamides, polyesters, polycarbonates and their blends, polystyrene and high performance polymers such as polyphenylene sulphide (PPS), PEI and polyetheretherketone

(PEEK). Incorporation of even small volumes of nanotubes into various polymers has already led to substantial and demonstrated increases in electrical conductivity, Young's modulus, hardness, and thermal conductivity as compared to the non-reinforced matrix material. However, the full potential of nanotube reinforced composites had not yet been achieved for reasons that are not fully understood. This section will address some of the issues related to the fabrication of nanotube-reinforced polymers.

2.4.1.1 Nanotube dispersion within the polymer

For the effective use of carbon nanotubes in polymer composite applications it is essential that the nanotubes are uniformly dispersed within the polymer matrix. Van der Waals attractive forces between nanotubes cause the nanotubes to assemble into ropes or bundles which reduce the reinforcing ability of the nanotubes due to slipping between nanotubes in contact with one another and a reduction in the aspect ratio (length/diameter) of the reinforcement. It is, however, a difficult task to uniformly disperse the nanotubes within the polymer matrix. Thus, maintaining separation of the nanotubes during the processing of nanotube-reinforced polymers without compromising the nanotube-polymer interface is an ongoing subject of NRP research.

Separation of individual nanotubes from the bundles has been achieved using both chemical and ultrasonic treatments. The homogeneity of the composite films are then investigated using electron microscopy. A uniform distribution of low volume fractions (1 wt%) of multi-walled nanotubes in a polystyrene matrix have been achieved by Qian *et al.* (2000) using a solution evaporation method assisted by high-energy sonication. The process consisted of separate dispersion and high-energy sonication of the polymer and the nanotubes in a tolurene solvent, followed by mixing, casting and solvent evaporation. The dispersion and orientation of the nanotubes within the polystyrene matrix can be seen in figure 2-14.

The use of a surfactant to improve nanotube dispersion by overcoming van der Waals attractive forces between nanotubes has been investigated by Gong *et al.* (2000). It is, however, unclear whether such processing agents might compromise the nanotube-polymer interface.

A summary of dispersion methods reviewed in literature is given in Appendix A.

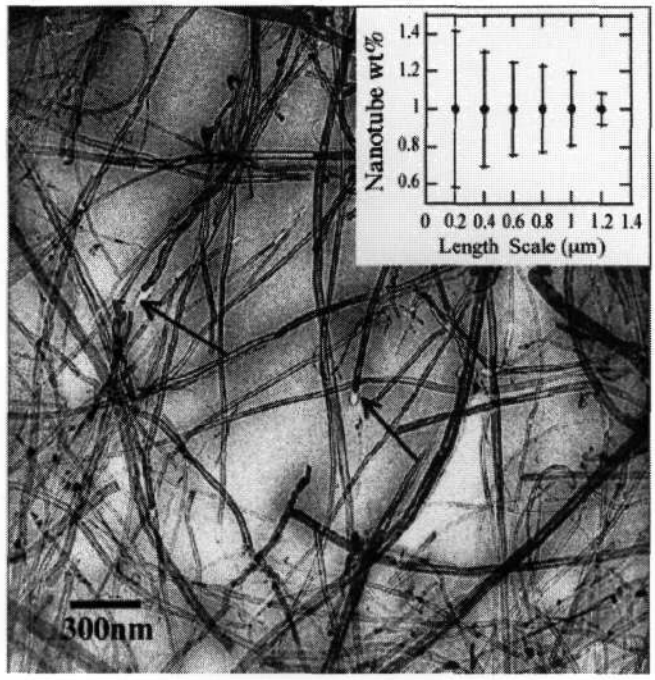

Figure 2-14 Transmission electron microscopy (TEM) image of arrangement of nanotubes in polymer showing good dispersion and random orientation (Qian *et al.* 2000).

2.4.1.2 Load transfer across the nanotube-polymer interface

For nanotubes to provide optimum reinforcement in composite materials, sufficient load needs to be transferred from the polymer matrix to the nanotubes. Load transferred from the polymer matrix to the nanotubes is a function of both the aspect ratio of the nanotubes and the nanotube-polymer interfacial shear stress. The limiting value of aspect ratio is found to be related to interfacial shear stress τ between the nanotube and the polymer by:

$$\frac{L}{d} > \frac{\sigma_{max}}{2\tau} \tag{2.5}$$

where σ_{max} is the maximum strength of the fibre.

Molecular mechanics studies of binding in nanotube-reinforced polymer composites using force-field-based molecular mechanics have demonstrated good interfacial bonding between the polymer and the nanotube. The key factor contributing to the interfacial bond has been attributed to a helical conformation of the polymer around the nanotube resulting in molecular entanglement of the two phases and forced long-range ordering of the polymer

(Lordi *et al.* 2000). Using molecular mechanics, Liao *et al.* (2001) estimated the interfacial shear stress for a polystyrene-nanotube composite to be 160 MPa.

Wagner *et al.* (1998) experimentally studied the fragmentation of multi-walled nanotubes within thin polymeric films (urethane/diacrylate oligomer EBECRYL 4858) under compressive and tensile strain. A nanotube-polymer interfacial shear stress in the order of 500 MPa was found. This value, if reliable, suggests the possibility of chemical bonding between the nanotubes and the polymer in their composites, and is an order of magnitude greater than the stress-transfer ability of current advanced composites. Successful transfer of tensile load across the interface between multi-walled nanotubes and polystyrene (Qian *et al.* 2000) and polyhydroxyaminoether (PHAE) (Jin *et al.* 1998) have been reported. TEM images of PPV and PHAE wetting the nanotubes are shown in figures 2-15 and 2-16 indicating good adherence between the polymers and the nanotubes. However, Raman spectroscopy investigations of stress transfer between nanotubes and epoxy matrices have indicated poor load transfer between nanotubes and epoxy. (Ajayan *et al.* 2000, Sandler *et al.* 1999) Transmission electron microscopy images of fracture surfaces in the nanotube/epoxy composites showed nanotube pullout and matrix fracture, confirming poor load transfer between the nanotubes and the epoxy matrix. Jia *et al.* (1999) showed that the nanotubes can be initiated by a free-radical initiator to open their π bonds allowing for a C-C bond between the nanotube and the matrix. While promising, a much better understanding of the factors that influence the nanotube-polymer interface is required.

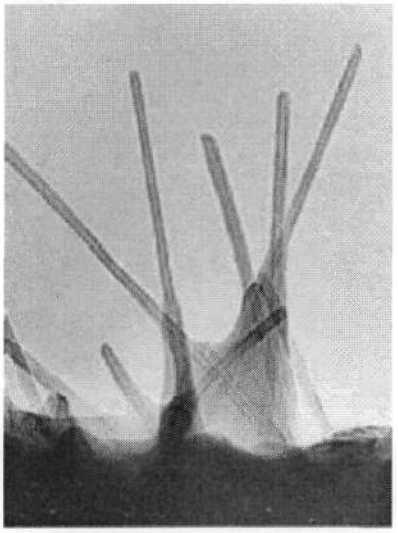

Figure 2-15 TEM image showing evidence of PPV wetting the nanotubes indicating good adherence between the polymer and the nanotubes. (Curran *et al.* 1998)

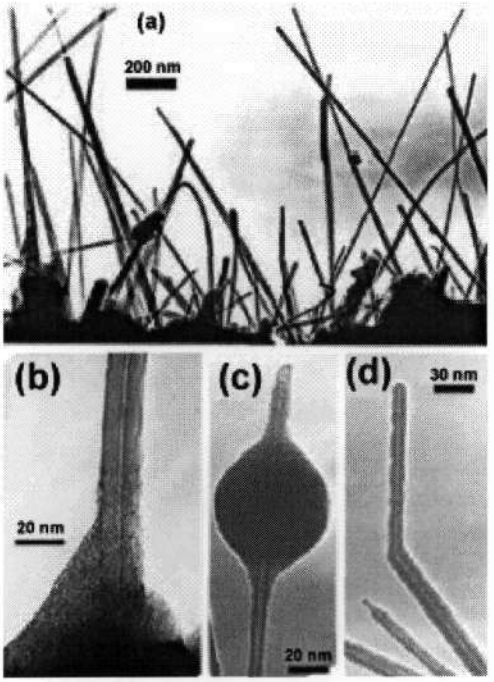

Figure 2-16 TEM images of MWNTs in PHAE. (a) Fracture surface. (b,c) Evidence of good adherence between the polymer and the MWNT. (d) Plastically deformed MWNT at fracture surface. (Bower *et al.* 1999).

2.4.1.3 Nanotube orientation within the polymer

The final properties of the carbon nanotube-reinforced composite materials depend on the controllability of the nanotube alignment within the composite material and several techniques have been employed to address this issue.

Ajayan *et al.* (1994) achieved alignment of multi-walled nanotubes in an epoxy matrix by making thin slices (on the order of 100 nm) of the composite with a diamond knife. Transmission electron microscopy (TEM) image analysis of the nanotube-reinforced epoxy films showed that longer and thinner nanotubes were oriented along the cutting direction, while thicker and shorter nanotubes were randomly oriented. This behaviour was attributed to shear flow created from the action of the knife. It was also noted that the length of the nanotubes did not change during cutting indicating either high nanotube strength or weak interfacial bonding between the nanotubes and the polymer. This flow orientation method has also been used to orient small amounts of nanotubes (0.1% wt) in a urethane acrylate polymer to thicknesses of up to 150 μm (Zhao *et al.* 1996; Wood *et al.* 2001).

Jin *et al.* (1998) demonstrated that the alignment of multi-walled nanotubes in a polyhydroxyaminoeter (PHAE) polymer could be obtained by mechanical stretching of the

composite at temperatures above the glass transition temperature of the polymer. After stretching, the samples were cooled at room temperature and then the load was released. The degree of orientation was determined by x-ray diffraction and TEM image analysis (See figure 2-17). It was noted that nanotube alignment increased with increased stretching ratio and was not effected by the thickness of the sample. Bower *et al.* (1999) further investigated the deformation of carbon nanotubes in these films. Haggenmueller *et al.* (2000) showed that melt spinning single-walled nanotubes in fibre form can also increase the alignment of the nanotubes in the fibre direction.

Wang et al. (2003) produced aligned SWNT buckypapers with a thickness of 15 to 30 μm by filtering well-dispersed SWNT suspensions under high magnetic fields (15 to 25 Tesla). Multiple layers of aligned buckypapers were then impregnated with epoxy resin and cured forming bulk solid composite samples. Significant alignment of nanotubes in the buckypapers was observed using the scanning electronic microscope (SEM). The SEM observations of the cross-section of the resultant composite also showed significant alignment of the nanotubes along the desired direction, which indicated the tube alignment in the magnetically aligned buckypaper was successfully transited into the solid nanocomposites (See figure 2-18).

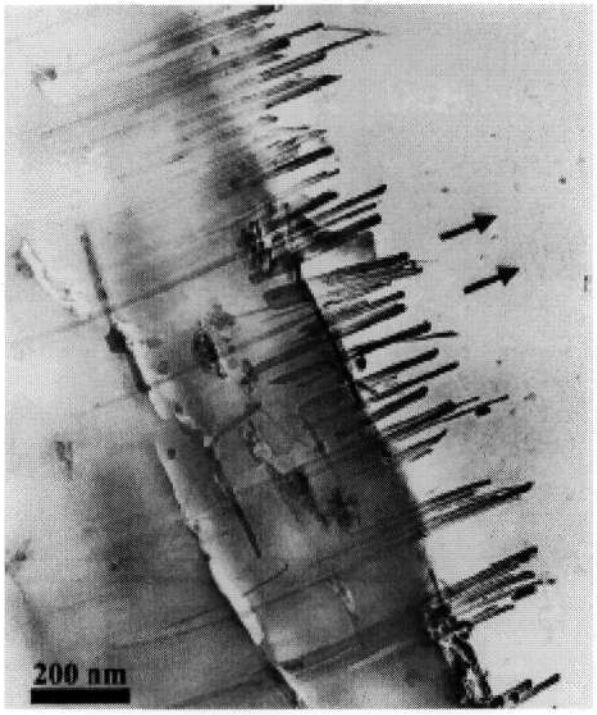

Figure 2-17 Alignment of nanotubes in PHAE via microtoming . The sample thickness is 90 nm. (Jin *et al.* 1998).

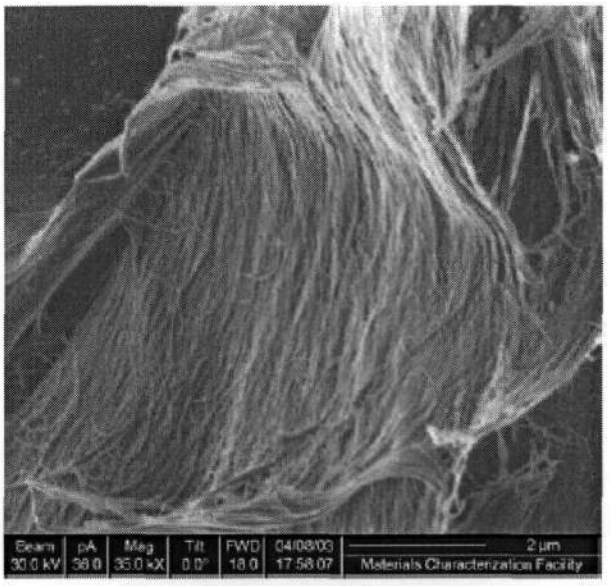

Figure 2-18 Micrograph showing nanotube alignment on the peeled-off surface of magnetically aligned buckypaper (Wang *et al.* 2003).

2.4.2 Properties of manufactured nanotube-reinforced polymers

A great deal of experimental work has gone into determining the effective physical and mechanical properties of carbon nanotube-reinforced polymer composites, however it is difficult to generalise across these studies due to the large number of parameters that can affect the properties. Factors that can affect the properties of a nanotube-reinforced polymer include the method of nanotube fabrication, size and form of the nanotube, nanotube-reinforced polymer processing technique, nanotube-polymer interaction, and the specifics of the polymer chemistry. However, one constant throughout much of the experimental work is that significant improvements in the properties of the NRP, with respect to that of the un-reinforced polymer, are obtained. In the following sections we highlight some of the relevant work in the literature.

2.4.2.1 Mechanical properties

Perhaps the first experimental investigation on the mechanical behaviour of nanotube-reinforced polymers was carried out by Schadler *et al.* (1998) on samples of 5 wt% multi-walled nanotubes mixed in an epoxy. Raman spectroscopy was used to qualitatively measure the strain induced in the nanotubes as the samples were loaded. The introduction of nanotubes into the epoxy matrix increased the compressive modulus by more than the tensile modulus, which was attributed to poor load transfer between the outer and inner layers of the

nanotubes. In tension, the load was not transferred from the outer layers to the inner layers by the van der Waals forces between the layers. However, in compression, the load was transferred to the inner layers through nanotube bent sections and geometrical constraints.

Lourie *et al.* (1998) demonstrated a high compressive strength for single multi-walled nanotubes in an epoxy matrix using TEM image analysis. The compressive stress was induced by the polymerisation shrinkage and the thermal effect associated with the electron beam in the transmission electron microscope.

Polymethyl methacrylate (PMMA) based nanotube-reinforced polymers studied by Jia *et al.* (1999) found that pre-processing of chemical vapour deposition grown multi-walled nanotubes using a ball mill resulted in an increase in tensile strength. The ball milling operation was attributed to separating individual nanotubes from entanglement thus improving load transfer between the nanotubes and the polymer. Scanning electron microscopy images of fracture surfaces showed wrapping of the nanotubes by the polymer indicating a strong interface between the two phases.

The tensile moduli and strength of multi-walled nanotube-reinforced polystyrene composites were studied by Qian *et al.* (2000) A homogeneous distribution of 1 wt% (0.5 vol%) multi-walled nanotubes was achieved by an ultrasound-assisted solution-evaporation method. Macroscopic testing of the samples determined an increase in strength of 25% and an increase in tensile modulus of 40% over that of the neat matrix material. Transmission electron microscopy images of fracture surfaces suggest that cracks propagate in regions of relatively low NT density, and that the multi-walled nanotubes tend to align and bridge the crack prior to failure (see Figure 2-19). Eventual failure of the nanotube-reinforced polymer was due to either nanotube fracture or pull-out from the matrix. Because nanotubes which were aligned parallel to the direction of crack propagation tended to break between the crack faces (rather than pull-out from the matrix), the authors concluded that a relatively strong interface exists between the two phases.

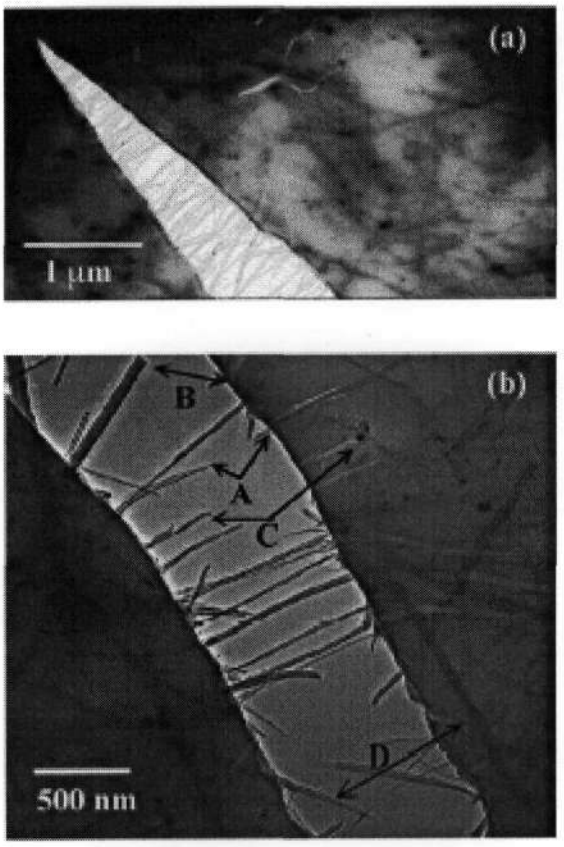

Figure 2-19 TEM observations of crack propagation and nanotube crack bridging in an epoxy-MWNT sample. (Qian *et al.* 2000)

Wang *et al.* (2003) performed dynamic mechanical analysis (DMA) on nanotube-reinforced epoxy bulk composites samples produced by impregnating multiple layers of SWNT buckypapers with epoxy. Samples made from magnetically-aligned and randomly oriented SWNTs were tested. The aligned NRP samples had a nanotube content as high as 59.8 wt% due to the close packing of the nanotubes, whilst the random oriented NRP samples had a nanotube content of 31.3 wt%. Storage moduli of 40.5 GPa and 15.1 GPa were found for the aligned nanotube and random oriented nanotube samples respectively.

Andrews *et al.* (1999) dispersed 5 wt% single-walled nanotubes in isotropic petroleum pitch improving the tensile strength by ~90% and the elastic modulus by ~150%. Because the pitch matrix is isotropic, the elastic modulus is orders of magnitude lower than mesophase pitch fibres used in composite materials. However, the exceptional flexibility demonstrated by the nanotube composite fibres suggest that further developments in the alignment of the nanotubes within the fibre could result in a new form of carbon fibre that has exceptional

stiffness, strength and flexibility. The exceptional flexibility of a carbon nanotube-based fibre is demonstrated in figure 2-20.

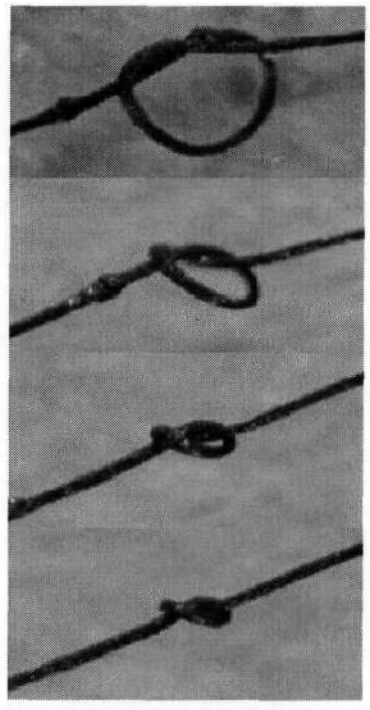

Figure 2-20 Micrographs showing the exceptional flexibility of a carbon nanotube-based fibre (Vigolo *et al.* 2000)

2.4.2.2 Thermal-mechanical properties

The thermal-mechanical properties of polymeric materials are important from both processing and applications perspectives. Nanotubes are on the same size scale as the polymer chains in nanotube-reinforced polymers and thus are expected to alter the thermo-mechanical properties of the nanotube-reinforced polymer with respect to neat polymer. A limited amount of experimental research has gone into studying the thermal-mechanical behaviour of nanotube-reinforced polymers.

Shaffer *et al.* (1999) studied the thermo-mechanical properties of multi-walled nanotubes in a poly(vinyl alcohol) (PVOH) matrix and found that the glass transition temperature, measured by dynamic analysis, moderately increased with the addition of nanotubes. The storage modulus at higher temperatures was found to increase substantially with increased fraction of nanotubes. This was attributed to a reduction in polymer chain mobility in the reinforced samples. Dynamical mechanical analysis of PVOH with different loadings of CVD grown nanotubes is shown in figure 2-21.

A study on the thermo-mechanical properties of 1 wt% multi-walled nanotubes in an epoxy matrix discovered that the glass transition temperature increased by a substantial amount (63°C to 88°C) when the nanotubes were well dispersed using a surfactant (Gong *et al.* 2000). A smaller shift in glass transition temperature was observed when a surfactant was not used to disperse the nanotubes. (See figure 2-22)

Both studies also found that the addition of nanotubes increased the stiffness of the polymer matrix, especially at higher temperatures, and increased the temperature at which the onset of degradation initiates. These results suggest that nanotube-reinforced polymers may be used as polymer modifiers for high-temperature uses.

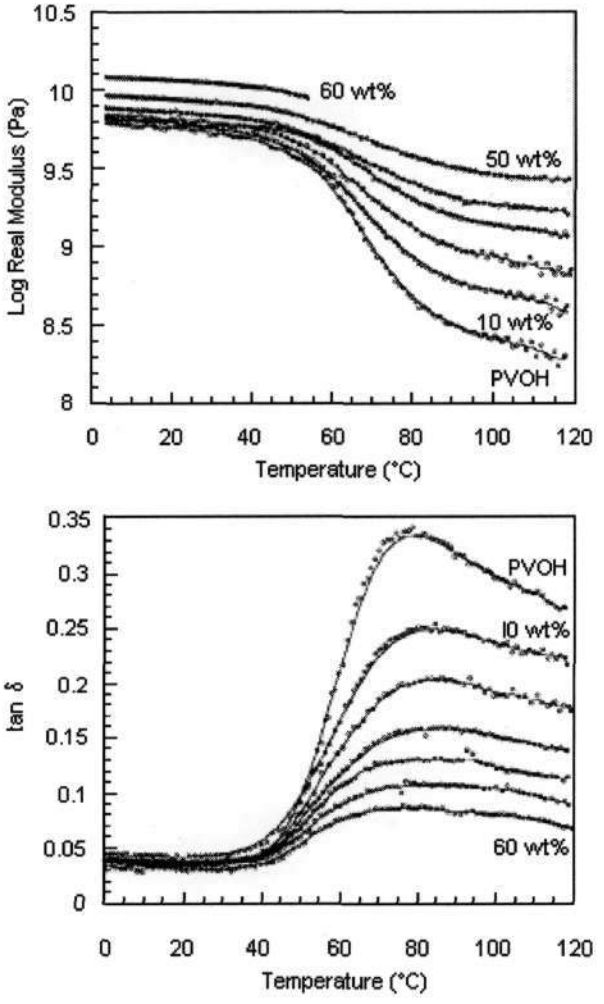

Figure 2-21 Dynamical mechanical analysis of PVOH with different loadings of CVD grown nanotubes. (Shaffer *et al.* 1999)

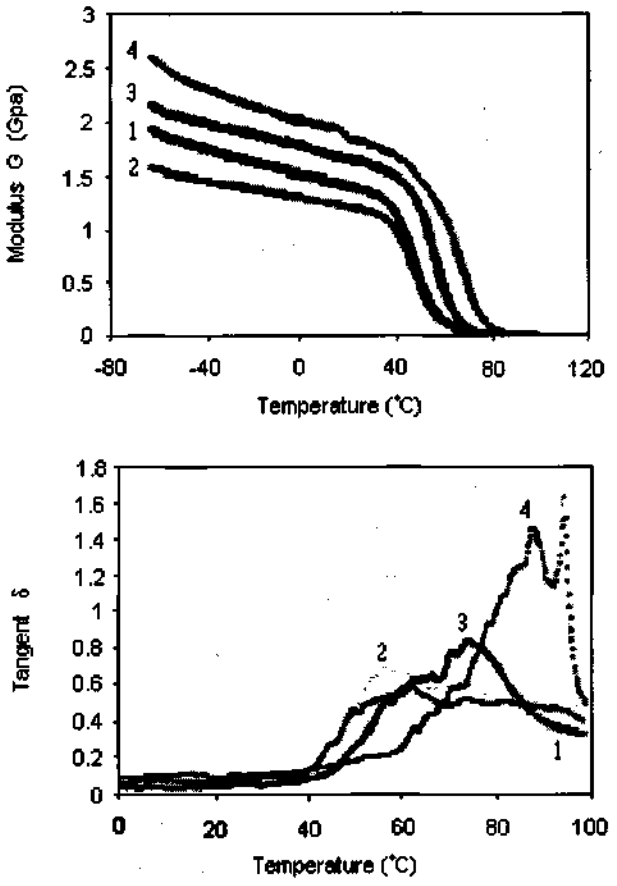

Figure 2-22 Storage modulus and loss tangent results via dynamic mechanical analysis for different epoxy samples. Curves are labelled as: (1) pure epoxy, (2) epoxy plus $C_{12}EO_8$ surfactant, (3) epoxy plus 1% wt multi-walled nanotubes, and (4) epoxy plus surfactant plus 1% wt multi-walled nanotubes (Gong *et al.* 2000).

2.4.2.3 Electrical and electronic properties

In addition to improving the mechanical properties of polymers, the addition of carbon nanotubes to polymer matrices also alters the electronic properties of the composite creating multifunctional composite materials. Applications for these multifunctional materials could include optoelectronics, electrostatic discharge, electromagnetic induction shielding, and membrane technologies.

The addition of nanotubes to an epoxy (Araldite LY556) matrix was found to significantly increase the electrical conductivity of the polymer as demonstrated in figure 2-23 (Sandler *et al.* 1999). The polymer matrix is usually used for aircraft applications where high electrical

conductivity is required to avoid electrostatic charging and electromagnetic radio frequency interference. Carbon black at a concentration of 0.5 vol% is traditionally used as a conductive filler for this application. Nanotubes can however achieve the same conductivity as the carbon black at a lower filler content (0.04 vol%) due to a favorable percolation behavior. The percolation phenomenon is characterized by the presence of a conductive path through the matrix due to the formation of a three-dimensional network of conductive fillers, which are the nanotubes. A sharp drop in electrical conductivity characterizes the percolation threshold in the electrical resistance. Improvements in mechanical properties in this case are seen as an additional benefit.

Nanotubes have also been combined with conjugate polymers creating active materials for electronic applications. Some of these applications include light-emitting diodes (Curran *et al.* 1998, Woo *et al.* 2000), field effect transistors, and photovoltaic devices (Ago *et al.* 1999).

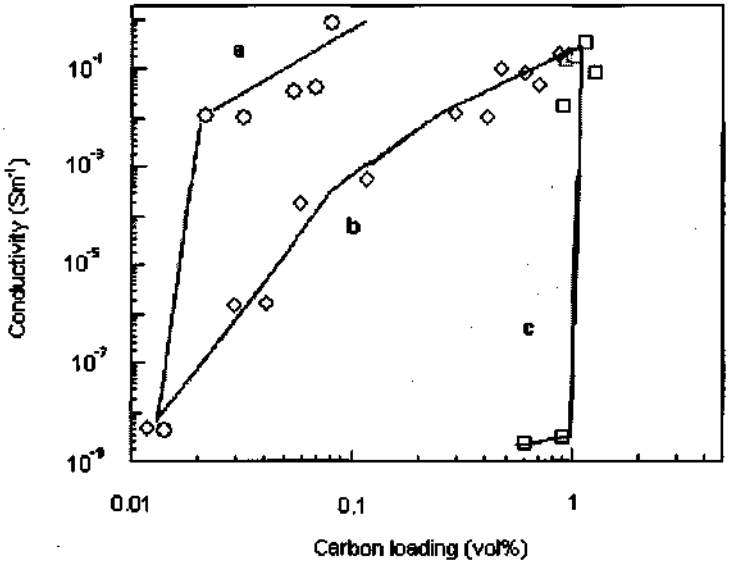

Figure 2-23 Electrical conductivity of CVD grown nanotubes in an epoxy. (a) CVD grown nanotubes. (b) carbon black with copper-chloride. (c) carbon black only. (Sandler *et al.* 1999)

Chapter 3

Modelling of Carbon Nanotubes

An understanding of the elastic behaviour of carbon nanotubes is important in the analysis and design of carbon nanotube-based composites. The elastic behaviour of nanotubes has been the subject of numerous experimental, atomistic modelling, and elastic continuum modelling studies. Experiments at this length scale are themselves still under development and thus have resulted in a range of reported values for various mechanical properties. Molecular dynamics simulations have been effective in simulating the deformation of carbon nanotubes under various loading conditions. However, the computational expense of molecular dynamics simulations limits the size of the nanotubes that can be studied with this technique. Most continuum modelling approaches use the continuum shell model to analyse the elastic behaviour of nanotubes. However, these models neglect the detailed characteristics of nanotube chirality and the forces acting on individual atoms. A modelling technique is thus needed that analyses the mechanical response of nanotubes at the atomistic scale but is not as computationally expensive as molecular dynamics simulations.

In this chapter we investigate the continuum-based model for predicting elastic properties of nanotubes recently proposed by Li *et al.* (2003). The model uses classical structural mechanics to simulate a nanoscopic nanotube as a marcoscopic frame-like structure and then establishing the linkage between molecular mechanics and structural mechanics to obtain the required parameters for structural analysis. The advantages of the proposed method are its simplicity and ability to analyse at an atomistic scale.

In the following sections, brief reviews of structural mechanics and molecular mechanics are first given and then a linkage between the two is established. The method is then demonstrated by a few computational examples. The possibility of extending the model to multi-walled nanotubes is also investigated.

3.1 A brief review of structural mechanics for space frames

Structural mechanics analysis enables the determination of the displacements, strains and stresses of a structure under a given loading condition. The most common method used for analysing structures is the stiffness matrix method, which can be readily applied to analyze structures of any geometry and can be used to solve linear elastic static problems as well as problems involving buckling, plasticity and dynamics. The stiffness matrix method for linearly elastic space frame problems employs an elemental equilibrium equation for each element in a space frame. These equations are then transformed from local coordinates to a common global reference system so that a set of simultaneous equations can be assembled according to the requirements of nodal equilibrium. By solving the system of equations and taking into account the boundary restraint conditions, the nodal displacements of the structure can be obtained.

The elemental equilibrium equation for structural analysis can be written as:

$$Ku = p \tag{3.1}$$

where K is the elemental stiffness matrix, u is the nodal displacement vector, and p is the nodal force vector of the element. For the present study, beam elements of uniform thickness are required. Beam elements connect two nodal points, each with six degrees of freedom. The nodal displacement vector, the nodal force vector, and the elemental stiffness matrix of a beam element may be written as:

$$u = \begin{bmatrix} u_{xi} & u_{yi} & u_{zi} & \theta_{xi} & \theta_{xi} & \theta_{xi} & u_{xj} & u_{yj} & u_{zj} & \theta_{xj} & \theta_{yj} & \theta_{zj} \end{bmatrix}^T, \tag{3.2}$$

$$p = \begin{bmatrix} f_{xi} & f_{yi} & f_{zi} & m_{xi} & m_{xi} & m_{xi} & f_{xj} & f_{yj} & f_{zj} & m_{xj} & m_{yj} & m_{zj} \end{bmatrix}^T, \tag{3.3}$$

and

$$K = \begin{bmatrix} K_{ii} & K_{ij} \\ K_{ij}^T & K_{jj} \end{bmatrix} \tag{3.4}$$

where

$$K_{ii}=\begin{bmatrix} EA/L & 0 & 0 & 0 & 0 & 0 \\ 0 & 12EI_x/L^3 & 0 & 0 & 0 & 6EI_x/L^2 \\ 0 & 0 & 12EI_y/L^3 & 0 & -6EI_y/L^2 & 0 \\ 0 & 0 & 0 & GJ/L & 0 & 0 \\ 0 & 0 & -6EI_y/L^2 & 0 & 4EI_y/L & 0 \\ 0 & 6EI_x/L^2 & 0 & 0 & 0 & 4EI_x/L \end{bmatrix}, \tag{3.5}$$

$$K_{ij}=\begin{bmatrix} -EA/L & 0 & 0 & 0 & 0 & 0 \\ 0 & -12EI_x/L^3 & 0 & 0 & 0 & 6EI_x/L^2 \\ 0 & 0 & -12EI_y/L^3 & 0 & -6EI_y/L^2 & 0 \\ 0 & 0 & 0 & -GJ/L & 0 & 0 \\ 0 & 0 & 6EI_y/L^2 & 0 & 2EI_y/L & 0 \\ 0 & -6EI_x/L^2 & 0 & 0 & 0 & 2EI_x/L \end{bmatrix} \tag{3.6}$$

and

$$K_{jj}=\begin{bmatrix} EA/L & 0 & 0 & 0 & 0 & 0 \\ 0 & 12EI_x/L^3 & 0 & 0 & 0 & -6EI_x/L^2 \\ 0 & 0 & 12EI_y/L^3 & 0 & 6EI_y/L^2 & 0 \\ 0 & 0 & 0 & GJ/L & 0 & 0 \\ 0 & 0 & 6EI_y/L^2 & 0 & 4EI_y/L & 0 \\ 0 & -6EI_x/L^2 & 0 & 0 & 0 & 4EI_x/L \end{bmatrix} \tag{3.7}$$

From the above elemental stiffness matrices, it can be observed that the stiffness parameters of tensile resistance EA, flexural resistance EI_x and EI_y, and torsional resistance GJ need to be determined to obtain the deformation of an element of known length.

3.2 Molecular mechanics

Molecular mechanics uses classical type models to predict the energy of a molecule as a function of the positions of its nuclei. The atomic nuclei are regarded as material points and

the forces between them are characterized by a force field, which depends solely on the positions of the atoms relative to each other within the molecule. In the most general form, the total molecular potential energy is described by the sum of many individual energy contributions.

$$E_{total} = \sum E_r + \sum E_\theta + \sum E_\varphi + \sum E_\omega + \sum E_{vdW} + \sum E_{el} \qquad (3.8)$$

where E_r, E_θ, E_φ, and E_ω, are the energies associated with bond stretching, angle variation, dihedral angle torsion, and improper (out-of plane) torsion respectively. The non-bonded interaction energies consist of van der Waals, E_{vdW}, and electrostatic, E_{el}, interactions. Various functional forms may be used for these energy terms, depending on the particular material and loading conditions. Energy forms for covalent systems under the assumption of small deformation are given below:

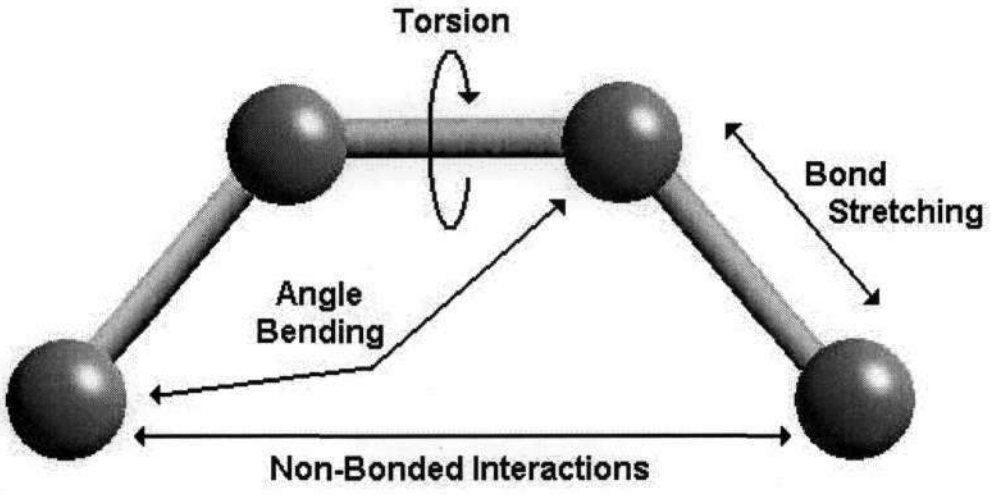

Figure 3-1 Interatomic interactions in molecular mechanics

3.2.1 Bond stretching

Whenever a bond is compressed or stretched, the energy increases. For small bond stretching increments, the harmonic approximation is adequate for describing the energy:

$$E_r = k_r\left(r - r_{eq}\right)^2 \qquad (3.9)$$

where k_r is the bond stretching force constant and r_{eq} is the equilibrium distance between a pair of bonded atoms. For a sp^2 bond between carbon atoms the equilibrium bond length r_{eq} = 1.409 Å, and the force constant k_r = 469 kcal/(mol.Å^2) (Cornell *et al.* 1995).

3.2.2 Angle variation

The bending energy equation estimates the energy associated with vibration about the equilibrium bond angle and can also be approximated by a harmonic function for small increments about the equilibrium angle.

$$E_\theta = k_\theta \left(\theta - \theta_{eq}\right)^2 \tag{3.10}$$

where k_θ is the bond angle bending force constant and θ_{eq} is the equilibrium bond angle. For a sp^2 bond between carbon atoms the equilibrium bond angle θ_{eq} = 120°, and the force constant k_θ = 63 kcal/(mol.rad^2) (Cornell *et al.* 1995).

3.2.3 Torsion

The dihedral angle torsion and improper torsion energies are modelled by simple periodic functions fitted to experimental data:

$$E_\tau = \frac{V_n}{2}\left[1 + \cos\left(n\varphi - \gamma\right)\right] \tag{3.11}$$

where E_τ is the torsional energy, φ is the rotational angle, V_n is the parameter for amplitude, n controls the periodicity and γ shifts the curve along the rotation axis. For a sp^2 bond between carbon atoms the values of n and γ are 2 and 180° respectively, whilst the values of $V_n/2$ for dihedral angle torsion and improper torsion are 14.5 kcal/mol and 1.1 kcal/mol respectively (Cornell *et al.* 1995). For simplicity, the dihedral and improper torsions are merged and for small changes in the rotational angle φ, the torsion energy equation may be approximated as:

$$E_\tau = 2k_\tau \left(\Delta\phi\right)^2 \tag{3.12}$$

where $\Delta\varphi$ is the change in rotational angle and $K_\tau = V_n/2$ for dihedral torsion and improper torsion = 15.6 kcal/mol

3.2.4 Non-bonded interactions

The non-bonded energy represents the pair-wise sum of the van der Waal's and electrostatic energies of all possible interacting non-bonded atoms. The van der Waals forces between atoms are modelled using the general Lennard-Jones potential and the electrostatic contribution is modelled using a Coulombic potential.

$$E = \left(\frac{A_{ij}}{r_{ij}^{12}} - \frac{B_{ij}}{r_{ij}^{6}} \right) + \frac{q_i q_j}{r_{ij}} \tag{3.13}$$

where A_{ij} and B_{ij} are the parameters used to describe the attraction and repulsion of the van der Waals forces respectively while q_i and q_j are the electrostatic potentials of the atoms. When modelling carbon atoms in a nanotube, there are no electrostatic forces between atoms and the van der Waals interactions are only significant when modelling the interactions between the layers of multi-walled nanotubes or buckling of single-walled nanotubes.

3.3 Linkage between sectional stiffness parameters and constants of force fields

The structure of a carbon nanotube can be visualised as carbon atoms covalently bonded together to form a hexagonal lattice structure on the wall of the tube. When a nanotube is subjected to external forces, the deformation of the nanotube is a result of the individual interactions between its atoms, which are constrained by the bonds between the atoms. The bonds between the atoms have characteristic bond lengths and bond angles in a three-dimensional space. If the covalent bonds between carbon atoms are considered to be connecting elements between carbon atoms, the nanotube can be simulated as a space frame-like structure with the carbon atoms acting like joints between connecting elements.

To establish a link between the molecular mechanics models of bonding between atoms and the structural mechanics models of structural elements between nodes, the relationships between force constants of molecular mechanics and stiffness parameters in structural mechanics need to be determined. The deformation of a space frame results in changes in strain energies of the elements. Thus the stiffness parameters of the elements can be determined by energy equivalence with energy terms in molecular mechanics. For convenience, it is assumed that the sections of the elements representing the carbon-carbon bonds are identical and uniformly round. Thus $I_x = I_y = I$ and only the stiffness parameters EA, EI and GJ are need to be determined.

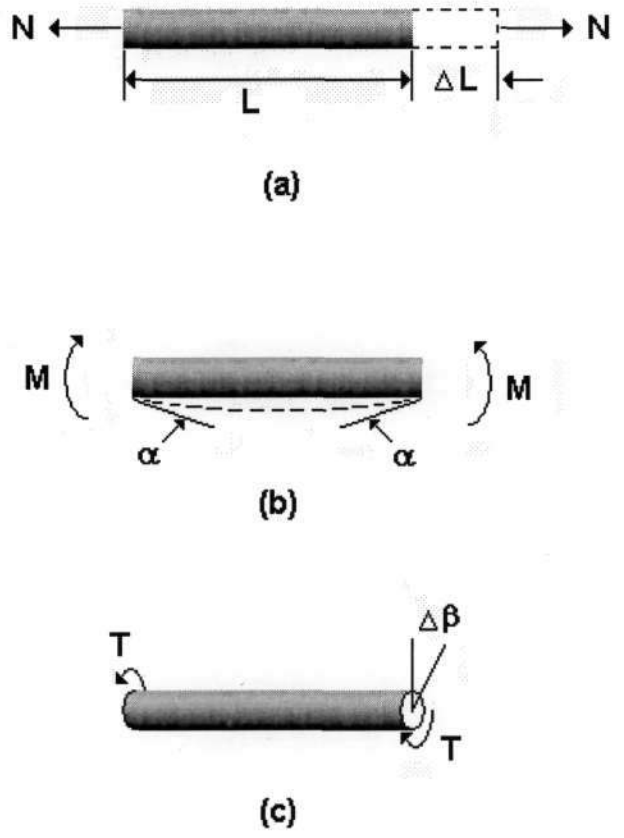

Figure 3-2 (a) Pure tension, (b) pure bending, and (c) pure torsion

The strain energy of a uniform beam of length L loaded in pure tension by an axial force N can be described by:

$$U_A = \frac{1}{2}\int_0^L \frac{N^2}{EA}dL = \frac{1}{2}\frac{N^2 L}{EA} = \frac{1}{2}\frac{EA}{L}(\Delta L)^2 \tag{3.14}$$

where ΔL is the axial stretching deformation. The strain energy of a uniform beam under pure bending moment M is:

$$U_M = \frac{1}{2}\int_0^L \frac{M^2}{EA}dL = \frac{2EI}{L}\alpha^2 = \frac{1}{2}\frac{EI}{L}(2\alpha)^2 \tag{3.15}$$

where α denotes the rotational angle at the ends of the beam. The strain energy of a uniform beam under pure torsion T is:

$$U_T = \frac{1}{2}\int_0^L \frac{T^2}{GJ} dL = \frac{1}{2}\frac{T^2 L}{GJ} = \frac{1}{2}\frac{GJ}{L}(\Delta\beta)^2 \tag{3.16}$$

where $\Delta\beta$ is the relative rotation between the ends of the beam.

It is noted that the mechanical strain energy due to pure tension U_A can be equated to stretching energy E_r, strain energy due to pure bending U_M can be equated to bending energy E_θ, and strain energy due to pure torsion U_T can be equated to torsion energy E_τ. It is reasonable to assume that the change in bond length (r - r_{eq}) is equivalent to the change in length of the beam ΔL, the change in bond angle (θ- θ_{eq}) is equivalent to the rotational angle at the ends of the beam 2α, and the change in rotational angle $\Delta\varphi$ is equivalent to the relative rotation between the ends of the beam $\Delta\beta$. Thus, a direct relationship between the structural mechanics parameters and the molecular force constants can be obtained by comparing molecular energy equations with strain energy equations. Stretching energy (3.9) can be equated to strain energy due to pure tension (3.14) to obtain the relationship between tensile resistance EA and bond stretching force constant k_r:

$$k_r = \frac{EA}{2L} \tag{3.17}$$

Bending energy (3.10) can be equated to strain energy due to pure bending (3.15) to obtain the relationship between bending resistance EI and bond angle force constant k_θ:

$$k_\theta = \frac{EI}{2L} \tag{3.18}$$

Torsion energy (3.12) can be equated to strain energy due to torsion (3.16) to obtain the relationship between torsion resistance and torsional force constant:

$$k_\tau = \frac{GJ}{L} \tag{3.19}$$

It follows that a structural mechanics theory can be used to model the mechanical behaviour of carbon nanotubes using force constants from molecular mechanics.

3.4 Molecular structural mechanics model

The modelling of molecular structures using a structural mechanics approach is achieved using the following main steps. First, an equivalent frame-like structure of the molecule is constructed with the atoms modelled as joints and bonds modelled as beams. The sectional properties of the beams are determined from energy equivalence of molecular force field energy with structural strain energy. Boundary constraint conditions are placed and finite element analysis software is then used to solve the displacements of atoms. The elastic properties of the molecule can be calculated from the displacement of the atoms.

Carbon nanotubes can be visualised as graphene sheets rolled into tubes. As the elastic properties of graphene sheets are well understood, a graphene sheet is first modelled to evaluate the molecular structural mechanics method. Single-walled nanotubes are then modelled to calculate their basic elastic properties, such as Young's modulus and shear modulus.

The initial bond length between carbon atoms is taken to be 0.1421 nm which is the widely accepted initial bond length between carbon atoms in a graphene sheet. The van der Waals forces between non-bonded atoms in the graphene sheet are ignored as they are negligible when compared to the bonding forces between atoms. Using the parameters for the AMBER force field (Cornell *et al.* 1995), the stiffness parameters of the beams representing interatomic bonds can be calculated using equations (3.17)-(3.19).

$$\frac{EA}{2L} = k_r = 46900 \frac{kcal}{mol.nm^2} = 3.26 \cdot 10^{-7} \frac{nJ}{bond.nm^2} \tag{3.20}$$

$$\frac{EI}{2L} = k_\theta = 63 \frac{kcal}{mol.rad^2} = 4.38 \cdot 10^{-10} \frac{nJ}{angle.rad^2} \tag{3.21}$$

$$\frac{GJ}{L} = k_\tau = 15.6 \frac{kcal}{mol.rad^2} = 1.08 \cdot 10^{-10} \frac{nJ}{angle.rad^2} \tag{3.22}$$

From the stiffness equations, the geometrical and material properties of the round beam elements representing the bonds between carbon atoms can be deduced as:

$$A = 0.01688 nm^2$$

$$E = 5491 \frac{nN}{nm^2}$$

$$I = 2.267 \cdot 10^{-5} nm^4$$

$$G = 676 \frac{nN}{nm^2}$$

$$J = 4.535 \cdot 10^{-5} nm^4$$

The finite element analysis software, MSC visual Nastran for Windows, was used to model the behaviour of the equivalent frame-like structures of graphene sheets and carbon nanotubes. Firstly, the geometric positions of the atoms in the model were calculated and nodes were placed at the atom locations. Beam elements with properties as given above were then placed between the nodes of bonded atoms. Boundary conditions were then placed on the structure so that the elastic properties of the molecule can be calculated from the displacement of the atoms.

3.4.1 Molecular structural mechanics model of a graphene sheet

Various model sizes of equivalent frame-like structures of graphene sheets were entered into a finite element models to determine their elastic moduli. The elastic modulus of a material is the linear relationship between normal stress and normal strain in uniaxial tension or compression test:

$$E = \frac{\sigma}{\varepsilon} = \frac{F / A_0}{\Delta H / H_0} \tag{3.23}$$

where F is the total force acting on the object, A_0 is the initial cross-sectional area of the object, ΔH is the change in length of the object, and H_0 is the initial length of the object. A graphene sheet has the thickness of a single carbon atom so to define the cross-sectional area of the graphene sheet, the thickness is taken to be the interlayer spacing of graphite, 0.34 nm (Dresselhaus et al. 1995).

Boundary conditions were placed on the models to represent uniaxial tension tests. The nodes on one side of the sheet were constrained and equal forces were placed on the nodes on the other side to load the sheet in tension. Finite element analysis was then performed on

the model and the increase in length of the sheet was determined from the displacement of the nodes. The graphene sheets were loaded in two fundamental directions, load case I and load case II (see figure 3-3), to determine the effect of bond orientation on the elastic behaviour of graphene sheets. In load case I, one third of the bonds are aligned perpendicular to the load direction, whilst in load case II, one third of the bonds are aligned parallel to the load direction. The elastic properties of various model sizes were calculated to determine the effect of model size on the elastic properties of the graphene sheets.

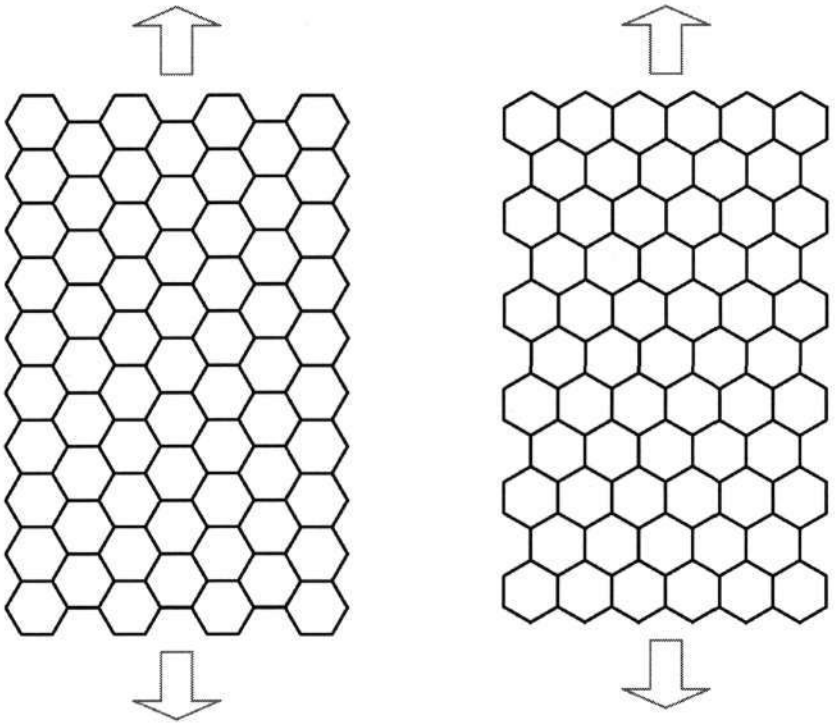

Figure 3-3 Models of graphene sheets loaded in tension.

The results calculated in table 3-1 show that the elastic moduli of graphene sheets in both directions are fairly close to the general accepted value of 1.025 TPa (Kelly 1981), validating the molecular mechanics method for determining the elastic constants of graphene sheets. The elastic modulus is weakly affected by model size, with the elastic modulus in the load case II direction being effected by a slightly higher degree.

	Length of Model (nm)	Width of Model (nm)	Elastic Modulus (TPa)
Load case I	443	85.26	1.03
	566.1	127.9	1.033
	1428	298.4	1.039
	3126	639.5	1.041
Load Case II	284.2	73.84	0.9959
	326.8	98.45	1.007
	624.2	123.1	1.015
	1009	196.9	1.025
	1478	295.3	1.031
	2032	418.4	1.034
	3226	639.9	1.037

Table 3-1 Elastic modulus of modelled graphene sheets loaded in two principal directions

3.4.2 Molecular structural mechanics model of SWNTs

The success of the structural mechanics modelling method for determining the elastic modulus of a graphene sheet established confidence that the method could be used to analyse the elastic behaviour of carbon nanotubes. Single-walled nanotubes with armchair chirality and zigzag chirality were considered. The geometric positions of the atoms in the nanotubes were calculated such that the atoms lay on a cylinder and the distances between bonded atoms were 0.1421 nm. Equivalent frame-like structures of the nanotubes were entered into finite element models using the same beam parameters as used for modelling graphene sheets. Boundary conditions were then placed to represent tests determining the elastic behaviour of the nanotubes.

3.4.2.1 Young's modulus

To determine the elastic modulus of SWNTs in the axial direction, boundary conditions were placed to represent loading the nanotube in tension and finite element analysis was performed to determine the displacement of the nodes. The nanotube was loaded in tension by constraining one end of the tube and applying a tensile force to the other end.

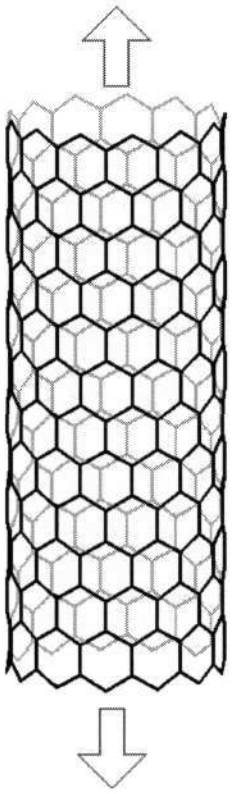

Figure 3-4 Model of a zigzag nanotube loaded in tension

To determine the elastic modulus of the carbon nanotubes, the cross-sectional is taken to be that of a hollow tube with a thickness equal to the interlayer spacing of graphite. The cross-sectional area may thus be approximated by the following equation:

$$A_0 = \pi dt \tag{3.24}$$

where d is the nanotube diameter and t is the interlayer spacing of graphite (0.34 nm). Figure 3-5 shows the elastic moduli of armchair and zigzag nanotubes calculated using equation (3.23). A trend of increasing elastic modulus with increasing nanotube diameter is observed for both armchair and zigzag nanotubes and the chirality of the nanotubes is shown to have little effect on their elastic modulus. For nanotubes with diameters less than 0.7 nm, the elastic modulus of nanotubes with an armchair chirality is slightly greater than the elastic modulus of nanotubes with a zigzag chirality, whilst for nanotubes with diameters greater than 0.7 nm, the elastic modulus of nanotubes with a zigzag chirality is slightly greater than the elastic modulus of nanotubes with an armchair chirality. The diameter of the nanotubes has a significant effect on their elastic modulus for nanotube diameters less than 1 nm, whilst the elastic modulus of nanotubes with greater diameters tends towards the elastic modulus

calculated earlier for graphene sheets. The results are comparable to the experimental results and the theoretical results reviewed in chapter 2.

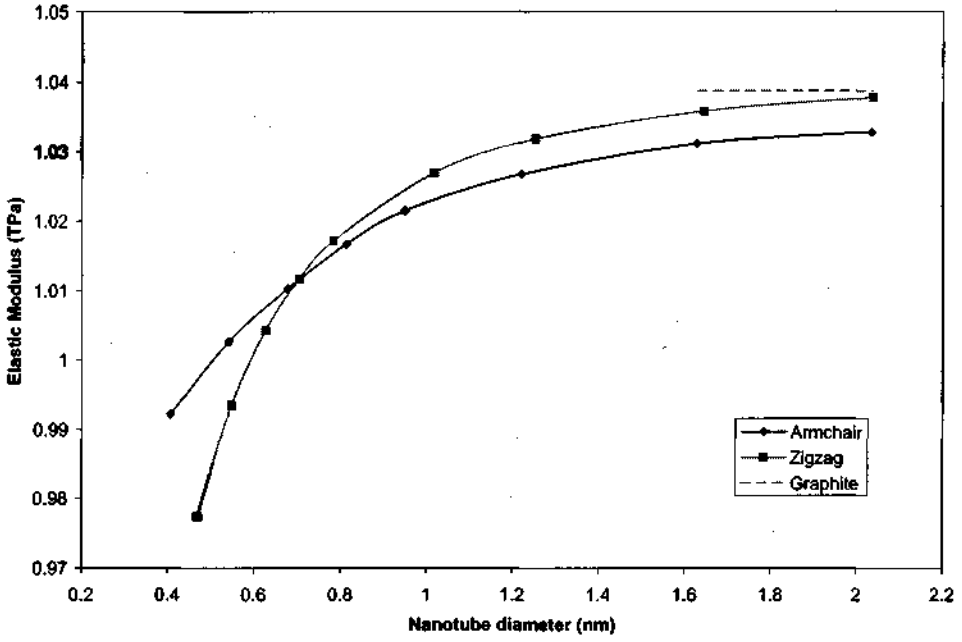

Figure 3-5 Elastic modulus of nanotubes versus nanotube diameter.

For the use of nanotubes as a filler phase in composite materials, the elastic modulus of the nanotube when the nanotube is considered to be solid fibre is also of interest. The cross-sectional area of the solid fibre is calculated using the following equation:

$$A_0 = \frac{\pi(d+t)^2}{4} \tag{3.27}$$

where d is the diameter of the nanotube and t is the interlayer spacing of graphite (3.4 nm). Figure 3-6 shows the elastic modulus of a nanotube considered to be a solid fibre versus nanotube diameter. The elastic modulus of the nanotubes decreases with increasing diameter due to the hollow tubular structure of the nanotubes. A solid tubular structure also means that the density of nanotubes decreases with increasing diameter, thus nanotube diameter needs to be considered when analysing and designing nanotube-reinforced polymer composite materials.

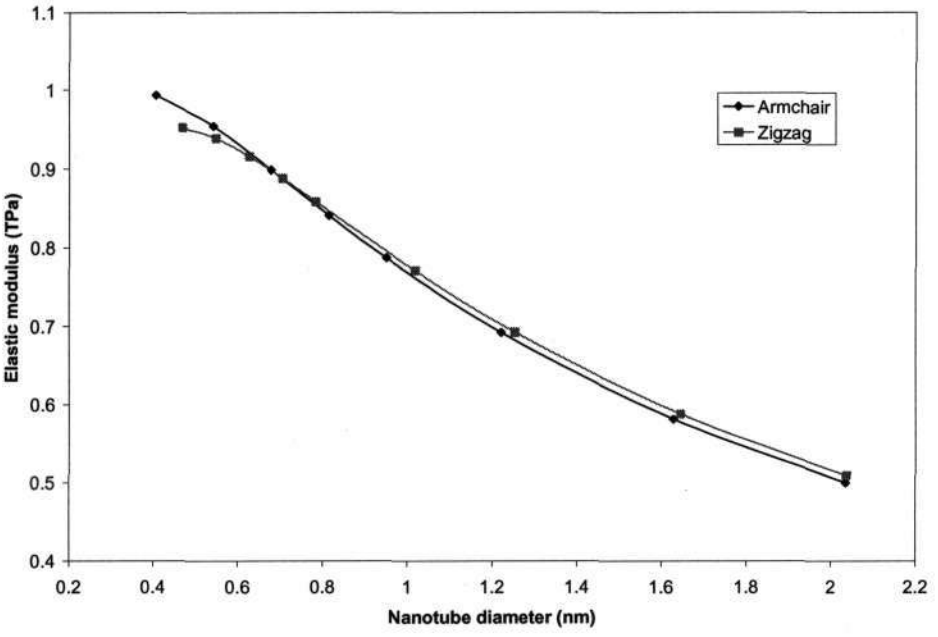

Figure 3-6 Elastic modulus of nanotubes considered to be solid fibres versus nanotube diameter

3.4.2.2 Shear modulus

The shear modulus of a nanotube was determined by subjecting the equivalent frame-like structure to a torsional moment at one end and constraining the other end.

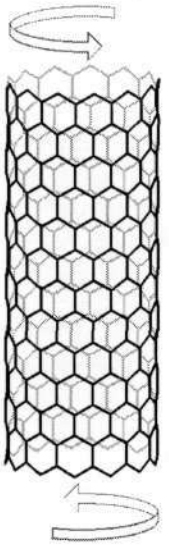

Figure 3-7 Model of a zigzag nanotube loaded in shear

The following formula, which is based on the theory of elasticity at the macroscopic scale, was used for obtaining the shear modulus:

$$G = \frac{T L_0}{\theta J_0} \tag{3.25}$$

where T is the torque acting at one end, L_0 is the original length, θ is the torsional angle, and J_0 is the cross-sectional polar inertia of the nanotube if the nanotube is treated as a hollow tube with a thickness equal to the interlayer distance of graphene sheets. Figure 3-8 shows the shear modulus of armchair and zigzag nanotubes. Similar trends to that of elastic modulus can be observed in that the shear modulus increases with increasing diameter for small nanotube diameters and chirality has little effect on the shear modulus. The shear modulus of the nanotubes again tends towards the shear modulus calculated for graphene sheets at large diameters. No experimental results are available for the shear modulus of nanotubes but the results are comparable to the theoretical results reviewed in chapter 2.

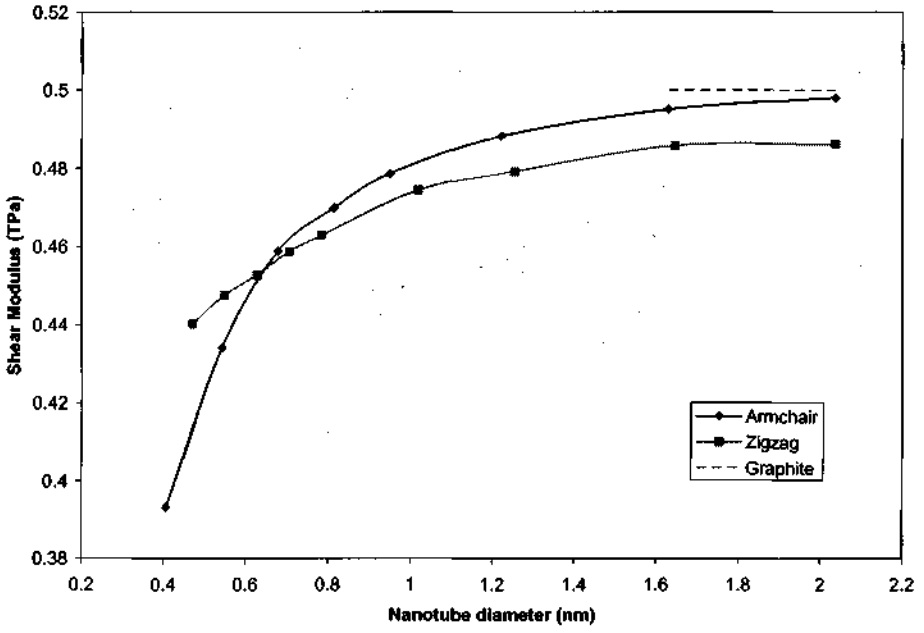

Figure 3-8 Shear moduli of nanotubes versus nanotube diameter

3.5 Extension of model to MWNTs

Multi-walled nanotubes consist of multiple layers held together through non-bonded van der Waals interactions. The van der Waals interaction results in a force between a pair of non-

bonded atoms dependant on the distance between the atoms. If the distance between the interacting atoms is less than the sum of their contact radii, a repulsive force exists between the two atoms and if the distance between the two interacting atoms is greater than the sum of their contact radii, an attractive force exists between the two interacting atoms. The van der Waals interaction between two atoms is often modelled using a Lennard-Jones potential:

$$E_{vdW} = 4\varepsilon\left[\left(\frac{\sigma}{r}\right)^{12} - \left(\frac{\sigma}{r}\right)^{6}\right] \tag{3.26}$$

where the distance between atoms is r and the constants, ε and σ for carbon atoms are 0.0556 kcal/mol and 3.4 Å respectively. (Battezzatti *et al.* 1975). Based on the Lennard-Jones potential, the force between interacting atoms can be expressed as:

$$F(r) = -\frac{dU(r)}{dr} = 24\frac{\varepsilon}{\sigma}\left[2\left(\frac{\sigma}{r}\right)^{13} - \left(\frac{\sigma}{r}\right)^{7}\right] \tag{3.27}$$

The force between interacting atoms due to van der Waals interactions is shown in figure 3-9. Each atom in a MWNT layer forms interacting pairs with other atoms in neighbouring layers. However, if the distance between atoms is greater than 2.5 σ, the interaction can be ignored without significant loss of accuracy.

In our analysis, we investigate the possibility of simulating the van der Waals forces between atoms with an equivalent structural mechanics approach. It is hypothesised that the van der Waals forces between non-bonded atoms may be represented by truss rod elements. Truss rod elements transmit only tensile or compressive forces between rotatable end joints. The tensile and compressive forces transmitted by truss rod elements could thus represent the attractive and repulsive van der Waals forces between non-bonded atoms, which are represented by nodes in the equivalent structural mechanics method.

As can be seen in figure 3-9, the van der Waals force between two atoms is highly non-linear. Therefore, the truss rods representing van der Waals forces need to be nonlinear, with a load-displacement relationship characterised by the van der Waals force. Due to the intrinsic nature of the van der Waals force, the force exerted by the truss rod element needs to be opposite to that of the van der Waals force. The stress in the truss elements may then be

calculated for a given cross-sectional area. Figure 3-10 shows examples of the stress versus strain behaviour of truss elements representing the interaction between atoms with different initial distances between the interacting atoms.

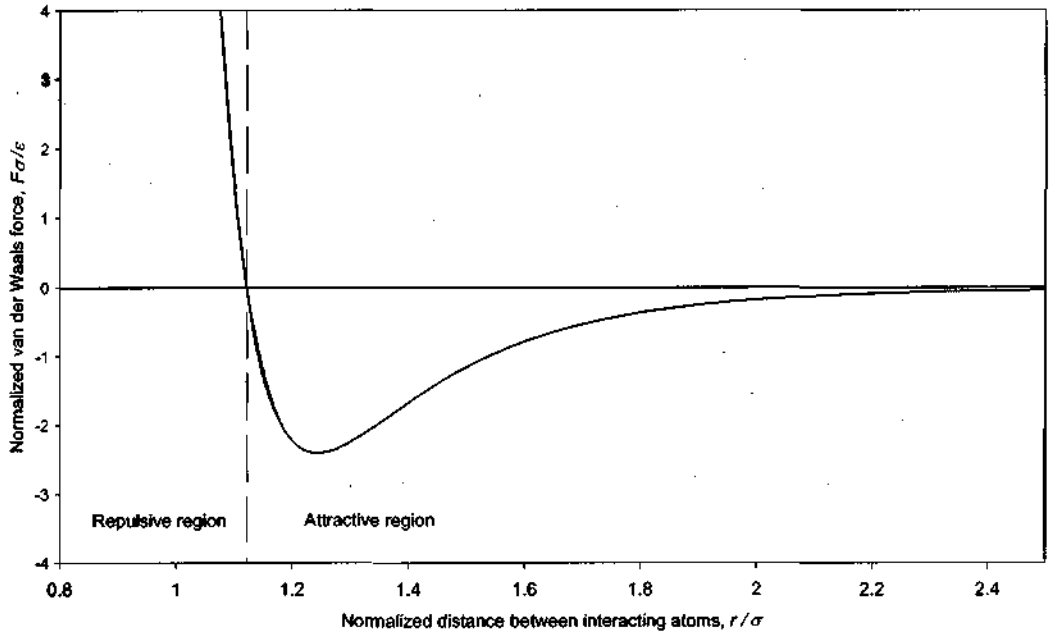

Figure 3-9 The variation of van der Waals force with the distance between two interacting atoms.

It is noticed that the stress-strain behaviour of the truss elements have distinct stages of loading and unloading and thus a suitable nonlinear analysis method is needed for simulation. For most nonlinear analyses, the Newton-Raphson method is used to converge the solution at each time step along the force deflection curve. The Newton-Raphson method increments the load a finite amount at each substep and keeps that load fixed throughout the equilibrium iterations. Because of this, it cannot converge if the slope of the force-deflection curve at any point is zero. To avoid this problem, the arc-length method may be used as it is able to handle zero and negative force-deflection curves. To handle zero and negative force-deflection curves, the arc-length treats the load-factor as a variable which is modified at each iteration so that the solution follows some specified path until convergence is achieved.

Simulations were carried out on examples of truss elements to determine the ability of the arc-length method in determining the relationship between force and displacement of van der Waals interactions. Truss elements with initial lengths of: 0.34 nm, 0.3816 nm, 0.4 nm and 0.5 nm were simulated using the MSC Nastran for Windows finite element analysis software. The truss elements had nonlinear elastic material properties with stress-strain

relationships as shown in figure 3-10. The arc-length non-linear analysis method was then used to determine the force-displacement relationships of the non-linear truss elements.

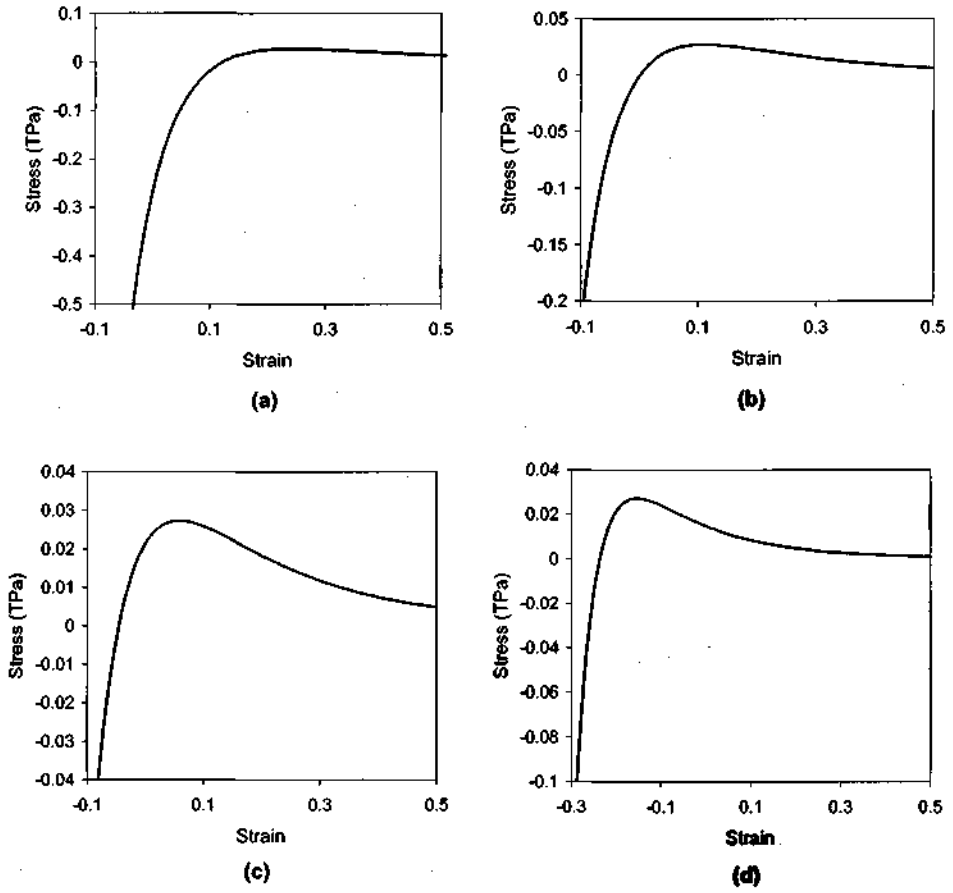

Figure 3-10 Stress versus strain of truss elements, with a cross-sectional area of 0.1 nm^2, representing the interaction between atoms with initial distances between interacting atoms of: (a) 0.34 nm, (b) 0.3816 nm, (c) 0.4 nm, and (d) 0.5 nm.

The arc-length method successfully simulated the force-displacement relationship for the truss with an initial length of 0.3816 nm. Truss elements with an initial length of 0.3816 nm have no initial force and the stress-strain curve is positive at zero strain. For initial truss lengths lower than 0.3816 nm, the arc-length method was able to simulate the force-displacement relationship for negative strain but was unable to get the solution to converge for positive strains. For initial truss lengths between 0.3816 nm and 0.4231 nm, the arc-length method was able to simulate the force-displacement relationship for positive strain but was unable to get the solution to converge for negative strains. At initial truss lengths of over 0.4231 nm, the stress-strain curve is negative at zero strain and the finite element software

would not accept such a nonlinear material. The finite element software used was thus not able to simulate MWNTs using the proposed method.

3.6 Summary

A structural mechanics approach to simulating a nanoscopic nanotube as a macroscopic frame-like structure has been presented. The bonds between the carbon atoms were modelled as beam elements with the cross-sectional properties of the beams being determined through energy equivalence with the molecular force field. Thus nanotubes were modelled at an atomistic scale using theories of solid mechanics and methods of computational mechanics. This allows advantages over more refined atomic simulation methods such as molecular dynamics in that the computation is more economical allowing for the simulation of larger systems over longer time periods.

The computational results for basic elastic properties are comparable to those obtained from other modelling techniques, giving us confidence that the method can accurately model the behaviour of nanotubes.

The ability of extending the model to MWNTs by introducing a nonlinear truss rod to represent van der Waals forces acting between the non-bonded atoms between MWNT layers was investigated. Modelling of the nonlinear truss elements was however not achievable with the finite element analysis software available.

Chapter 4

Micromechanical Methods

For the application of carbon nanotubes in nanotube-reinforced polymer (NRP) composite structures, detailed models of the effective properties of the composite at the macroscopic level need to be developed. Molecular dynamic or other atomistic models are too computationally intensive for modelling NRPs thus micromechanical methods need to be developed to describe the behaviour of these materials. In this chapter, the stiffening effect of carbon nanotubes is quantitavely investigated by an extension of traditional micromechanical methods. The results from the micromechanical investigation are used to determine the engineering constants for a NRP composite.

Although some encouraging results have been reported on experimental analysis of manufactured NRP composites, most experiments demonstrate only moderate improvements in strength and stiffness. Some of the characteristics observed in manufactured NRP composites that could contribute to the mechanical properties being lower than expected are: random orientation of the nanotubes, curvature of the nanotubes and poor distribution of the nanotubes in the matrix. In our investigation, we include some of these characteristics in an extension of traditional micromechanical models to determine their effect on the overall properties of the composite. Other characteristics that may reduce the stiffening effect of the nanotubes, such as the nanotube-polymer interface are not included in the model.

The Mori-Tanaka effective field method is first employed to calculate the effective elastic moduli of composites with aligned or randomly oriented straight nanotubes. Then the influence of nanotube agglomeration on the effective stiffness is analysed using an Eshelby's inclusion model. Analytical expressions derived for the effective elastic stiffness of NRP composites with the effects of random orientation and agglomeration show the reduction in the stiffening effect of nanotubes to be significant. The results of this study may also be useful for improving and tailoring the mechanical properties of nanotube composites.

4.1 The Model

A micromechanics model is developed to determine the effective elastic moduli of a single-walled nanotube-reinforced polymer. First a polymer reinforced with aligned nanotubes is investigated, then the model is extended to a random oriented nanotube-reinforced polymer and finally, a random oriented, agglomerated nanotube-reinforced polymer is investigated. The unsatisfactory improvement of mechanical properties in experimental results on NRPs have also been attributed to observed waviness of the SWNTs and weak bonding between the nanotubes and the polymer, however these characteristics are not included in the model.

The SWNTs in this model are considered to be long, straight and have a diameter of 2 nm. A diameter of 2 nm was chosen as it is the mean diameter of commercially available SWNTs. Bonding at the polymer-nanotube interface is considered to be perfect. The SWNTs are modelled as solid fibres with transversely isotropic material properties. Transversely isotropic material properties account for the tubular structure of the nanotubes. Representative values of the elastic constants of the SWNTs are taken from the analytical results of Popov *et al.* (2000), who calculated the elastic moduli of nanotubes using a perturbation approach to study the long-wave atomic vibrations.

Polystyrene is chosen for the polymer matrix as theoretical and experimental results have demonstrated a good nanotube-polymer interface in nanotube-reinforced polystyrene composites. Good dispersion of the nanotubes in polystyrene matrices has also been demonstrated.

Representative volume elements of the composite are chosen and the Mori-Tanaka method is used to estimate the overall properties of the composite. The Mori-Tanaka method assumes that each inclusion is embedded in an infinite pristine matrix subjected to an effective stress or an effective strain in the far field.

4.2 Composites Reinforced with Aligned Nanotubes

For this model, a linear elastic polymer matrix reinforced by a large number of dispersed nanotubes that are straight, aligned and of infinite length is considered. An elementary cell of such a unidirectional composite material can be considered as a fibre embedded in a cylinder

of matrix. The cell has an axis of revolution in a direction parallel to the fibres, referred to as the longitudinal direction. Every direction normal to the fibre is called the transverse direction, and the composite is considered as being transversely isotropic.

4.2.1 Stiffness Matrices

Taking direction 1 in the longitudinal direction and directions 2 and 3 in the transverse directions, the elastic behaviour of an elementary cell of a unidirectional composite material can be expressed as:

$$\begin{bmatrix}\sigma_{11}\\ \sigma_{22}\\ \sigma_{33}\\ \sigma_{23}\\ \sigma_{13}\\ \sigma_{12}\end{bmatrix}=\begin{bmatrix}n & l & l & 0 & 0 & 0\\ l & k+m & k-m & 0 & 0 & 0\\ l & k-m & k+m & 0 & 0 & 0\\ 0 & 0 & 0 & 2m & 0 & 0\\ 0 & 0 & 0 & 0 & 2p & 0\\ 0 & 0 & 0 & 0 & 0 & 2p\end{bmatrix}\begin{bmatrix}\varepsilon_{11}\\ \varepsilon_{22}\\ \varepsilon_{33}\\ \varepsilon_{23}\\ \varepsilon_{13}\\ \varepsilon_{12}\end{bmatrix} \tag{4.1}$$

where k, l, m, n, and p are the Hill's elastic moduli; n is the uniaxial tension modulus in the fibre direction (direction 1), k is the plane-strain bulk modulus normal to the fibre direction, l is the associated cross modulus, m and p are the shear moduli in planes normal and parallel to the fibre direction respectively. A composite with a reinforcing phase volume fraction c_r, matrix Young's modulus E_m and matrix Poisson's ratio ν_m is considered. Using the Mori-Tanaka method, the Hill's elastic moduli are found to be (Shi *et al.* 2004):

$$k=\frac{E_m\{E_m c_m+2k_r(1+\nu_m)[1+c_r(1-2\nu_m)]\}}{2(1+\nu_m)[E_m(1+c_r-2\nu_m)+2c_m k_r(1-\nu_m-2\nu_m^2)]} \tag{4.2}$$

$$l=\frac{E_m\{c_m\nu_m[E_m+2k_r(1+\nu_m)]+2c_r l_r(1-\nu_m^2)\}}{(1+\nu_m)[2c_m k_r(1-\nu_m-2\nu_m^2)+E_m(1+c_r-2\nu_m)]} \tag{4.3}$$

$$\begin{aligned}n=&\frac{E_m^2 c_m(1+c_r-c_m\nu_m)+2c_m c_r(k_r n_r-l_r^2)(1+\nu_m)^2(1-2\nu_m)}{(1+\nu_m)\{2c_m k_r(1-\nu_m-2\nu_m^2)+E_m(1+c_r-2\nu_m)\}}\\ &+\frac{E_m[2c_m^2 k_r(1-\nu_m)+c_r n_r(1-2\nu_m+c_r)-4c_m l_r\nu_m]}{2c_m k_r(1-\nu_m-2\nu_m^2)+E_m(1+c_r-2\nu_m)}\end{aligned} \tag{4.4}$$

$$m = \frac{E_m\left[E_m c_m + 2m_r(1+\nu_m)(3+c_r-4\nu_m)\right]}{2(1+\nu_m)\left\{E_m\left[c_m+4c_r(1-\nu_m)\right]+2c_m m_r\left(3-\nu_m-4\nu_m^2\right)\right\}} \tag{4.6}$$

$$p = \frac{E_m\left[E_m c_m + 2(1+c_r)p_r(1+\nu_m)\right]}{2(1+\nu_m)\left[E_m(1+c_r)+2c_m p_r(1+\nu_m)\right]} \tag{4.5}$$

where k_r, l_r, m_r, n_r and p_r are the Hill's elastic moduli for the reinforcing phase.

4.2.2 Engineering Constants

For the application of composite structures, the engineering constants need to be determined. The engineering constants are the Young's Moduli, the Poissons ratios, and the shear moduli. They are determined by imposing a known stress field and the measuring the strain field. Simple tests such as uniaxial tension or shear tests are performed to obtain the engineering constants. The expressions for the moduli as functions of the stiffness constants are determined for a unidirectional composite material by considering various fundamental tests. The reader is referred to Appendix B for detailed calculations of the engineering constants. Expressions for elastic moduli as functions of the stiffness constants are:

$$E_L = n - \frac{l^2}{k} \tag{4.7}$$

$$E_T = \frac{4m\left(kn-l^2\right)}{kn-l^2+mn} \tag{4.8}$$

$$G_{LT} = 2p. \tag{4.9}$$

$$\nu_{LT} = \frac{l}{2k} \tag{4.10}$$

4.2.3 Evaluating the Engineering constants

The effective elastic moduli, Poison's ratios, and shear moduli are calculated for a polystyrene composite reinforced by aligned, straight single-walled carbon nanotubes. The Young's modulus and Poissin's ratio of polystyrene are E_m=1.9 GPa and ν_m=0.3, respectively. The single walled nanotubes considered have a diameter of 10Å and the Hill's elastic moduli are taken from the analytical results of Popov *et al.* (2004) which are as

follows: n_r=450 GPa, k_r=30 GPa, m_r=p_r=1 GPa, and l_r=10 GPa. It can be noted that the carbon nanotubes are transversely isotropic, with the Young's modulus in the longitudinal direction two orders of magnitude greater than the Young's modulus in the transverse direction.

A Matlab script file was compiled to calculate the engineering constants from the analytical expressions derived for the effective elastic stiffness of a unidirectional NRP composite with increasing volume fraction of nanotubes (See Appendix C.1).

Figure 4-1 shows the relationship between the longitudinal and transverse Young's moduli with increasing volume fraction of nanotubes. The longitudinal Young's modulus increases more rapidly with increasing volume fraction of nanotubes than the Young's modulus in the transverse direction. This is due to the transversely isotropic property of the nanotubes. It is also evident that there is a large magnitude of increase of Young's modulus at low volume fraction of nanotubes. The Poisson's ratio ν_{LT} and transverse shear modulus G_{LT} are plotted against increasing volume fraction of nanotubes in Figure 4-2 and Figure 4-3 respectively.

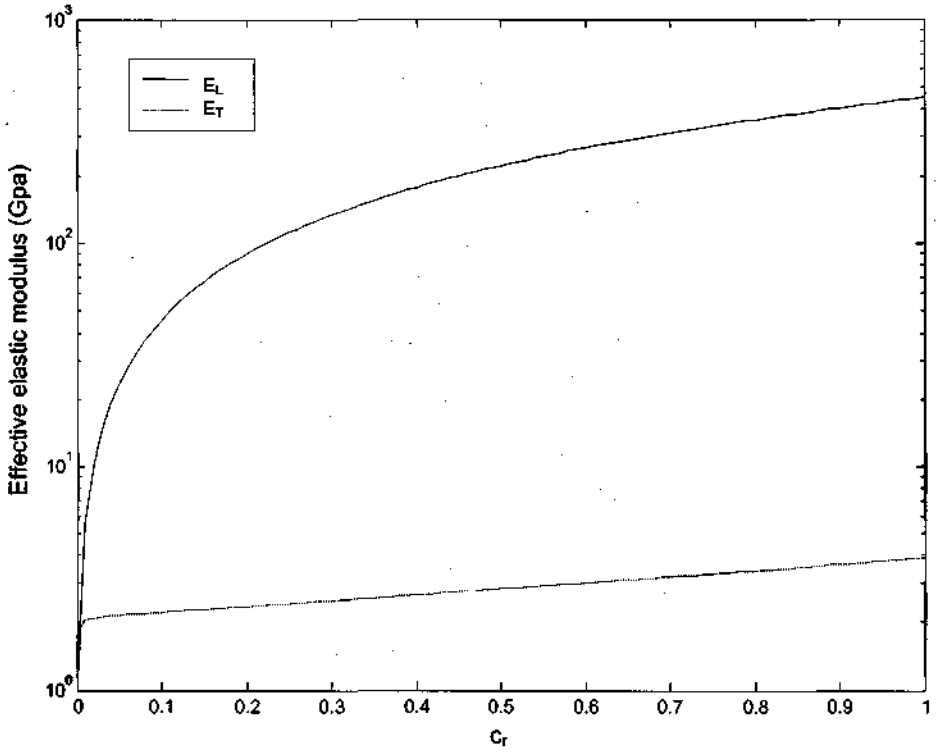

Figure 4-1 Effective elastic moduli of a composite reinforced with aligned nanotubes

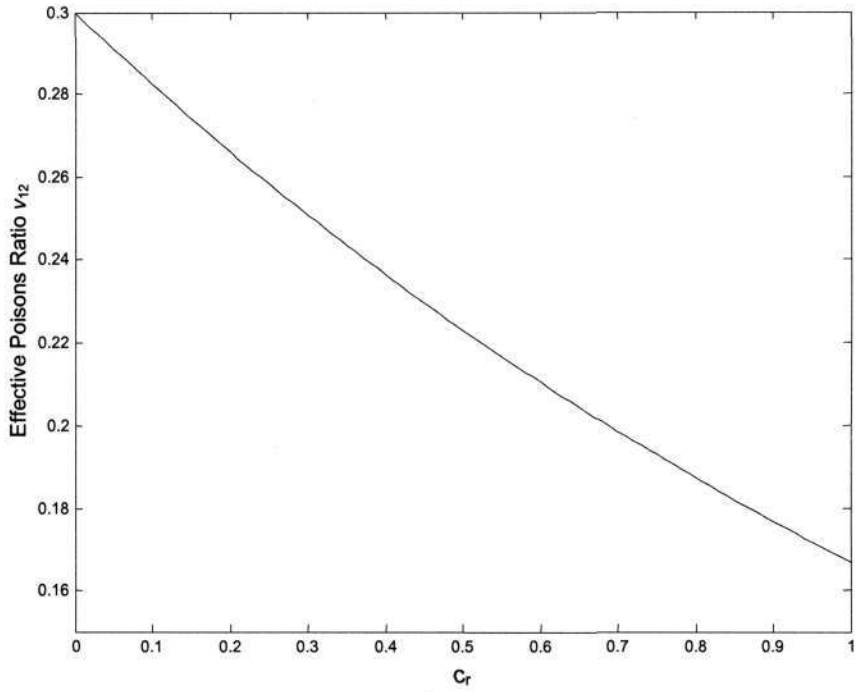

Figure 4-2 Effective Poisson's ratios of a composite reinforced with aligned nanotubes

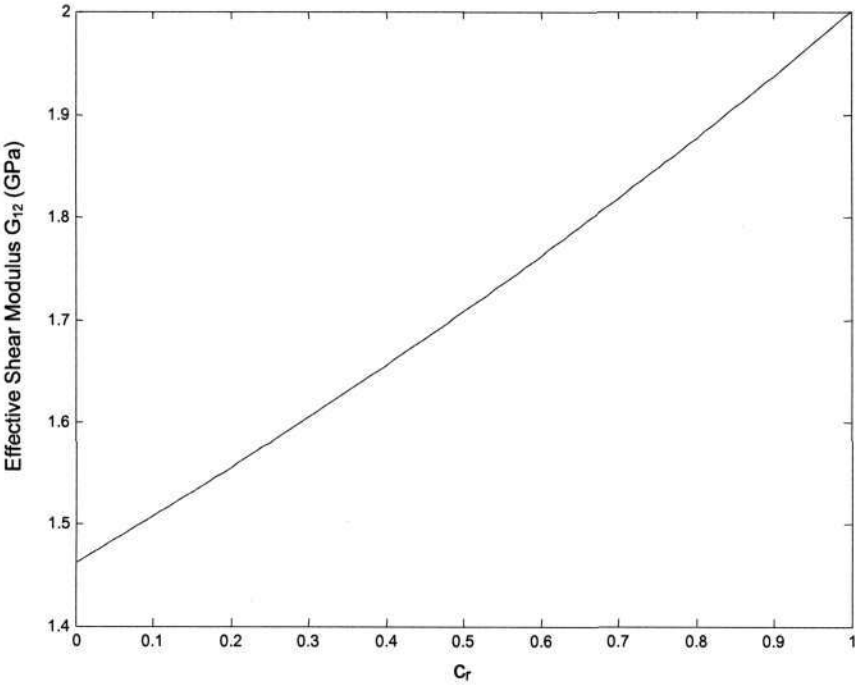

Figure 4-3 Effective shear moduli of a composite reinforced with aligned, straight nanotubes

4.3 Composites Reinforced with Randomly Oriented Nanotubes

In this model, polymers reinforced with randomly oriented, straight nanotubes are investigated. The orientation of the nanotube is characterized by two Euler angles so that the local coordinate system can be related to the global coordinate system and the orientation distribution of nanotubes in the composite is characterized by a probability density function for completely randomly oriented nanotubes. When nanotubes are randomly oriented in the matrix, the composite is then isotropic. Shi *et al.* (2004) derived expressions for the bulk modulus and shear modulus of a composite reinforced with randomly oriented, straight nanotubes using the Mori-Tanaka method. The bulk modulus K and shear modulus G were derived as follows:

$$K = K_m + \frac{c_r(\delta_r - 3K_m\alpha_r)}{3(c_m + c_r\alpha_r)} \tag{4.11}$$

$$G = G_m + \frac{c_r(\eta_r - 2G_m\beta_r)}{2(c_m + c_r\beta_r)} \tag{4.12}$$

where

$$\alpha_r = \frac{3(K_m + G_m) + k_r - l_r}{3(G_m + k_r)} \tag{4.13}$$

$$\beta_r = \frac{1}{5}\left\{\begin{array}{l}\dfrac{4G_m + 2k_r + l_r}{3(G_m + k_r)} + \dfrac{4G_m}{G_m + p_r} \\ + \dfrac{2[G_m(3K_m + G_m) + G_m(3K_m + 7G_m)]}{G_m(3K_m + G_m) + m_r(3K_m + 7G_m)}\end{array}\right\} \tag{4.14}$$

$$\delta_r = \frac{1}{3}\left[n_r + 2l_r + \frac{(2k_r + l_r)(3K_m + 2G_m - l_r)}{G_m + k_r}\right] \tag{4.15}$$

$$\eta_r = \frac{1}{5}\left[\begin{array}{l}\frac{2}{3}(n_r - l_r) + \frac{8G_m p_r}{G_m + p_p} + \frac{2(k_r - l_r)(2G_m + l_r)}{3(G_m + k_r)} \\ + \frac{8m_r G_m(3K_m + 4G_m)}{3K_m(m_r + G_m) + G_m(7m_r + G_m)}\end{array}\right] \tag{4.16}$$

K_m and G_m are the bulk and shear moduli of the matrix respectively. The effective Young's modulus E and Poisson's ratio v are given by:

$$E = \frac{9KG}{3K + G} \tag{4.17}$$

$$\nu = \frac{3K - 2G}{6K + 2G} \tag{4.18}$$

A Matlab script file was compiled to calculate the Young's modulus and Poisson's ratio of a randomly oriented NRP for increasing nanotube volume fraction. (See Appendix C.2).

Figure 4-4 shows the effective Young's modulus versus the volume fraction of randomly oriented, straight nanotubes in the same polystyrene matrix studied in 4.2.1. Substantial increases in Young's modulus are demonstrated with the addition of a low volume fraction of nanotubes. The Young's modulus of the polystyrene matrix can be doubled with the addition of only 0.025 vol% single-walled nanotubes. Figure 4-5 shows the Poisson's ratio versus the volume fraction of randomly oriented, straight nanotubes in the same polystyrene matrix. The Poisson's ratio decreases with increasing nanotube volume fraction until a nanotube volume fraction of 0.085 vol%, then the Poisson's ratio increases with increasing nanotube volume fraction.

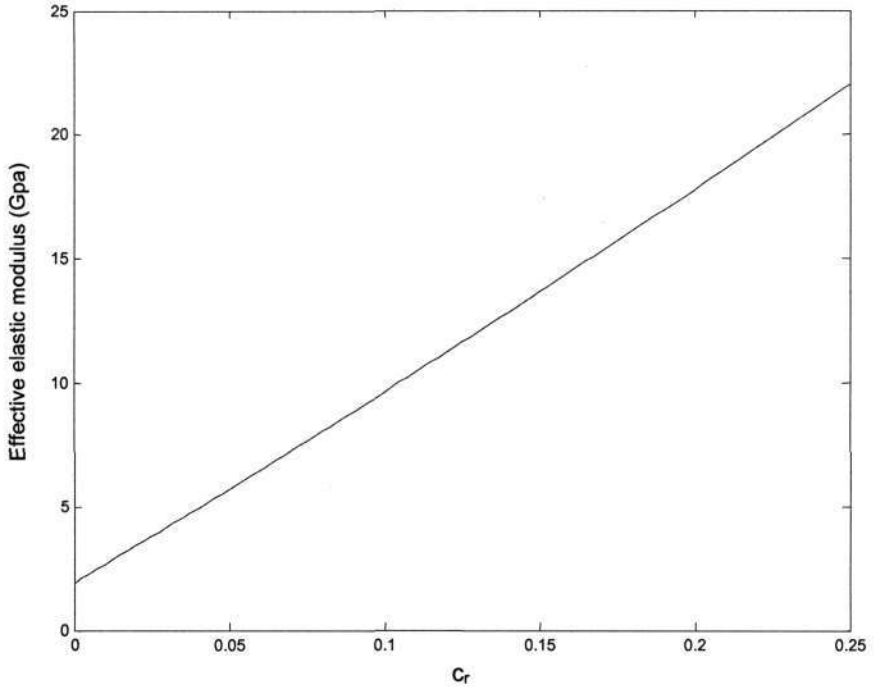

Figure 4-4 Effective elastic modulus of a composite reinforced with randomly oriented nanotubes

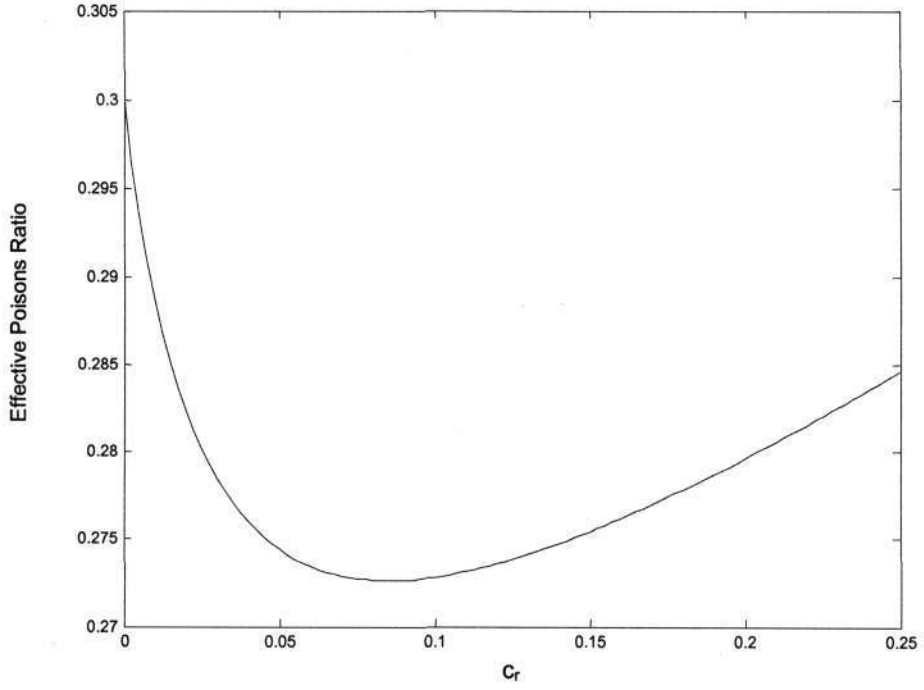

Figure 4-5 Poisson's ratio of a composite reinforced with randomly oriented, straight nanotubes

4.4 Agglomeration of Nanotubes

It has been observed in carbon nanotube-reinforced composites that a large amount of the nanotubes are concentrated in agglomerates. The van der Waals attractive forces between nanotubes cause them to agglomerate into bundles. SWNT tend to have a higher degree of agglomeration compared to MWNTs due to their lower bending stiffness and higher aspect ratios. In this section, a two parameter micromechanics model of agglomeration is used to determine the effect of nanotube agglomeration on the elastic properties of randomly oriented NRP composites. The regions with concentrated nanotubes are assumed to be spherical in shape and are considered as inclusions with different elastic properties from the surrounding material. The total volume V_r of the nanotubes in the representative volume element V can be divided into the following two parts:

$$V_r = V_r^{inclusion} + V_r^m \tag{4.19}$$

where $V_r^{inclusion}$ and V_r^m denote the volumes of nanotubes dispersed in the inclusions and in the matrix respectively. The average volume fraction c_r of nanotubes in the composite is:

$$c_r = \frac{V_r}{V} \tag{4.20}$$

The two parameters used to describe the agglomeration are introduced.

$$\xi = \frac{V_{inclusion}}{V} \tag{4.21}$$

$$\zeta = \frac{V_r^{inclusion}}{V_r} \tag{4.22}$$

ξ denotes the volume fraction of inclusions, $V_{inclusion}$ with respect to total volume of the composite V and ζ denotes the volume fraction of nanotubes in the inclusions with respect to the total volume of nanotubes. When ξ=1, the nanotubes are uniformly dispersed in the matrix, and with the decrease in ξ, the agglomeration degree increases. When ζ=1, all the nanotubes are concentrated in the inclusions with the concentration of nanotubes in the

inclusions decreasing with decreasing ζ. When $\xi=\zeta_{,,}$ the nanotubes are uniformly distributed within the matrix and ζ must be greater than ξ for agglomeration to be present.

The volume fractions of nanotubes in the inclusions and in the matrix are expressed respectively as:

$$\frac{V_r^{inclusion}}{V_{inclusion}} = \frac{c_r \zeta}{\xi} \tag{4.23}$$

$$\frac{V_r^m}{V - V_{inclusion}} = \frac{c_r(1-\zeta)}{1-\xi} \tag{4.24}$$

It is noted that the volume fractions of nanotubes in the inclusions and in the matrix must be less than 1. The effective elastic moduli of the composite are calculated using different micromechanics methods. Two methods are used to determine the elastic properties of the inclusions and the matrix. For the first method, the Voigt model, the anisotropy of the nanotubes is neglected and they are considered to be isotropic. The Voigt model provides the effective modulus of inclusions E_{in} and their surrounding E_{out} as (Jones 1999):

$$\begin{aligned} E_{out} = {} & \frac{3}{8}\left\{\frac{c_r(1-\zeta)}{1-\xi}E_{CNT} + \left[1 - \frac{c_r(1-\zeta)}{1-\xi}\right]E_m\right\} \\ & + \frac{5}{8}\left\{\frac{(1-\xi)E_{CNT}E_m}{\left[(1-\xi) - c_r(1-\zeta)\right]E_{CNT} + c_r(1-\zeta)E_m}\right\} \end{aligned} \tag{4.25}$$

$$E_{in} = \frac{3}{8\xi}\left[c_r \xi E_{CNT} + (\xi - c_r\zeta)E_m\right] + \frac{5}{8}\left[\frac{\xi E_m E_{CNT}}{(\xi - c_r\zeta)E_{CNT} + c_r\zeta E_m}\right] \tag{4.26}$$

The effective Young's modulus E of the composite may thus be calculated.

$$E = E_{out}\frac{E_{out} + (E_{in} - E_{out})\xi^{2/3}}{E_{out} + (E_{in} - E_{out})\xi^{2/3}(1-\xi^{1/3})} \tag{4.27}$$

In the second method, the nanotubes are considered to be transversely isotropic. The elastic moduli of the inclusions and the matrix are estimated using the Mori-Tanaka method, as

described in section 4.3. The effective bulk moduli K_{in} and K_{out} and the effective shear moduli G_{in} and G_{out} of the inclusions and the matrix respectively are given by:

$$K_{in} = K_m + \frac{(\delta_r - 3K_m\alpha_r)c_r\zeta}{3(\xi - c_r\zeta + c_r\zeta\alpha_r)} \tag{4.28}$$

$$K_{out} = K_m + \frac{c_r(\delta_r - 3K_m\alpha_r)(1-\zeta)}{3[1-\xi - c_r(1-\zeta) + c_r(1-\zeta)\alpha_r]} \tag{4.29}$$

$$G_{in} = G_m + \frac{c_r\zeta(\eta_r - 2G_m\beta_r)}{2(\xi - c_r\zeta + c_r\zeta\beta_r)} \tag{4.30}$$

$$G_{out} = G_m + \frac{c_r(1-\zeta)(\eta_r - 2G_m\beta_r)}{2[1-\xi - c_r(1-\zeta) + c_r(1-\zeta)\beta_r]} \tag{4.31}$$

The effective bulk modulus K and the effective shear modulus G of the composite are derived using an Eshelby's inclusion model.

$$K = K_{out}\left[1 + \frac{\xi\left(\frac{K_{in}}{K_{out}} - 1\right)}{1 + \alpha(1-\xi)\left(\frac{K_{in}}{K_{out}} - 1\right)}\right] \tag{4.32}$$

$$G = G_{out}\left[1 + \frac{\xi\left(\frac{G_{in}}{G_{out}} - 1\right)}{1 + \beta(1-\xi)\left(\frac{G_{in}}{G_{out}} - 1\right)}\right] \tag{4.33}$$

with

$$\alpha = \frac{1+\nu_{out}}{3(1-\nu_{out})} \quad , \quad \beta = \frac{2(4-5\nu_{out})}{15(1-\nu_{out})} \tag{4.34}$$

where ν_{out} is the Poisson's ratio of the hybrid matrix:

$$\nu_{out} = \frac{3K_{out} - 2G_{out}}{2(3K_{out} + G_{out})} \tag{4.35}$$

Thus the effective Young's modulus E and Poisson's ratio ν are described by

$$E = \frac{9KG}{3K + G} \tag{4.36}$$

$$\nu = \frac{3K - 2G}{6K + 2G} \tag{4.37}$$

Matlab script files were compiled to calculate the influence of agglomeration on the elastic properties on NRPs. Firstly, the nanotubes were considered to be isotropic and then they were considered to be transversely isotropic. The representative values for Young's modulus and Poisson's ratio of the isotropic nanotubes and the polystyrene matrix material were taken as E_{CNT} = 450 GPa, E_m = 1.9 GPa and $\nu_r = \nu_m = 0.3$ respectively. The Hill's elastic moduli of the transversely isotropic nanotubes were taken as follows: n_r=450 GPa, k_r=30 GPa, m_r=p_r=1 GPa, and l_r=10 GPa. (See Appendix C.3).

The Young's moduli of agglomerated composites are shown as a fraction of evenly distributed composites in figures 4-6 and 4-7. In figure 4-6, the nanotubes are considered to be isotropic and in figure 4-7, the nanotubes are considered to be transversely isotropic.

To illustrate the effect of agglomeration more clearly, two more specific cases of agglomeration are presented. In the first case, all the nanotubes are concentrated in the inclusions, i.e., ζ=1. The agglomeration models above are thus reduced to having only one agglomeration parameter, ξ. The relationships between the volume fraction of inclusions ξ and the effective Young's modulus E of composites with various average volume fractions of nanotubes c_r are shown in figure 4-8(a). In the second model, the nanotubes are considered to be transversely isotropic. The representative values of elastic constants of nanotubes that were used in section 4.2.1 are used to determine the effective elastic properties of a composite with agglomeration. The effective Young's moduli of composites with various average volume fractions of nanotubes are plotted against volume fraction of inclusions in figure 4-9(b).

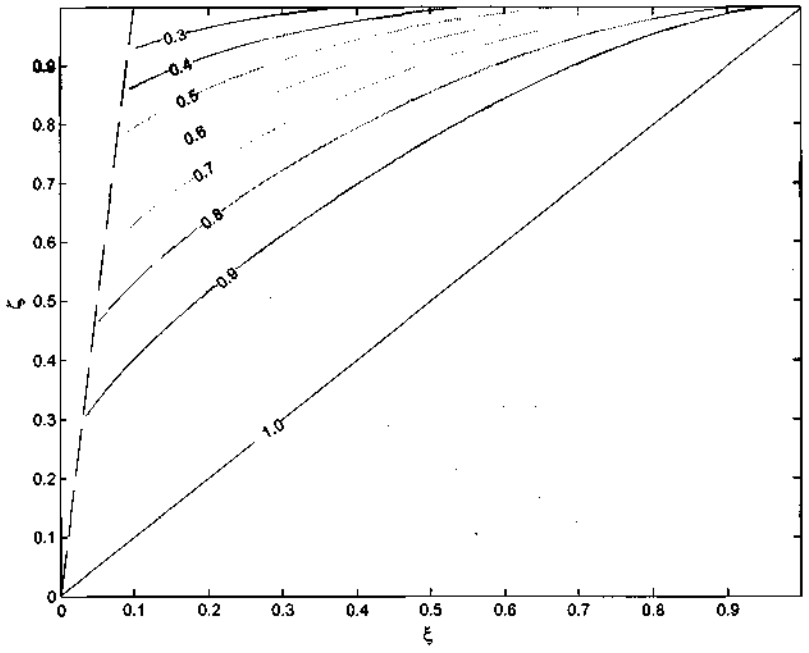

Figure 4-6 Contour plot showing the effect of agglomeration on Young's modulus with respect to a uniformly distributed composite ($E_{agglomerated}/E_{distributed}$). The nanotubes are considered to be isotropic and the nanotube volume fraction is 0.1. ($\zeta > \xi$, and $\xi > c_r\,\zeta$)

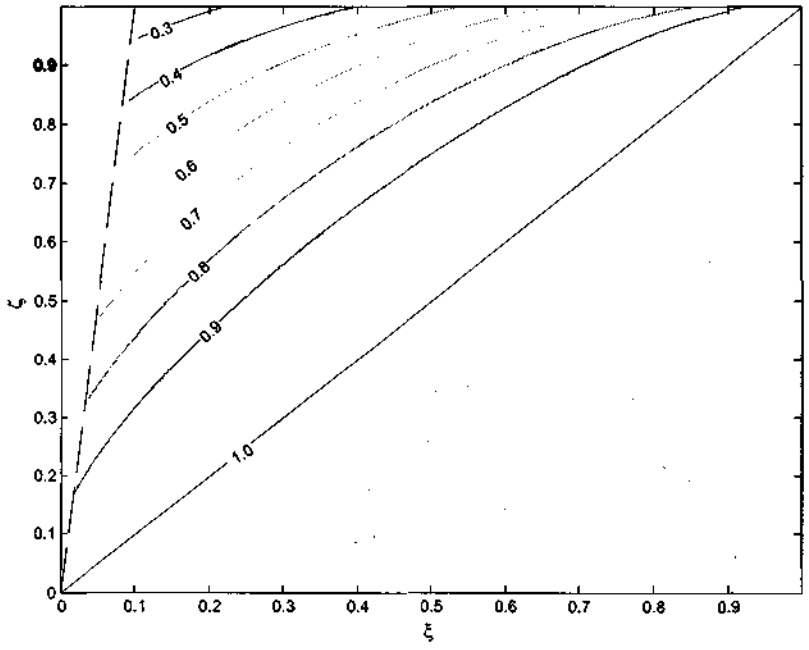

Figure 4-7 Contour plot showing the effect of agglomeration on Young's modulus with respect to a uniformly distributed composite ($E_{agglomerated}/E_{distributed}$). The nanotubes are considered to be transversely isotropic and the nanotube volume fraction is 0.1. ($\zeta > \xi$, and $\xi > c_r\,\zeta$)

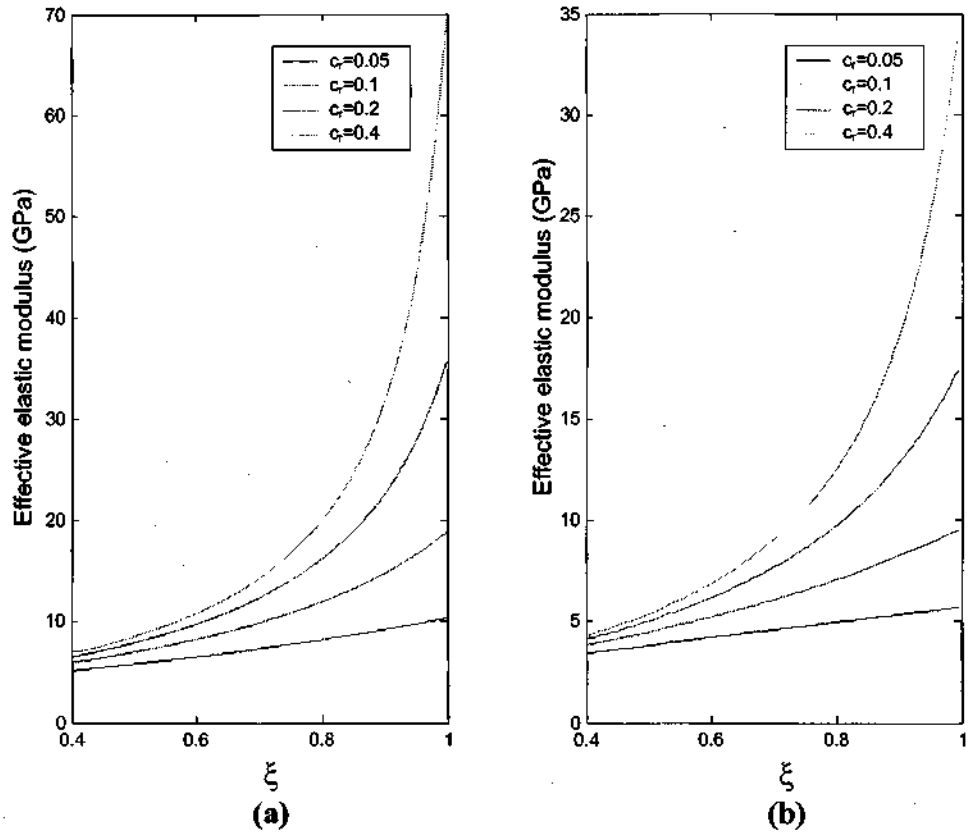

Figure 4-8 Effect of nanotube agglomeration on the effective elastic modulus with ζ=1, in which the nanotubes are considered to be: (a) isotropic, and (b) transversely isotropic

Analysis of the graphs reveals that the value of elastic modulus for agglomerated composites has a maximum value when the nanotubes are completely dispersed within the matrix, i.e. ξ=1. The value of elastic modulus then decreases rapidly with increasing agglomeration parameter ξ. Values of ξ lower than 0.6 yield very low increases in effective elastic modulus with addition of nanotubes.

In the second case, ξ=0.5 and the stiffening effect of the nanotubes is investigated with varying ζ. The effective elastic moduli for various average volume fraction of nanotubes c_r are plotted against volume ration of nanotubes concentrated in the inclusions. Figure 4-7(a) shows the reduction of stiffening effect of the nanotubes with an increase in the volume ratio of nanotubes situated in the inclusions. In figure 4-7(a) the nanotubes are considered to be isotropic and show a similar curve changing tendency to figure 4-7(b) where the nanotubes are considered to be transversely isotropic. However, when the nanotubes are considered to

be transversely isotropic, the values of elastic modulus are lower than those of composites where the nanotubes are considered to be isotropic.

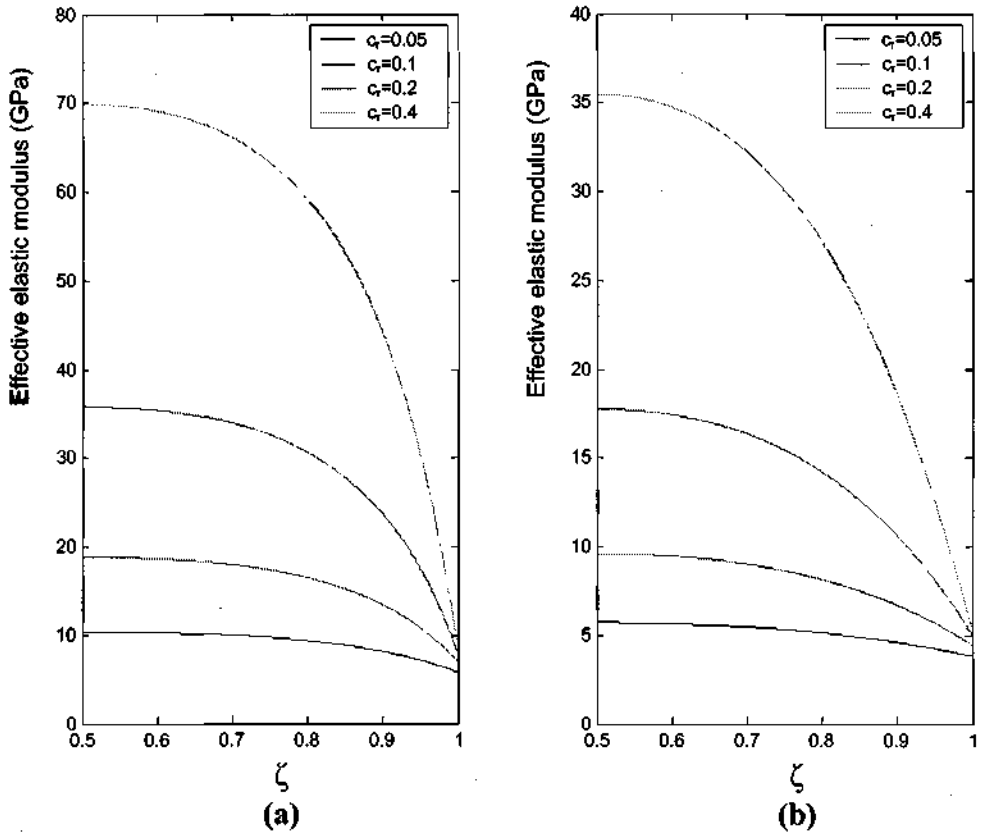

Figure 4-9 The effective modulus of a nanotube-reinforced composite with agglomeration effect with ξ=0.5, in which the nanotubes are assumed to be (a) isotropic, and (b) transversely isotropic

4.5 Summary

The effects of nanotube orientation and agglomeration on the elastic properties of single-walled nanotube-reinforced polymers were examined theoretically using analytical micromechanics methods. Polystyrene reinforced with well dispersed, aligned single-walled nanotubes showed a rapid increase of Young's modulus in the fibre direction with increasing volume fraction of nanotubes. However, the Young's modulus normal to the fibre direction only increased marginally with increasing nanotube volume fraction due to the transversely isotropic properties of nanotubes. Remarkable improvements in the elastic properties of

Polystyrene were demonstrated for the addition of straight, randomly oriented nanotubes. These results suggest the possibility of tailoring the properties of NRP composites by controlling the orientation of the nanotubes. However, these results require that the nanotubes are straight, long and well dispersed.

Experimental studies on nanotube-reinforced polymers have shown limited ability to control the distribution of nanotubes within the matrix. The influence of distribution of the nanotubes within the matrix was analysed using an Eshelby's inclusion model, where the composite is assumed to have spherical inclusions with concentrated nanotubes. Results showed a significant effect on the elastic properties when nanotubes are concentrated in agglomerations.

Observations of manufactured NRP have shown waviness of the nanotubes within the polymer. This observed waviness of the nanotubes would also affect the elastic properties of the NRPs indicating the need to develop models to analyse the effects of nanotube waviness on the properties of NRPs.

Chapter 5

Structural Application of Nanotube-Reinforced Polymers

The predicted high-stiffness and high-strength of nanotube-reinforced composite materials has created a great deal of interest in their use in structural applications. Reducing structural weight, whilst maintaining critical material properties such as strength and stiffness, is one of the key design criteria for many applications. The aim of this chapter is to analyze carbon nanotube-reinforced composite structures to determine their mechanical performance enabling a comparison with traditional materials.

Using the micromechanical results obtained in chapter 4, the performance of composite beams reinforced with both aligned and randomly oriented nanotubes are analyzed. For composites reinforced with aligned nanotubes, classical laminate theory is used to analyse the structural performance of a laminate beam. The results are then compared to traditional carbon fibre-reinforced polymer composites. Randomly oriented NRPs have isotropic material properties so the best measure of their structural performance is their specific modulus which can be compared to the specific moduli of other materials used in weight-critical applications.

The structure chosen to analyse the performance of aligned NRPs is a symmetrical laminate beam element in bending. Analysis of beam elements is important for both the mechanical characterization by bending tests, and the use of beams as basic elements of structures. The beam is loaded simply about three points with the measure of structural performance being taken as the deflection of the beam at its mid-point.

5.1 Classical laminate theory

For the case of a straight, aligned nanotube-reinforced composite, the composite structure is considered to be a symmetric laminate. General expressions, needed to describe the deflection and the stresses within a symmetric laminate are taken from Berthelot (1998).

In the case of pure bending of a symmetric laminate, the constituitive equation reduces to:

$$\begin{bmatrix} M_x \\ M_y \\ M_{xy} \end{bmatrix} = \begin{bmatrix} D_{11} & D_{12} & D_{16} \\ D_{12} & D_{22} & D_{26} \\ D_{11} & D_{16} & D_{66} \end{bmatrix} \begin{bmatrix} \kappa_x \\ \kappa_y \\ \kappa_{xy} \end{bmatrix} \tag{5.1}$$

The differential equation used to describe the deflection curve of a beam in the case of bending only along the x-axis is:

$$\frac{d^2 w_0}{dx^2} = -D_{11}^* M_x \tag{5.2}$$

where:

$$D_{11}^* = \frac{1}{\Delta}\left(D_{22}D_{66} - D_{26}^2\right) \tag{5.3}$$

and Δ is the determinant of the matrix $[D_{ij}]$ in equation 5.1:

$$\Delta = D_{11}D_{22}D_{66} + 2D_{12}D_{16}D_{26} - D_{11}D_{26}^2 - D_{22}D_{16}^2 - D_{66}D_{12}^2 \tag{5.4}$$

On introducing the terms of effective bending modulus E_x, quadratic moment I of the cross-section of the beam with respect to the (x,y) plane, and the bending moment M:

$$\begin{aligned} E_x &= \frac{12}{h^3 D_{11}^*} \\ I &= I_{xy} = \frac{bh^3}{12} \\ M &= bM_x \end{aligned} \tag{5.5}$$

It is usual to write equation 5.2 in the form:

$$\frac{d^2 w_0}{dx^2} = -\frac{M}{E_x I} \tag{5.6}$$

The stresses in the *k*th layer of the laminate may be written as:

$$\begin{aligned}\sigma_{xx}^{k} &= z a_{xx}^{k} \frac{M}{I} \\ \sigma_{yy}^{k} &= z a_{yy}^{k} \frac{M}{I} \\ \sigma_{xy}^{k} &= z a_{xy}^{k} \frac{M}{I}\end{aligned} \tag{5.7}$$

with:

$$\begin{aligned}a_{xx}^{k} &= \left(Q_{11}^{k} D_{11}^{*} + Q_{12}^{k} D_{12}^{*} + Q_{16}^{k} D_{16}^{*}\right)\frac{h^3}{12} \\ a_{yy}^{k} &= \left(Q_{12}^{k} D_{11}^{*} + Q_{22}^{k} D_{12}^{*} + Q_{26}^{k} D_{16}^{*}\right)\frac{h^3}{12} \\ a_{xx}^{k} &= \left(Q_{16}^{k} D_{11}^{*} + Q_{26}^{k} D_{12}^{*} + Q_{66}^{k} D_{16}^{*}\right)\frac{h^3}{12}\end{aligned} \tag{5.8}$$

These stresses are correct only at a significant distance (>*h*) from the edge of the beam. The preceding results are therefore applicable only to the case of beams that have a high ratio b/h. The shear stress in the layers is deduced as:

$$\sigma_{xz}^{k} = -a_{xx}^{k}\tau_0\left[4\left(\frac{z}{h}\right)^2 + d_k\right] \tag{5.9}$$

and d_k are new constants to be determined by assuring the continuity of σ_{xz} within the thickness of the beam and τ_0 is the maximum shear stress at z=0, that is:

$$\tau_0 = \frac{3Q}{2bh} \tag{5.10}$$

where:

$$Q = \frac{dM}{dx} \tag{5.11}$$

5.2 Three-point bending

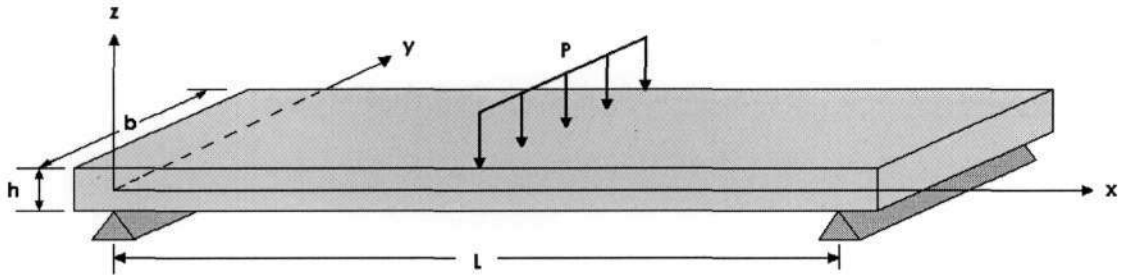

Figure 5-1 Three-point bending

For the application, a beam bending about three points was chosen. Due to the symmetry of the problem, only half of the beam is considered. The bending moment is expressed by the relation:

$$M = -\frac{Px}{2} \quad , \quad 0 \le x \le \frac{L}{2} \tag{5.12}$$

where P is the total load applied at the centre of the beam. The differential equation of the deflection curve of a beam is (6.2):

$$\frac{d^2 w_0}{dx^2} = \frac{M}{E_x I} = \frac{Px}{2E_x I} \quad , \qquad 0 \le x \le \frac{L}{2} \tag{5.13}$$

In the case of simple supports the boundry conditions for $x=0$ are:

$$M = w_0 = 0 \tag{5.14}$$

The symmetry of the beam requires that, for $x=L/2$:

$$\frac{dw_0}{dx} = 0 \tag{5.15}$$

Integration of equation (5.13) coupled with the boundary conditions of (5.14) and (5.15) leads to:

$$w_0 = -\frac{PL^2}{48E_x I} x\left[3-\left(\frac{2x}{L}\right)^2\right] \tag{5.16}$$

The deflection at the centre of the beam ($x=L/2$) is:

$$w_c = \frac{PL^3}{48E_x I} = \frac{PL^3}{48b} D_{11}^* \tag{5.17}$$

In the case of an isotropic material, the effective bending modulus of the beam E_m is the Young's modulus of the material. For a symmetrical laminate beam, the bending stresses in the kth layer are given by (5.7):

$$\sigma_{xx}^k = -6a_{xx}^k \frac{P}{bh^3} xz \tag{5.18}$$

These stresses are maximum for $x=L/2$, that is:

$$\sigma_{xx}^k = -3a_{xx}^k \frac{PL}{bh^3} z \sigma_{xx}^k = -2a_{xx}^k \sigma_0 \frac{z}{h} \tag{5.19}$$

where σ_0 is the maximum tensile stress which is reached on the lower face ($z=-h/2$):

$$\sigma_0 = \frac{3PL}{2bh^2} \tag{5.20}$$

The shear stresses in the kth layer may be written as (5.9):

$$\sigma_{xz}^k = -a_{xx}^k \tau_0 \left[4\left(\frac{z}{h}\right)^2 + d_k\right] \tag{5.21}$$

where (5.10)

$$\tau_0 = -\frac{3P}{4bh} \tag{5.22}$$

5.3 Straight, aligned nanotube-reinforced laminate

As an example of straight, aligned nanotube reinforced laminates, three symmetric laminates made of eight layers of the same thickness and oriented at 0°, ±45°, and 90° were considered. The stacking sequences of the three laminates considered were: [0°/45°/-45°/90°]s, [90°/45°/-45°/0°]s, and [45°/0°/-45°/90°]s. The engineering constants for the unidirectional nanotube reinforced composites were calculated in section 4.2. These values were used in Matlab script files (Appendix C.4) to determine the deflection at the centre of the beam w_c (5.17) for increasing volume fraction of nanotubes c_r. The decrease in deflection versus the increase in volume fraction of nanotubes for the three stacking sequences is shown in figure 5-2. It is evident that the deflection of the beam decreases dramatically at low volume fractions of nanotubes. This illustrates the substantial increase in stiffness of a polymer with the addition of a small volume of nanotubes.

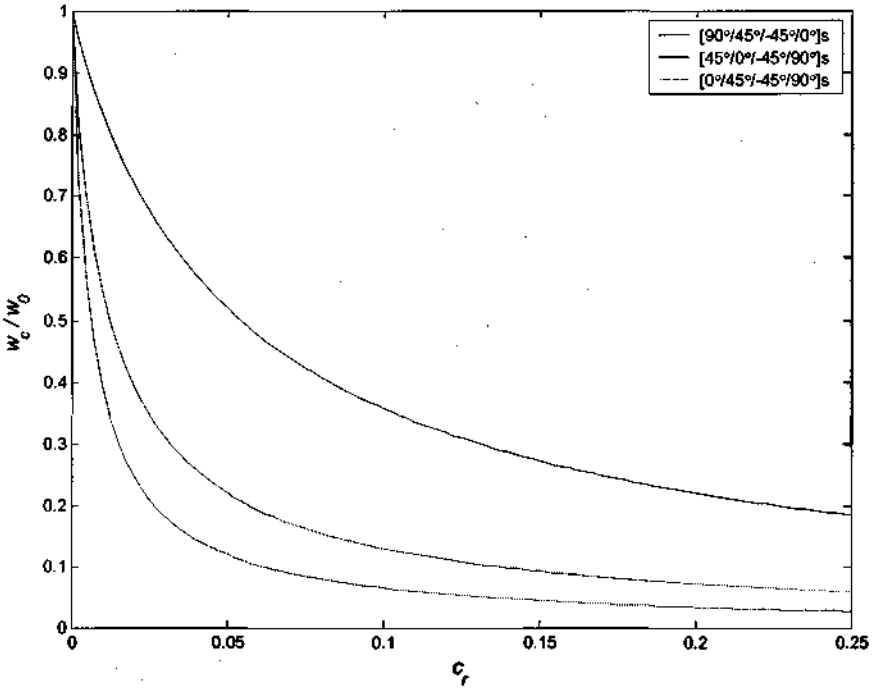

Figure 5-2 Influence of volume fraction of nanotubes c_r on the deflection of a nanotube-reinforced composite beam w_c with respect to a non-reinforced beam w_0.

The variation of the bending stress σ_{xx} (5.19) and the variation of the shear stress σ_{xz} (5.21) across the thickness of a nanotube-reinforced composite beam, with a nanotube volume ratio of 0.1, are plotted in figure 5-3 and figure 5-4 respectively. Bending and shear stresses for an

isotropic material are plotted for comparison. From the plots it is noticed that most of the load is carried in the nanotube direction. The variation of stress across the laminate is important when considering failure methods.

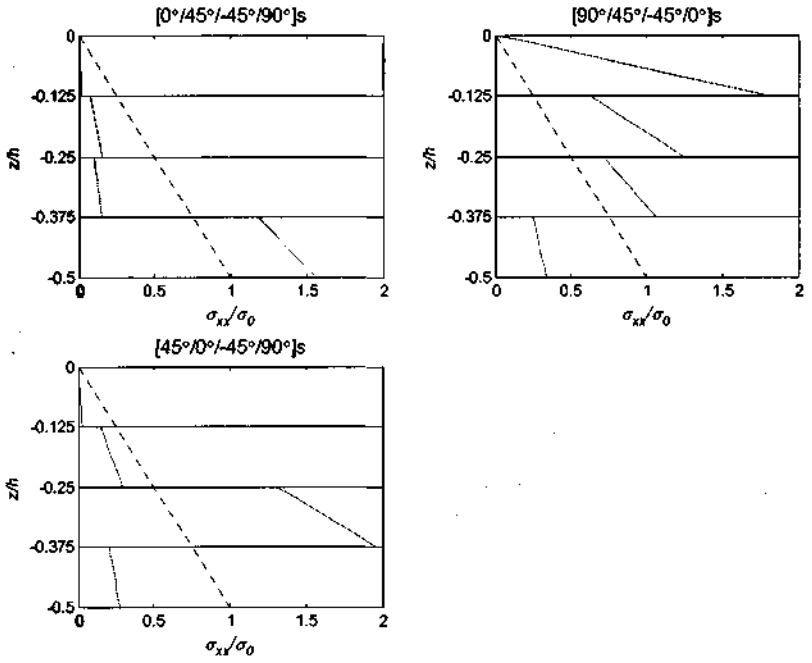

Figure 5-3 Influence of stacking sequence on variation of shear stress σ_{xx} across the laminate thickness

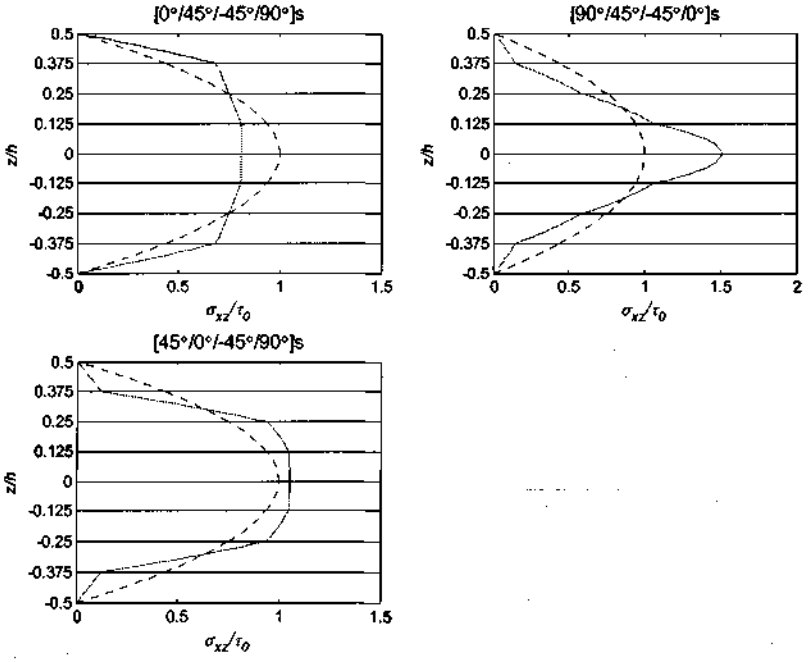

Figure 5-4 Variation of shear stress σ_{xz} across the thickness of the laminate

To determine the performance of a nanotube-reinforced composite a comparison with a traditional, well established composite material is needed. The composite material chosen to compare against is a high modulus, high strength unidirectional carbon fibre-reinforced epoxy with the following characteristics:

E_{11}= 159 GPa, E_{22}= 14 GPa, G_{12}= 4.8 GPa, ν_{12}= 0.32, V_f= 0.6, ρ= 1570 kg/m^3.

Symmetric carbon fibre-reinforced composite beams with a length-to-height ratio, L/h = 20 and fibre orientations as in the previous examples are used as a comparisons against nanotube-reinforced composite beams with the same orientations and length but varying thickness h and nanotube volume fraction c_r. The deflections of the nanotube-reinforced composite beams for varying nanotube volume fraction and thickness are calculated and the results of the deflection of the nanotube-reinforced composite beams w_c are plotted as a fraction of the deflection of the carbon fibre-reinforced beam w_0 in figure 5-5.

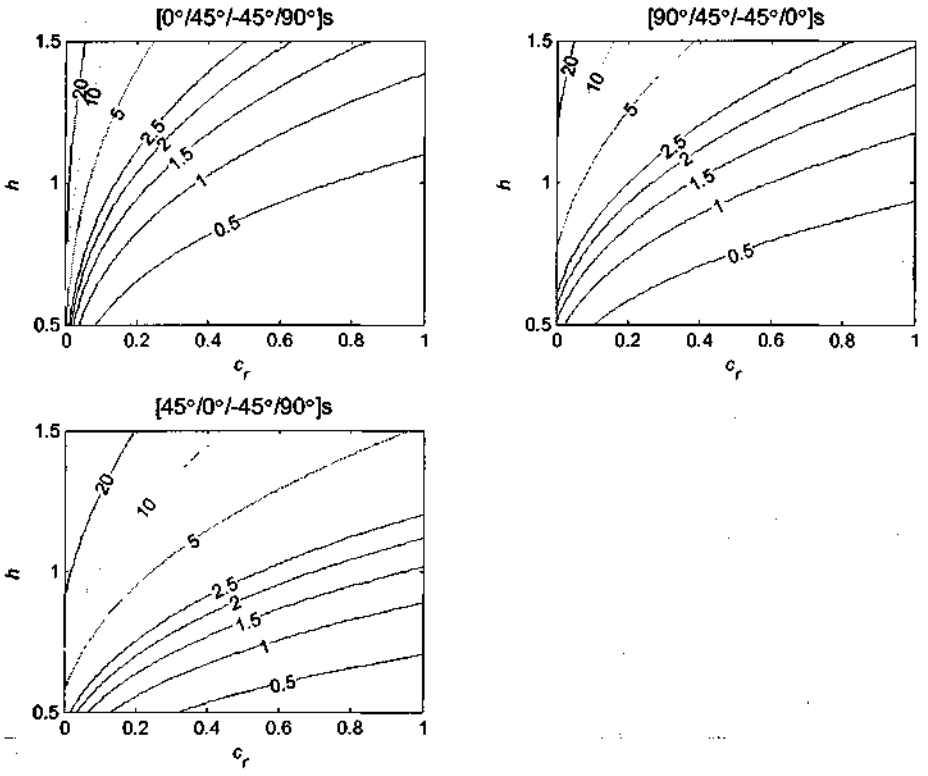

Figure 5-5 Contour graphs showing the effect of nanotube volume fraction c_r and thickness h on the deflections of NRP laminate beams. The deflection is expressed as a fraction of the deflection of a comparison carbon fibre-reinforced beam (w_c / w_0).

The main driving force for nanotube reinforced composites is the predicted high strength-to-weight and stiffness-to-weight ratios. Thus a comparison of the masses of the nanotube-reinforced beam and the carbon fibre-reinforced beam is needed. The mass of the nanotube–reinforced composite beam as a fraction of the mass of the comparison carbon fibre-reinforced composite beam (m/m_c) can be expressed by:

$$m/m_c = \frac{\left(\rho_{NT} c_r + \rho_{polystyrene}(1 - c_r)\right) h_{NT}}{\rho_{carbon-fibre-composite} h_{carbon-fibre-composite}} \tag{5.23}$$

where ρ_{NT} is the density of a SWNT with a diameter of 2 nm.

The masses of the nanotube–reinforced composite beams m are plotted as a function of the mass of the carbon fibre-reinforced beam m_0 in figure 5-6.

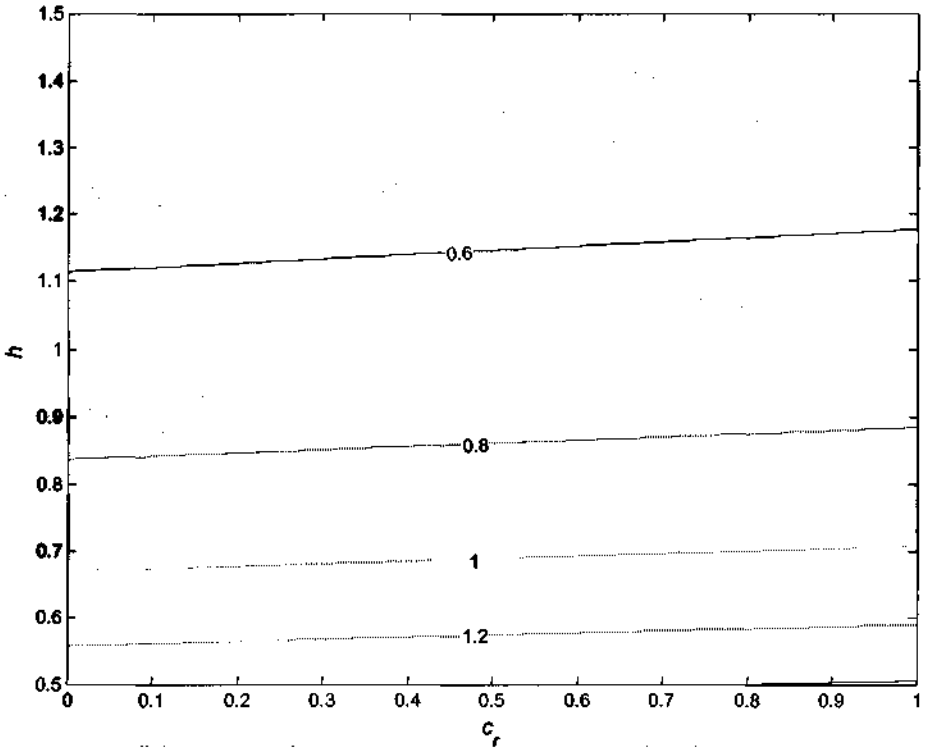

Figure 5-6 Contour graph of mass of the nanotube–reinforced composite beam as a fraction of mass of the comparison composite beam m/m_0 as a function of nanotube volume fraction c_r and thickness h of the beam

When the contours graphs in figure 5-5 and 5-.6 are combined, it is possible to compare the deflection of and the mass of nanotube-reinforced composite beams with a carbon fibre-reinforced composite beam. It is evident that for a nanotube-reinforced polystyrene beam with a low volume fraction of reinforcement is able have the same mass and deflection under pure bending as a carbon fibre-reinforced beam. Some examples of nanotube-reinforced polystyrene beams which experience the same deflection as the carbon fibre-epoxy comparison beam are shown in table 5-.1

	[0°/45°/-45°/90°]s		[90°/45°/-45°/0°]s		[45°/0°/-45°/90°]s	
h	c_r	m/m_c	c_r	m/m_c	c_r	m/m_c
0.5	0.039	1.341	0.024	1.339	0.132	1.348
0.75	0.151	0.899	0.220	0.903	0.592	0.922
1	0.373	0.683	0.603	0.692	-	-
1.25	0.737	0.558	-	-	-	-

Table 5-1 Nanotube volume fraction c_r and mass ratio m/m_c of nanotube-reinforced composite beams which have the same deflection under three-point bending as the comparison carbon fibre-reinforced composite beam.

5.4 Random oriented, straight nanotubes

For the case of a composite reinforced with randomly oriented, straight nanotubes, the material is considered to be isotropic at the macroscopic level. Thus it is best to compare the specific modulus (modulus/density) of random oriented NRP with that of bulk materials to determine their performance in weight-critical structural applications. The Young's moduli of randomly oriented NRPs calculated in chapter 4 are divided by the density of the respective NRP to calculate the specific modulus of the NRP material.

The specific modulus of polystyrene reinforced with an increasing nanotube volume fraction of well dispersed, randomly oriented randomly oriented nanotubes is shown in figure 5-8. These values can be compared to the specific moduli of other materials commonly used in weight-critical applications given in table 5-2. It is noted that a high volume fraction of nanotubes is needed to provide structural performance equal to existing bulk materials, thus demonstrating the need to align nanotubes within their polymer composites to obtain high performance materials.

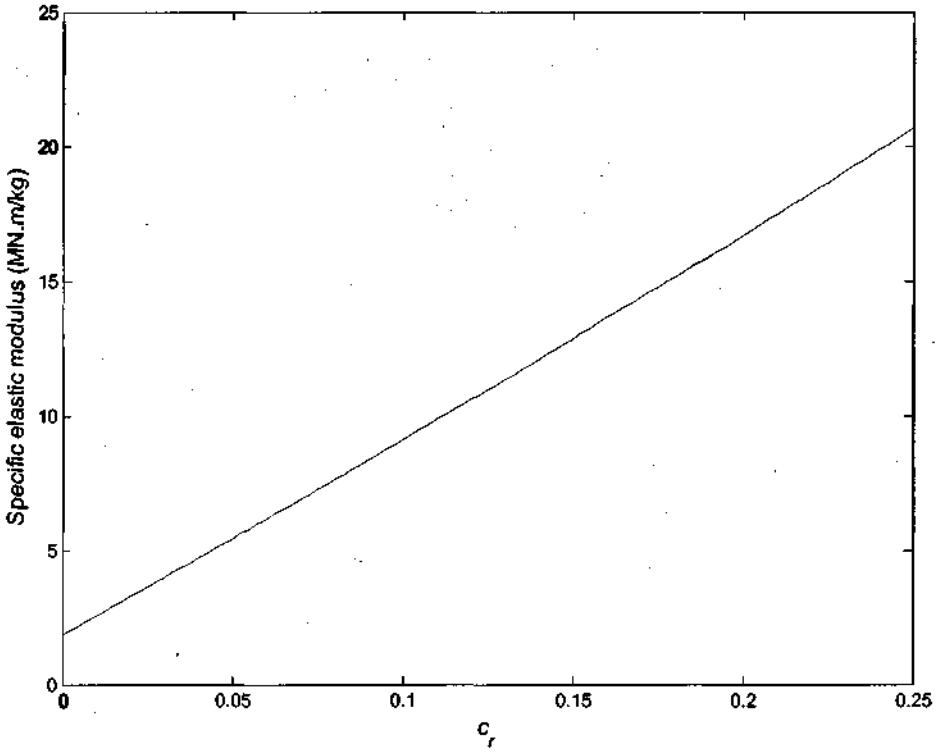

Figure 5-7 Specific modulus versus nanotube volume fraction of randomly oriented nanotube-reinforced polystyrene composite

Material	Specific Modulus (MN.m/kg)	Density (kg/m^3)
Steel	26.9	7800
Aluminum alloys	25.9	2700
Titanium	26.7	4500

Table 5-2 Specific Modulus of common bulk materials

The effect of nanotube agglomeration studied in section 4.4 reduces the Young's modulus of a randomly oriented NRP by a significant amount and thus will have the same effect on the specific modulus of the NRP.

5.5 Summary

The addition of well dispersed straight, aligned SWNTs to polymer matrices greatly increases the elastic modulus of the composite in the nanotube axis direction. Elastic moduli of carbon fibre-reinforced composite materials can be matched with the addition of a low

volume fraction of nanotubes and unmatched elastic moduli are achievable with the addition of high volume fractions of nanotubes.

However, the elastic modulus of aligned NRPs perpendicular to the nanotube axis direction is only moderately increased with the addition of nanotubes. This is due to the transverse isotropy of the nanotubes, traditional fibres used to reinforce polymer composites are considered to be isotropic. The resulting elastic modulus of aligned nanotube-reinforced polystyrene perpendicular to the nanotube axis direction is an order of magnitude lower than that of carbon-fibre-reinforced epoxy. This is due to both the elastic modulus of epoxy being greater than polystyrene and the nanotubes offering less reinforcement in the direction perpendicular to the nanotube axis.

The higher degree of transverse isotropy of aligned NRPs compared to carbon fibre-reinforced polymers results in NRP laminates designed to take advantage of the higher degree of transverse isotropy outperforming carbon fibre-reinforced composites by a substantial amount. For a [0/45/-45/90]s laminate loaded in pure bending about the x-axis, most of the load is carried by the outer layers which have fibre orientations in the load direction. NRP laminates with this orientation thus outperformed carbon fibre-reinforced polymer composites substantially.

Due to the hollow tubular structure of SWNTs, their density is lower than the density of carbon fibres which have a solid cylindrical structure. A polymer reinforced with nanotubes will thus have a lower density than a polymer reinforced with carbon fibres. The low density of the nanotubes in relation to carbon-fibres and the lower density of polystyrene in relation to epoxy results in a nanotube-reinforced polystyrene having a substantially lower density than carbon fibre-reinforced epoxy.

The addition of well dispersed straight, randomly oriented SWNTs to polymer matrices greatly increases the elastic modulus of the polymer. However, unachievable high volume fractions are required to equal the specific moduli of traditional bulk materials used in weight critical structural applications. The use of random oriented NRPs in purely structural applications is thus not viable. However, the specific modulus of polymers already used in weight-critical applications may be increased by the addition of randomly oriented nanotubes. The increase in specific modulus of the resulting polymer will allow for a reduction in component size whilst maintaining its structural properties.

Chapter 6

Conclusions

The outstanding physical properties predicted for carbon nanotubes have lead to a great deal of research into the use of nanotubes as a reinforcing filler material in polymer-based composites. The potential benefits of carbon nanotube reinforced polymers are not only structural but also include an increase in the working temperature range, the thermal stability and the electrical conductivity of the composite. This multifunctionality suggests that the materials may be designed to meet both mechanical and secondary material property specifications. Initial experimental work on carbon nanotube-reinforced polymers (NRPs) has demonstrated that large increases in effective moduli and strength can be attained with the addition of small amounts of carbon nanotubes.

For the analysis and design of nanotube-reinforced polymer materials, accurate models of NRP behavior are needed. This is complicated by the range of length scales characteristic of these materials. The structure of carbon nanotubes is at an atomistic scale which has been modeled successfully using molecular dynamics simulations. Molecular dynamics simulations are however computationally expensive and limited to small systems and short time periods. Molecular dynamics is thus not able to simulate at a size scale needed for NRP composite applications. Thus, continuum methods need to be developed that are able to describe the mechanical behavior of NRPs. However, careful consideration needs to be taken when using continuum methods to model carbon nanotubes which are at an atomistic size scale.

In this dissertation, a structural mechanics approach to modelling the deformation of carbon nanotubes at the atomistic scale was presented. Fundamental to the concept is the notion that a carbon nanotube may be modelled as a geometrical frame-like structure with the bonds between neighbouring atoms acting as load-bearing members. The sectional property parameters of these beams were established through energy equivalence between structural mechanics strain energy and molecular mechanics force field energy. This modelling technique is able to analyse the mechanical response of carbon nanotubes at the atomic scale using existing theories of solid mechanics and methods of computational mechanics. The

method is not perplexed in the time scales, thus it is more economical in computation than refined atomistic simulation methods, such as molecular dynamics. The major advantages of the method are the simplicity of the concept and the improved computational efficiency allowing for the simulation of large systems.

Structural mechanics models of graphene sheets were first modelled to verify the reliability and efficiency of the structural mechanics approach to the modelling carbon molecules. The computational results of in-planar Young's modulus were comparable to the commonly accepted value of in-planar Young's modulus of graphene sheets. The successful prediction of the Young's moduli of graphene sheets established confidence in applying the structural mechanics approach to modelling of single-walled carbon nanotubes (SWNTs). Boundary conditions were placed on various diameter SWNTs of armchair and zigzag chirality to determine the axial Young's modulus and shear modulus of the nanotubes. Both Young's modulus and shear modulus of the nanotubes tended to increase with increasing nanotube diameter, approaching the modulus of graphene sheets at nanotube diameters greater than 1 nm. The nanotube chirality had little effect on the moduli. These computational results are comparable to those obtained from other modelling techniques. Building on the structural mechanics approach to modelling SWNTs, we expect to also be able to address the bending and buckling behaviour of SWNTs.

A method of extending the model to multi-walled nanotubes (MWNTs) by introducing a nonlinear truss rod model to represent van der Waals forces acting between the non-bonded atoms between MWNT layers was proposed. However, computational results of the nonlinear truss elements were not achievable with the finite element analysis software available. The use of nonlinear truss rod elements to represent the van der Waal's forces would also enable the simulation of the nanotube-polymer interface in nanotube-reinforced polymer composites. Thus a NRP composite may be simulated with a frame-like structure representing the nanotubes and nonlinear truss rod elements connecting the nanotube with the polymer which could be modelled as a continuum.

For the analysis and design of nanotube-reinforced polymer composite structures, detailed models of the elastic properties of the composite material at a macroscopic scale are needed. Atomistic modelling techniques are efficient at simulating material behaviour at an atomic scale but are too computationally intensive for simulating systems of the macroscopic size scale. Thus analytical micromechanical analysis methods that take into account the nanoscale

characteristics of the nanotubes need to be developed for describing the stiffening effect of nanotubes in a polymer matrix.

Analysis of experimental results reported for NRPs have shown moderate improvements in the mechanical properties of polymers by the addition of nanotubes as a filler material. While encouraging, these results indicate that the full reinforcing ability of the nanotubes is still not being achieved. The unsatisfactory improvements in mechanical properties have been attributed to a wide range of parameters that are expected to impact the effective response of the NRP composite. Examples of these parameters are: the orientation and dispersion of the nanotubes within the polymer, observed waviness on the nanotubes within the polymer, and poor load transfer between the nanotubes and the polymer. Accurate models of how these parameters influence the effective properties of the NRP will be necessary for both the optimization of the fabrication of NRPs and for tailoring of the effective properties of the NRP composites.

A micromechanics model was presented that takes into account the nanoscale characteristics of the nanotubes. The Mori-Tanaka method was used to determine the overall properties of an isotropic, elastic matrix material reinforced by a large number of dispersed SWNTs that were aligned, straight and of infinite length. The nanotubes were modelled as long fibres with transversely isotropic elastic properties, with the elastic properties of the nanotubes being taken from analytical results in literature. The calculated results for polystyrene reinforced with uniformly distributed, aligned, 2 nm diameter SWNTs showed a large magnitude of increase of Young's modulus in the fibre direction for low volume fractions of nanotubes. However, the Young's modulus in the transverse direction only increased slightly with increasing nanotube volume fraction due to the nanotubes being highly transversely isotropic.

The effects of nanotube orientation and agglomeration on the overall elastic properties of NRPs were then investigated using extensions of the model. The elastic modulus of polystyrene reinforced with randomly oriented, uniformly dispersed, straight SWNTs was calculated for increasing volume fraction of nanotubes. The orientation distribution of the nanotubes was characterised by a completely random probability density function. A substantial increase in Young's modulus of the resulting composite was demonstrated. It was however not in the same magnitude of increase as the Young's modulus of uniformly oriented NRP in the nanotube axis direction.

The effect of distribution of the nanotubes on the elastic properties of randomly oriented nanotubes was then investigated. An Eshelby's inclusion model, where the composite is considered to have spherical inclusions with concentrated nanotubes, was used to model the influence of agglomeration of nanotubes on the effective stiffness of a NRP composite. The degree of agglomeration was described using a two parameter model and the reduction of stiffening effect, when compared to a uniformly oriented NRP composite, was calculated. The results indicated a significant decrease in Young's modulus of agglomerated NRP composites when compared to uniformly oriented composites.

From the results, it is evident that for the full potential of nanotube as a reinforcing material to be achieved, the nanotubes need to be well dispersed, straight and uniformly oriented. The model presented may be improved by extended it to include other characteristics that may have reducing effect on the overall properties of NRPs, such as nanotube curvature and poor load transfer at the nanotube-polymer interface. The development of experimental methods that enable the isolation of individual parameters of NRPs would be desirable in the development and analysis of these modelling techniques.

A structural application was presented to determine the performance of polystyrene reinforced with well dispersed, straight, aligned SWNTs. The structural application chosen was a beam element in bending. Analysis of beam elements is important for both mechanical characterization by bending tests, and the use of beams as basic elements of structures. Symmetric laminate beams with different stacking sequences were analysed when loaded about three points. The measurement of performance was taken to be the deflection of the beam at its mid-point. Classical laminate theory was applied to a material with elastic properties calculated using the micromechanics model proposed for well dispersed, straight, uniformly oriented nanotubes. The deflections of the beams were shown to decrease dramatically at low volume fractions of nanotubes.

The performances of the nanotube-reinforced polystyrene beams were then compared against carbon fibre-reinforced epoxy composite beams with the same stacking sequence but varying thickness. The lower density of the NRP and the large magnitude of increase in longitudinal Young's modulus with increasing nanotube volume fraction allowed for the NRPs to outperform traditional carbon fibre-reinforced composite materials in a weight-critical application.

Polymers reinforced with randomly oriented, straight nanotubes have isotropic material properties at the macroscopic scale. Consequently, a measure of their performance in weight-critical applications is their specific modulus. The specific modulus of polystyrene reinforced with well dispersed, randomly oriented nanotubes was calculated. The results indicated that a high volume fraction of nanotubes is needed to provide structural performance equal to existing bulk materials, thus demonstrating the need to align nanotubes within their polymer composites to obtain high performance structural materials.

Appendix A

Summary of dispersion methods used for preparing nanotube-reinforced polymers reviewed in literature

Preparation Method	Nanotubes	Polymer
Ultrasonic dispersion (Ajayan et al. 2000)	SWNT	Epoxy (Epon 828)
Mixing in ultrasonic bath and spin coating (Stephan et al. 2000)	SWNT	PMMA
Ultrasonic dispersion (Haggenmueller et al. 2000)	SWNT	PMMA
Mixing followed by in situ polymerization (Jia et al. 1999)	SWNT, MTWNT	PMMA
Electrochemical method (Chen et al. 2000)	SWNT	Polypropylene
Mixing and ultrasonic treatment (Chang et al. 2000)	SWNT	Polypropylene
Tube sonication followed by mixing with polymer (Lourie et al. 1998a, Sandler et al. 1999)	SWNT, MWNT	Epoxy (Araldite LY556)
Ultrasonic dispersion before curing (Schadler et al. 1998)	MWNT	Epoxy (Epon 828)
Solution evaporation assisted by high-energy sonication (Qian et al. 2000)	MWNT	Polystyrene
Tube sonication, drying, and dispersion on a glass surface, spreading of polymer by blade (Lourie et al. 1998b, 1999)	MWNT	Epoxy (Araldite LY564)
Mixing with the polymer, casting, and controlled water evaporation after chemical treatment of the tubes (Shaffer et al. 1999)	MWNT	Poly (vinyl alcohol)
Casting of nanotube suspension, polymer, and chloroform after sonication (Jin et al. 1998, Bower et al. 1999)	MWNT	PHAE
Tube sonication in ethanol, drying, and dispersion on a glass surface, polymer spreading by blade (Wagner et al. 1998)	MWNT	Urethane/diacrylate EBECRYL 4858
Tube sonication and mixing with polymer (Ajayan et al. 1994)	MWNT	Epoxy (Epon 812)
Chemical oxidation and spin coating (Ago et al. 1999)	MWNT	PPV
Mixing and sonication (Curran et al. 1998, Coleman et al. 1998, Woo et al. 2000)	MWNT	PmPV
Surfactant (Gong et al. 2000)	MWNT	Epoxy

Appendix B

Engineering constants of unidirectional composite materials

The engineering constants of Young's Moduli, Poissons ratios, and shear moduli as functions of the stiffness constants are determined by imposing a known stress field and the measuring the strain field.

B.1 Stiffness matrix

The elastic behaviour of a unidirectional composite material can be described by the stiffness constants:

$$\begin{bmatrix}\sigma_{11}\\ \sigma_{22}\\ \sigma_{33}\\ \sigma_{23}\\ \sigma_{13}\\ \sigma_{12}\end{bmatrix} = \begin{bmatrix} n & l & l & 0 & 0 & 0\\ l & k+m & k-m & 0 & 0 & 0\\ l & k-m & k+m & 0 & 0 & 0\\ 0 & 0 & 0 & 2m & 0 & 0\\ 0 & 0 & 0 & 0 & 2p & 0\\ 0 & 0 & 0 & 0 & 0 & 2p \end{bmatrix}\begin{bmatrix}\varepsilon_{11}\\ \varepsilon_{22}\\ \varepsilon_{33}\\ \varepsilon_{23}\\ \varepsilon_{13}\\ \varepsilon_{12}\end{bmatrix}$$

B.2 Longitudinal tensile test

For the longitudinal tensile test, all the stresses are zero except for the stress in the longitudinal direction.

$$\sigma_{11} \neq 0,$$
$$\sigma_{ij} = 0.$$

The elasticity equations may thus be written as functions of the stiffness constants:

$$\sigma_{11} = n\varepsilon_{11} + l\varepsilon_{22} + l\varepsilon_{33}$$
$$0 = l\varepsilon_{11} + (k+m)\varepsilon_{22} + (k-m)\varepsilon_{33}$$
$$0 = l\varepsilon_{11} + (k-m)\varepsilon_{22} + (k+m)\varepsilon_{33}$$
$$\varepsilon_{23} = \varepsilon_{13} = \varepsilon_{12} = 0.$$

From these relations we deduce:

$$\varepsilon_{22} = \varepsilon_{33} = -\frac{l}{2k}\varepsilon_{11}$$

and

$$\sigma_{11} = \left(n - \frac{l^2}{k}\right)\varepsilon_{11}$$

Thus we deduce the longitudinal Young's modulus E_L and the Poisson ratio ν_{LT} for longitudinal tension:

$$E_L = n - \frac{l^2}{k}, \qquad \nu_{LT} = \frac{l}{2k}$$

B.3 Transverse tensile test

For the transverse tensile test, a stress field is imposed such that the stress in one of the transverse directions is not zero, while the stress in the longitudinal and the other transverse direction are zero.

$$\sigma_{22} \neq 0,$$
$$\sigma_{ij} = 0.$$

The elasticity equations may thus be written:

$$0 = n\varepsilon_{11} + l\varepsilon_{22} + l\varepsilon_{33}$$
$$\sigma_{22} = l\varepsilon_{11} + (k+m)\varepsilon_{22} + (k-m)\varepsilon_{33}$$
$$0 = l\varepsilon_{11} + (k-m)\varepsilon_{22} + (k+m)\varepsilon_{33}$$
$$\varepsilon_{23} = \varepsilon_{13} = \varepsilon_{12} = 0.$$

From these we deduce:

$$\varepsilon_{11} = \frac{2ml}{l^2 - n(k+m)}\varepsilon_{22}$$
$$\varepsilon_{33} = \frac{n(k-m)-l^2}{n(k+m)-l^2}\varepsilon_{22}$$
$$\sigma_{22} = \frac{4m(kn-l^2)}{kn-l^2+mn}\varepsilon_{22}$$

Thus we deduce the transverse Young's modulus E_T and the Poisson ratios for transverse tension:

$$E_T = \frac{4m(kn-l^2)}{kn-l^2+mn},$$
$$\nu_{TL} = \frac{2ml}{kn-l^2+mn},$$
$$\nu_{TT'} = \frac{kn-l^2-mn}{kn-l^2+mn}.$$

It can be shown that the coefficients E_L, E_T, ν_{TL} and ν_{LT} are connected by the relation:

$$\frac{E_L}{\nu_{LT}} = \frac{E_T}{\nu_{TL}}$$

B.4 Longitudinal shear test

For the longitudinal shear test all stresses are zero except the shear stress in the longitudinal-transverse direction.

$$\begin{cases}\sigma_{13} \neq 0, \\ \sigma_{ij} = 0 \quad if \quad i \neq 1, j \neq 3\end{cases} \qquad \begin{cases}\sigma_{12} \neq 0, \\ \sigma_{ji} = 0 \quad if \quad i \neq 1, j \neq 2.\end{cases}$$

In the second case the elasticity equations are:

$$\varepsilon_{11} = \varepsilon_{22} = \varepsilon_{33} = \varepsilon_{23} = \varepsilon_{13} = 0,$$
$$\sigma_{12} = 2p\varepsilon_{12}.$$

From this we deduce:

$$G_{LT} = 2p.$$

Because the directions T and T' are equivalent we have:

$$G_{LT'} = G_{LT} = 2p.$$

B.5 Transverse shear test

For the longitudinal shear test all stresses are zero except the shear stress in the transverse-transverse direction.

$$\sigma_{23} \neq 0,$$
$$\sigma_{ij} = 0 \quad if \quad i \neq 2, j \neq 3.$$

Hence the elasticity equations are:

$$\varepsilon_{11} = \varepsilon_{22} = \varepsilon_{33} = \varepsilon_{13} = \varepsilon_{12} = 0,$$
$$\sigma_{23} = 2m\varepsilon_{23}.$$

The transverse shear modulus $G_{TT'}$ is thus written:

$$G_{TT'} = 2m.$$

The transverse shear modulus $G_{TT'}$ is related to the transverse Young's modulus E_T and the Poisson ratio $\nu_{TT'}$ by the expression:

$$G_{TT'} = \frac{E_T}{2(1+\nu_{TT'})}.$$

B.6 Lateral hydrostatic compression

A lateral hydrostatic compression test without longitudinal deformation also allows a simple characterization of materials. In such a test the applied stress and strain fields are such that:

$$\sigma_{22} = \sigma_{33} = -P,$$
$$\sigma_{23} = \sigma_{13} = \sigma_{12} = 0,$$
$$\varepsilon_{11} = 0,$$
$$\sigma_{11} \neq 0.$$

Where P is the applied pressure.

The elasticity equations are then written as:

$$\sigma_{11} = l\varepsilon_{22} + l\varepsilon_{33},$$
$$-P = (k+m)\varepsilon_{22} + (k-m)\varepsilon_{33}$$
$$-P = (k-m)\varepsilon_{22} + (k+m)\varepsilon_{33}$$
$$\varepsilon_{23} = \varepsilon_{13} = \varepsilon_{12} = 0.$$

From these equations we deduce:

$$\varepsilon_{22} = \varepsilon_{33},$$
$$-P = 2k\varepsilon_{22},$$
$$\sigma_{11} = 2l\varepsilon_{22}.$$

The surface dilation e_s is:

$$e_s = \varepsilon_{22} + \varepsilon_{33} = -\frac{P}{k}$$

or

$$P = -ke_s$$

From this we deduce the lateral compression modulus K_L without longitudinal deformation:

$$K_L = k$$

The modulus K_L is related to the Young's modulus E_L and the Poisson ratio ν_{LT} by the expression:

$$K_L = \frac{n - E_L}{4\nu_{LT}^2}.$$

Appendix C

Matlab script files

C.1 Aligned nanotubes

A Matlab script file created to determine the elastic moduli of NRPs reinforced with straight, aligned nanotubes. The inputs are the Hill's elastic moduli of the nanotubes considered and the elastic properties of the polymer. The Hills elastic moduli of the composite are then calculated at increasing volume fractions of nanotubes (equations 5.2 to 5.6). The elastic moduli of the composite are then calculated from functions of the stiffness constants. (equations 5.7 to 5.10). The outputs are the engineering constants of the NRP.

```
clear all;
% INPUTS
% Representative Elastic Moduli for SWNT (Popov et al. 2000):
kr=30; lr=10; mr=1; nr=450; pr=1;  %(GPa)

% Properties of polymer:
Em=1.9;          %Young's Modulus (GPa)
vm=0.3;          %Poisson's ratio

%CALCULATIONS
%Loop to determine engineering constants
N=1000;     %No. of increments
t=1/N;
cr=0:t:1;   %Volume fraction of nanotubes=cr

for i=1:N+1

        cm(i)=1-cr(i); % Volume fraction of matrix=cm

        %Hills Elastic Moduli
        k(i)=(Em*(Em*cm(i)+2*kr*(1+vm)*(1+cr(i)*(1-2*vm))))/(2*(1+vm)*(Em*(1+cr(i)-2*vm)
                +2*cm(i)*kr*(1-vm-2*vm^2)));

        l(i)=(Em*(cm(i)*vm*(Em+2*kr*(1+vm))+2*cr(i)*lr*(1-vm^2))) / ((1+vm)*(2*cm(i)* kr*
                (1-vm-2*vm^2)+Em*(1+cr(i)-2*vm)));

        n(i)=(Em^2*cm(i)*(1+cr(i)-cm(i)*vm)+2*cm(i)*cr(i)*(kr*nr-lr^2)*(1+vm)^2*(1-2* vm))
                /((1+vm)*(2*cm(i)*kr*(1-vm-2*vm^2)+Em*(1+cr(i)-2*vm)))+(Em*(2*cm(i)^2
        *kr*
                (1-vm)+cr(i)*nr*(1-2*vm+cr(i))-4*cm(i)*lr*vm))/(2*cm(i)*kr*(1-vm-2*vm^2)
                +Em*(1+cr(i)-2*vm));

        p(i)=(Em*(Em*cm(i)+2*(1+cr(i))*pr*(1+vm)))/(2*(1+vm)*(Em*(1+cr(i))+2*cm(i)*pr
```

```
        *(1+vm)));

    m(i)=(Em*(Em*cm(i)+2*mr*(1+vm)*(3+cr(i)-4*vm)))/(2*(1+vm)*(Em*(cm(i)+4*cr(i)*
        (1-vm))+2*cm(i)*mr*(3-vm-4*vm^2)));

    %Engineering Constants
    E11(i)=n(i)-(l(i)^2/k(i));
    v12(i)=l(i)/(2*k(i));
    E22(i)=(4*m(i)*(k(i)*n(i)-l(i)^2))/(k(i)*n(i)-l(i)^2+m(i)*n(i));
    v21(i)=v12(i)*(E22(i)/E11(i))
    v23(i)=(k(i)*n(i)-l(i)^2-m(i)*n(i))/(k(i)*n(i)-l(i)^2+m(i)*n(i));
    G12(i)=2*p(i);
    G23(i)=2*m(i);

end

%OUTPUT
%graphs
figure(1)
clf
semilogy(cr,E11,cr,E22)
xlabel('cr','FontSize',12)
ylabel('Effective elastic modulus (Gpa)','FontSize',12)
title('Effective elastic modulus','FontSize',12)
legend('EL','ET')
plotedit on
figure(2)
clf
plot(cr,v12)
xlabel('cr','FontSize',12)
ylabel('Effective Poisons Ratio v12','FontSize',12)
title('Effective Poisons Ratio','FontSize',12)
figure(3)
clf
plot(cr,G12)
xlabel('cr','FontSize',12)
ylabel('Effective Shear Modulus G12 (GPa)','FontSize',12)
title('Effective Shear Modulus','FontSize',12)
plotedit on
```

C.2 Random oriented nanotubes

A Matlab script file created to determine the elastic moduli of NRPs reinforced with straight, random oriented nanotubes. The inputs are the Hill's elastic moduli of the nanotubes considered and the elastic properties of the polymer. The bulk moduli of the composite are then calculated at increasing volume fractions of nanotubes (equations 5.11 to 5.16). The elastic moduli of the composite are then calculated from the bulk moduli (equations 5.17 and 5.18). The outputs are the Young's modulus and Poisson's ratio of the resulting isotropic material.

```
clear all
%INPUTS
% Representative Elastic Moduli for SWNT (Popov et al. 2000):
kr=30; lr=10; mr=1; nr=450; pr=1;  %(GPa)

% Moduli for polymer:
Em=1.9;          %GPa
vm=0.3;

%CALCULATIONS
% Bulk and Shear Moduli of polymer:
Km=Em/(3*(1-2*vm));     %GPa
Gm=Em/(2*(1+vm));

%Loop
N=1000;
t=0.25/N;
cr=0:t:0.25;   % Volume fraction of nanotubes=cr

for i=1:N+1
        cm(i)=1-cr(i);     % Volume fraction of matrix=cm=

        ar(i)=(3*(Km+Gm)+kr-lr)/(3*(Gm+kr));

        br(i)=((4*Gm+2*kr+lr)/(3*(Gm+kr))+(4*Gm)/(Gm+pr)+(2*(Gm*(3*Km+Gm)+Gm*
                (3*Km+7*Gm)))/(Gm*(3*Km+Gm)+mr*(3*Km+7*Gm)))/5;

        dr(i)=(nr+2*lr+((2*kr+lr)*(3*Km+2*Gm-lr))/(Gm+kr))/3;

        nnr(i)=((2/3)*(nr-lr)+(8*Gm*pr)/(Gm+pr)+(8*mr*Gm*(3*Km+4*Gm))/(3*Km*(mr+Gm)+
                Gm*(7*mr+Gm))+(2*(kr-lr)*(2*Gm+lr))/(3*(Gm+kr)))/5;

        K(i)=Km+(cr(i)*(dr(i)-3*Km*ar(i)))/(3*(cm(i)+cr(i)*ar(i)));

        G(i)=Gm+(cr(i)*(nnr(i)-2*Gm*br(i)))/(2*(cm(i)+cr(i)*br(i)));

        E(i)=9*K(i)*G(i)/(3*K(i)+G(i));

        v(i)=(3*K(i)-2*G(i))/(6*K(i)+2*G(i));

end
```

```
%OUTPUT
%graphs
figure(1)
clf
plot(cr,E)
xlabel('cr','FontSize',12)
ylabel('Effective elastic modulus (Gpa)','FontSize',12)
title('Effective elastic modulus','FontSize',12)
figure(2)
clf
plot(cr,v)
xlabel('cr','FontSize',12)
ylabel('Effective Poisons Ratio','FontSize',12)
title('Effective Poisons Ratio','FontSize',12)
```

C.3 Agglomerated isotropic nanotubes

A Matlab script file created to determine the effect of agglomeration on the elastic properties of nanotubes if the nanotubes are considered to be isotropic. A two part model is used to describe the degree of agglomeration. The inputs are the volume fraction of nanotubes and the representative values of elastic moduli for the nanotubes and the polymer matrix. The Voigt model is used to determine the effective modulus of the inclusions and the matrix (equations 5.25 to 5.26) and thus allow for the determination of the effective elastic modulus of the composite material (equation 5.27). The output is the Young's modulus of the resulting isotropic material.

```
clear all
% INPUTS
%Representative values of nanotubes & matrix
Ecnt=450   %GPa
Em=1.9     %GPa
vr=0.3;
vm=0.3;

%Volume fraction of nanotubes
cr=0.1;

%CALCULATIONS
%loops
N=1000;
t=1/N;
x=0:t:1-t;
z=0:t:1-t;
for i=1:N
   for j=1:N

        %Voigt model
        Eout=(3/8)*(((cr*(1-z(j)))/(1-x(i)))*Ecnt+(1-((cr*(1-z(j)))/(1-x(i))))*Em)+(5/8)*(((1-x(i))*
              Ecnt*Em) /(((1-x(i))-cr*(1-z(j)))*Ecnt+cr*(1-z(j))*Em));

        Ein=(3/(8*x(i)))*(cr*z(j)*Ecnt+(x(i)-cr*z(j))*Em)+(5/8)*((x(i)*Em*Ecnt)/((x(i)-
              cr*z(j))*Ecnt+cr*z(j)*Em));

        %Effective Young's modulus

        E(j,i)=Eout*(Eout+(Ein-Eout)*(x(i)^(2/3)))/(Eout+(Ein-Eout)*(x(i)^(2/3))*(1-
              (x(i)^(1/3))));

        xx(j,i)=x(i);

        zz(j,i)=z(j);

        if x(i)>z(j)              %x can not be greater than z from definition of model of
              E(j,i)=NaN;         %agglomeration
        end
```

```
        if x(i)<(1.1*cr*z(j))        %x must be greater than cr*z from definition of model of
                E(j,i)=NaN;          % agglomeration
        end

    end
end

EE=E/E(2,2)     %Young's modulus with respect to uniformly dispersed composite

%graphs
v=[0.3 0.4 0.5 0.6 0.7 0.8 0.9];
figure(1)
[C,h] = contour(xx,zz,EE,v)
clabel(C,h,'manual')
xlabel('\xi','FontSize',12)
ylabel('\zeta','FontSize',12)
plotedit on
```

C.4 Agglomerated anisotropic nanotubes

A Matlab script file created to determine the effect of agglomeration on the elastic properties of nanotubes if the nanotubes are considered to bean isotropic. A two part model is used to describe the degree of agglomeration. The inputs are the volume fraction of nanotubes, the Hill's elastic moduli of the nanotubes considered, and the elastic properties of the polymer. The effective bulk moduli of the inclusions and the matrix are calculated (equations 5.28 to 5.31). The effective bulk moduli of the composite material are derived (equations 5.32 to 5.35). The elastic moduli of the composite may then be calculated from the bulk moduli (equations 5.36 and 5.37). The outputs are the Young's modulus and Poisson's ratio of the resulting isotropic material.

```
clear all
% INPUTS
% Representative Elastic Moduli for SWNT (Popov et al. 2000):
kr=30; lr=10; mr=1; nr=450; pr=1;  %(GPa)

% Properties of polymer:
Em=1.9;     %GPa
vm=0.3;

%CALCULATIONS
% Bulk and Shear Moduli of polymer:
Km=Em/(3*(1-2*vm));     %GPa
Gm=Em/(2*(1+vm));

N=1000;
t=1/N;
x=0:t:1-t;
z=0:t:1-t;
cr=0.1;
for i=1:N
   for j=1:N
        ar=(3*(Km+Gm)+kr-lr)/(3*(Gm+kr));

        br=((4*Gm+2*kr+lr)/(3*(Gm+kr))+(4*Gm)/(Gm+pr)+(2*(Gm*(3*Km+Gm)+Gm*
                (3*Km+7*Gm))) /(Gm*(3*Km+Gm)+mr*(3*Km+7*Gm)))/5;

        dr=(nr+2*lr+((2*kr+lr)*(3*Km+2*Gm-lr))/(Gm+kr))/3;

        nnr=((2/3)*(nr-
        lr)+(8*Gm*pr)/(Gm+pr)+(8*mr*Gm*(3*Km+4*Gm))/(3*Km*(mr+Gm)+Gm*
                (7*mr+Gm))+(2*(kr-lr)*(2*Gm+lr))/(3*(Gm+kr)))/5;

        % Bulk moduli inside and outside of the inclusions
        Kin=Km+((dr-3*Km*ar)*cr*z(j))/(3*(x(i)-cr*z(j)+cr*z(j)*ar));
        Kout=Km+(cr*(dr-3*Km*ar)*(1-z(j)))/(3*(1-x(i)-cr*(1-z(j))+cr*(1-z(j))*ar));

        Gin=Gm+(cr*z(j)*(nnr-2*Gm*br))/(2*(x(i)-cr*z(j)+cr*z(j)*br));
        Gout=Gm+(cr*(1-z(j))*(nnr-2*Gm*br))/(2*(1-x(i)-cr*(1-z(j))+cr*(1-z(j))*br));
```

```
        vout=(3*Kout-2*Gout)/(2*(3*Kout+Gout));

        a=(1+vout)/(3*(1-vout));
        b=2*(4-5*vout)/(15*(1-vout));

        %Bulk Moduli of composite
        K=Kout*(1+(x(i)*(Kin/Kout-1))/(1+a*(1-x(i))*(Kin/Kout-1)));
        G=Gout*(1+(x(i)*(Gin/Gout-1))/(1+b*(1-x(i))*(Gin/Gout-1)));

        E(j,i)=9*K*G/(3*K+G);
        v(j,i)=(3*K-2*G)/(6*K+2*G);

        xx(j,i)=x(i);       %for graph
        zz(j,i)=z(j);       %for graph

        if x(i)>z(j)                %x can not be greater than z from definition of model of
                E(j,i)=NaN;         %agglomeration
        end

        if x(i)<(1.1*cr*z(j))       %x must be greater than cr*z from definition of model of
                E(j,i)=NaN;         % agglomeration
        end
    end
end

%OUTPUT
EE=E/E(2,2)     %elastic modulus/elastic modulus with no agglomeration
%graphs
v=[0.3 0.4 0.5 0.6 0.7 0.8 0.9];
figure(1)
[C,h] = contour(xx,zz,EE,v)
clabel(C,h,'manual')
xlabel('\xi','FontSize',12)
ylabel('\zeta','FontSize',12)
plotedit on
```

C.5 Deflection of an aligned nanotube-reinforced composite beam

A Matlab script file created to determine the deflection of an aligned nanotube-reinforced composite beam under pure bending. The inputs are the Hill's elastic moduli of the nanotubes considered, the elastic properties of the polymer, the orientations and thicknesses of the layers of the laminate beam, and the load on the beam. The engineering constants of the composite are determined for increasing nanotube volume fraction as in Appendix C.1. The reduced stiffness matrix is calculated for each layer which are used to calculate the bending stiffness matrix of the laminate. The bending stiffness matrix is then used to calculate the output of the deflection of the beam at its centre (equation 6.17).

```
clear all
% INPUTS
% Representative Elastic Moduli for SWNT (Popov et al. 2000):
kr=30; lr=10; mr=1; nr=450; pr=1;  %(GPa)

% Polymer Properties:
Em=1.9;     %GPa
vm=0.3;

% Laminate properties
M=8;   %no of layers
orientt=[0 pi/4 -pi/4 pi/2 pi/2 -pi/4 pi/4 0; pi/2 pi/4 -pi/4 0 0 -pi/4 pi/4 pi/2;
        pi/4 0 -pi/4 pi/2 pi/2 -pi/4 0 pi/4];          %orientations


h=[-0.5 -0.375 -0.25 -0.125 0 0.125 0.25 0.375 0.5];       %thickness

% Beam properties
P=1;   %force [N]
L=10;  %length [mm]
bredth=1;    %bredth [mm]

% CALCULATIONS
N=1000;
t=0.25/N;
cr=0:t:0.25;       % Volume fraction of nanotubes=cr
for z=1:3
        orient=orientt(z,:)
        for i=1:N+1
                %MICROMECHANICS CALCULATIONS

                cm(i)=1-cr(i);     % Volume fraction of matrix=cm


                k(i)=(Em*(Em*cm(i)+2*kr*(1+vm)*(1+cr(i)*(1-
                2*vm))))/(2*(1+vm)*(Em*(1+cr(i)-
                        2*vm)+2*cm(i)*kr*(1-vm-2*vm^2)));

                l(i)=(Em*(cm(i)*vm*(Em+2*kr*(1+vm))+2*cr(i)*lr*(1-vm^2)))/((1+vm)*
                        (2*cm(i)*kr*(1-vm-2*vm^2)+Em*(1+cr(i)-2*vm)));
```

```
n(i)=(Em^2*cm(i)*(1+cr(i)-cm(i)*vm)+2*cm(i)*cr(i)*(kr*nr-lr^2)*(1+vm)^2*
        (1-2*vm))/((1+vm)*(2*cm(i)*kr*(1-vm-2*vm^2)+Em*(1+cr(i)-2*vm)))
        +(Em*(2*cm(i)^2*kr*(1-vm)+cr(i)*nr*(1-2*vm+cr(i))-4*cm(i)*lr*vm))
        /(2*cm(i)*kr*(1-vm-2*vm^2)+Em*(1+cr(i)-2*vm));

p(i)=(Em*(Em*cm(i)+2*(1+cr(i))*pr*(1+vm)))/(2*(1+vm)*(Em*(1+cr(i))+2*cm(i)
        *pr*(1+vm)));

m(i)=(Em*(Em*cm(i)+2*mr*(1+vm)*(3+cr(i)-4*vm)))/(2*(1+vm)*(Em*(cm(i)+4*
        cr(i)*(1-vm))+2*cm(i)*mr*(3-vm-4*vm^2)));

%Engineering Constants
E11(i)=n(i)-(l(i)^2/k(i));
v12(i)=l(i)/(2*k(i));
E22(i)=(4*m(i)*(k(i)*n(i)-l(i)^2))/(k(i)*n(i)-l(i)^2+m(i)*n(i));
v21(i)=2*m(i)*l(i)/(k(i)*n(i)-l(i)^2+m(i)*n(i));
G12(i)=2*p(i);

%LAMINATE CALCULATION

Q11=E11(i)/(1-(v12(i)*v21(i)));
Q22=E22(i)/(1-(v12(i)*v21(i)));
Q12=v21(i)*E11(i)/(1-(v12(i)*v21(i)));
Q33=G12(i);
Qtheta0=[Q11 Q12 0; Q12 Q22 0; 0 0 Q33];

for j=1:M
        theta=orient(j);
        m=cos(theta);
        n=sin(theta);
        T=[m^2 n^2 2*m*n; n^2 m^2 -2*m*n; -m*n m*n m^2-n^2];
        R=[1 0 0;0 1 0;0 0 2];
        Qtheta1=(T^-1)*Qtheta0*R*T*(R^-1);

        d11(j)=Qtheta1(1,1)*(h(j+1)^3-h(j)^3);
        d12(j)=Qtheta1(1,2)*(h(j+1)^3-h(j)^3);
        d13(j)=Qtheta1(1,3)*(h(j+1)^3-h(j)^3);
        d21(j)=Qtheta1(2,1)*(h(j+1)^3-h(j)^3);
        d22(j)=Qtheta1(2,2)*(h(j+1)^3-h(j)^3);
        d23(j)=Qtheta1(2,3)*(h(j+1)^3-h(j)^3);
        d31(j)=Qtheta1(3,1)*(h(j+1)^3-h(j)^3);
        d32(j)=Qtheta1(3,2)*(h(j+1)^3-h(j)^3);
        d33(j)=Qtheta1(3,3)*(h(j+1)^3-h(j)^3);
end
D(1,1)=sum(d11)/3;
D(1,2)=sum(d12)/3;
D(1,3)=sum(d13)/3;
D(2,1)=sum(d21)/3;
D(2,2)=sum(d22)/3;
D(2,3)=sum(d23)/3;
D(3,1)=sum(d31)/3;
D(3,2)=sum(d32)/3;
D(3,3)=sum(d33)/3;

Dstar(1,1)=(1/det(D))*(D(2,2)*D(3,3)-D(2,3)^2);
```

```
                %BEAM DEFLECTION
                wc(i)=P*L^3*Dstar(1,1)/(48*bredth);

                wcc(i)=wc(i)/wc(1);        %deflection as a function of maximum deflection
                wwcc(z,i)=wcc(i)
        end
end

%DISPLAY
figure(1)
clf
plot(cr,wwcc(2,:),cr,wwcc(3,:),cr,wwcc(1,:))
xlabel('\it{c_{r}}','FontSize',12)
ylabel('\it{w_{c} / w_{0}}','FontSize',12)
legend('[90\circ/45\circ/-45\circ/0\circ]s','[45\circ/0\circ/-45\circ/90\circ]s','[0\circ/45\circ/-
45\circ/90\circ]s')
```

References

Ago H, Petritsch K, Shaffer MSP, Windle A,and Friend RH. (1999), *Composites of carbon nanotubes and conjugated polymers for photovoltaic devices*, Adv. Mater., Vol.11, pp.1281-1281

Ajayan PM and Schandler LS. (2000), *Single-walled carbon nanotube-polymer composites: strength and weakness*, Adv. Mat., Vol.12, pp. 750-753

Ajayan PM, Stephan O, Colliex C, and Trauth D. (1994), *Aligned carbon nanotube arrays formed by cutting a polymer resin-nanotube composite*, Science, Vol.26, pp. 1212-1214

Andrews R, Jacques D, Rao AM, Rantell T, Derbyshire F, Chen Yatal (1999), *Nanotube composite carbon fibers*, Appl. Phys. Lett., Vol.75(9), pp. 1329-1331

Battezzatti L., Pisani C., and Ricca F. (1975), *Equilibrium conformation and surface motion of hydrocarbon molecules physisorbed on graphite*, J. Chem. Soc.,Vol.71, pp.1629-1639

Belytschko T, Xiao S.P, Schatz G.C, and Ruoff R.S. (2002), *Atomistic simulations of nanotube fracture*, Physical Review B, Vol. 65, pp.235430

Berthelot J-M. (1998), *Composite Materials: Mechanical Behavior and Structural Analysis*, Springer, Vol., pp. 420-424

Bower C, Rosen R, Jin L, Han J, Zhou O. (1999), *Deformation of carbon nanotubes in nanotube-polymer composites*, Appl. Phys. Lett., Vol. 74, pp.3317-3319

Bower C, Zhu W, Jin S, Zhou O. (2000), *Plasma-induced alignment of carbon nanotubes*, Appl. Phys. Lett., Vol. 77(6), pp. 830-832

Collins, P. G. and P. Avouris (2000), *Nanotubes for electronics*, Scientific American, December pp. 62-69

Cornell W.D., Cieplak P., Bayly C.I., Gould I.R., Merz K.M., Ferguson D.M., Spellmeyer D.C., Fox T., Caldwell J.W., and Kollman P.A. (1995), *A second generation force field for the simulation of proteins, nucleic acids, and organic molecules*, J. Am. Chem. Soc., Vol. 117, pp. 5179-5197

Curran S, Ajaian PM, Blau WJ, Carrol DL, Coleman JN, Dalton ABS, Davey AP, Drury A, McCarthy B, Maier S, and Strevens S. (1998), *A composite from poly(m-phenylenevinylene-co-2,5-dioctoxy-p-pnenylenevinylene) and carbon nanotubes: a novel material for molecular optoelectronics*, Adv. Mater., Vol. 10, pp. 1091-1093

Dresselhaus M.S., Dresselhaus G., Saito R. (1995), *Physics of carbon nanotubes*, Carbon, Vol. 33, pp. 883

Falvo MR, Clary GJ, Taylor RM, Chi V, Brooks FP, Washburn S, and Superfine R. (1997), *Bending and buckling of carbon nanotubes under large strain*, Nature (London), Vol. 389(6651), pp. 582-584

Gong X, Liu J, Baskaran S, Voise RD, and Young J. (2000), *Surfactant-assisted processing of carbon nanotube / polymer composites*, Chem. Mater., Vol. 12, pp. 1049-1062

Haggenmueller R, Gommans HH, Rinzler AG, Fischer JE, Winey KI. (2000), *Aligned single-wall carbon nanotubes in composites by melt processing methods*, Chem. Phys. Lett., Vol. 330, pp. 219-225

Harris, P. J. F. (1999), *Carbon Nanotubes and Related Structures: New Materials for the 21st Century*. Cambridge, Cambridge University Press.

Hernandez E, Goze C, Bernier P, and Rubio A, (1998), *Elastic properties of C and $B_xC_yN_z$ composite nanotubes*, Phys. Rev. Lett., Vol. 80(20), pp. 4502-4505

Iijima, S. (1991), *Helical microtubules of graphitic carbon*, Nature (London), Vol. 354, pp. 56-58

Jia Z, Wang Z, Xu C, Liang j, Wei B, Wu D, and Zu S. (1999), *Study on polymethylmethacrylate / carbon nanotube composites*, Mater. Sci. Eng., Vol. 271A, pp. 395-400

Jin L, Bower C, and Zou O. (1998), *Alignment of carbon nanotubes in a polymer matrix by mechanical stretching*, Appl. Phys. Lett., Vol. 73, pp. 1197-1199

Jones, R. M. (1999), *Mechanics of composite materials*, Taylor & Francis, Philadelphia

Journet, C., W. K. Maser, P. Bernier, A. Loiseau, M. L. de la Chapelle, S. Lefrants, P.Deniard, R. Lee and J. E. Fischer (1997), *Large-scale production of single-walled carbon nanotubes by the electric-arc technique*, Nature, Vol. 388, pp. 756-758

Kelly B.T. (1981), *Physics of graphite*, Applied Science, London

Krishnan A, Dujardin E, Ebbesen TW, Yianilos PN, and Treacy MMJ. (1998), *Young's modulus of single -walled nanotubes*, Phys. Rev. B, Vol. 58(20), pp. 14013-14019

Li C, Chou TW (2003), *A structural mechanics approach for the analysis of carbon nanotubes*, Int J Solids Struct., Vol. 40(10), pp. 2487-2499

Liao, K. and S. Li (2001), *Interfacial characteristics of a carbon nanotube-polystyrene composite system*, Appl. Phys. Lett., Vol. 79(25), pp. 4225-4227

Lordi V, Yao N. (2000), *Molecular mechanics of binding in carbon-nanotube-polymer composites*, Appl. Phys. Lett., Vol. 15(12), pp. 2770-2779

Lourie O, Cox DM, and Wagner HD. (1998), *Buckling and collapse of embedded carbon nanotubes*, Phys. Rev. Lett., Vol. 81(8), pp. 1638-1641

Lu JP. (1997), *Elastic properties of carbon nanotubes and nanoropes*, Phys. Rev. Lett., Vol. 79(7), pp. 1297-1300

Odegard GM, Gates TS, Nicholson LM, and Wise KE. (2002), *Equivalent-continuum modelling of nanostructured materials*, Compos. Sci. Tech., Vol. 62, pp. 1869-1880

Overney G, Zhong W, and Tomanek D. (1993), *Structural rigidity and low-frequency vibrational-modes of long carbon tubules*, Zeitschrift Fur Physik D-Atoms Molecules and Clusters, Vol. 27(1), pp. 93-96

Poncharal P, Wang ZL, Ugarte D, and de Heer WA. (1999), *Electrostatic deflections and electromechanical resonances of carbon nanotubes*, Science, Vol. 283(5407), pp. 1513-1516

Popov VN, Van Doren VE, Balkanski M. (2000a), *Elastic properties of single-walled carbon nanotubes*, Phys. Rev. B, Vol. 61(4), pp. 3078-3084

Popov V.N, Doren V.E, and Balkanski M. (2000b), *Elastic properties of crystals of single-walled carbon nanotubes*, Solid state Commun., Vol. 114, pp. 395-399

Qian D, Dickey E.C, Andrews R, and Rantell T. (2000), *Load transfer and deformation mechanisms in carbon nanotube-polystyrene composites*, Appl. Phys. Lett., Vol. 76(20), pp. 2868-2870

Ren ZF, Huang ZP, Xu JW, Wang JH, Bush P, Siegal MP. (1998), *Synthesis of large arrays of well-aligned carbon nanotubes on glass*, Science, Vol. 282, pp. 1105-1107

Robertson DH, Brenner DW, and Mintmire JW. (1992), *Energetics of nanoscale graphitic tubules*, Phys. Rev. B, Vol. 45(21), pp. 12592-12595

Ru, C.Q. (2000a), *Effective bending stiffness of carbon nanotubes*, Physical Review B, Vol. 62, pp. 9973-9976

Ru, C.Q. (2000b), *Elastic buckling of single-walled carbon nanotube ropes under high pressure*, Physical Review B, Vol. 62, pp. 10405-10408

Saito Y, Nishikubo K, Kawabata K,and Matsumoto T. (1996), *Carbon nanocapsules and single-layered nanotubes produced with platinum-group metals by arc discharge*, J. Appl. Phys., Vol. 80, pp. 3062-3067

Salvetat JP, Kulik AJ, Bonard JM, Briggs GAD, Stockli T, Metenier K, Bonnamy S, Beguin F, Burnham NA, and Forro L. (1999a), *Elastic modulus of ordered and disordered multiwalled carbon nanotubes*, Adv. Mater., Vol. 11(2), pp. 161-165

Salvetat JP, Briggs GAD, Bonard JM, Bacsa RR, Kulik AJ, Stockli T, Burnham NA, and Forro L. (1999b), *Elastic and shear moduli of single -walled carbon nanotube ropes*, Phys. Rev. Lett., Vol. 82(5), pp. 944-947

Sanchez-Portal D, Artacho E, Solar JM, Rubio A, and Ordejon P. (1999), *Ab inito structural, elastic, and vibrational properties of carbon nanotubes*, Phys. Rev. B, Vol. 59, pp. 12678-12688

Sandler J, Shaffer MSP, Prasse T, Bauhofer W, Schulte, and Windle AH. (1999), *Development of a dispersion process for carbon nanotubes in an epoxy matrix and the resulting electrical properties*, Polymer, Vol. 40, pp. 5967-5971

Schadler LS, Giannaris SC, and Ajaian PM. (1998), *Load transfer in carbon nanotube epoxy composites*, Appl. Phys. Lett., Vol. 73, pp. 3842-3844

Schlittler RR, Seo JW, Gimzewski JK, Durkan C, Saifullah MSM, Welland ME. (2001), *Single crystals of single-walled carbon nanotubes formed by self-assembly*, Science, Vol. 292, pp. 1136-1139

Shaffer MSP,and Windle AH. (1999), *Fabrication and characterization of carbon nanotube / poly(vinyl alcohol) composites*, Composite Sci. Technol., Vol. 59, pp. 975-977

Shi D-L, Huang Y, Hwang, K-C, Gao H. (2004), *The effect of nanotube waviness and agglomeration on the elastic property of carbon nanotube-reinforced composites*, Journal of engineering materials and technology, Vol. 126, pp. 250-257

Terrones M, Grobert N, Olivares J, Zhang JP, Terrones H, Kordatos k, Hsu WK, Hare JP, Townsend PD, Prassides K, Cheetham AK, Kroto HW, Walton DRM. (1997), *Controlled production of aligned-nanotube bundles*, Nature (London), Vol. 388, pp. 52-55

Tersoff, J. (1992), *Energies of fullerenes*, Phys. Rev. B, Vol. 46, pp. 15546-15549

Thostenson ET, Zhifeng R,and Chou T-W. (2001), *Advances in the science and technology of carbon nanotubes and their composites: a review*, Composites Science and Technology, Vol. 61, pp. 1899-1912

Tibbetts GG. (1984), *Why are carbon filaments tubular*, Journal of Crystal Growth, Vol. 66(3), pp.632-638

Treacy MMJ, Ebbesen TW, and Gibson JM. (1996), *Exceptionally high young's modulus observed for individual carbon nanotubes*, Nature, Vol. 381(6584), pp. 678-680

Vigolo B, Pe'nicaud A, Coulon C, Sauder C, Pailler R, Journet C et al.(2000), *Marcoscopic fibers and ribbons of oriented carbon nanotubes*, Science, Vol. 290, pp. 1331-1334

Wagner HD, Lourie O, Feldman Y, and Tenne R. (1998), *Stress-induced fragmentation of multiwall carbon nanotubes in a polymer matrix* , Appl. Phys. Lett., Vol. 72, pp.188-190

Wang B, Liang Z, Ravi Shankar K, Barefield K, Zhang C,and Kramer L. (2003), *Fabrication and characterization of inplane aligned nanotube composites with magnetically aligned carbon nanotube bucky papers*, International conference ICCM-14

Wong EW, Sheehan PE, and Lieber CM. (1997), *Nanobeam mechanics: Elasticity, strength, and toughness of nanorods and nanotubes*, Science, Vol. 277(5334), pp. 1971-1975

Woo HS, Czerw R, Webster S, Carrol DL, Ballato J, Strevens AE, O'Brien D, and Blau WJ. (2000), *Hole blocking in carbon nanotube-polymer composite organic light emitting diodes based on poly(m-phenylenevinylene-co-2,5-dioctoxy-p-pnenylenevinylene)*, Appl. Phys. Lett., Vol. 77, pp. 1393-1395

Wood, J. R., Q. Zhao and H. D. Wagner (2001), *Orientation of carbon nanotubes in polymers and its detection by Raman spectroscopy* , Composites: Part A, Vol. 32, pp. 391-399

Yakobson BI and Avouris P. (2001), *Mechanical properties of carbon nanotubes,* Carbon Nanotubes, pp. 287-327

Yakobson BI, Brabec CJ, and Bernholc J, (1996), *Nanomechanics of carbon tubes: Instabilities beyond linear response*, Phys. Rev. Lett., Vol. 76(14), pp. 2511-2514

Yu MF, Dyer MJ, Chen J, and Bray K. (2001), *Multiprobe nanomanipulation and functional assembly of nanomaterials inside a scanning electron microscope*, International conference IEEE-NANO2001(eds), Maui

Yu MF, Files BS, Arepalli S, and Ruoff RS. (2000a), *Tensile loading of ropes of single wall carbon nanotubes and their mechanical properties*, Phys. Rev. Lett., Vol. 84(24), pp. 5552-5555

Yu MF, Lourie O, Dyer MJ, Moloni K, Kelly TF, and Ruoff RS. (2000b), *Strength and breaking mechanism of multiwalled carbon nanotubes under tensile load*, Science, Vol. 287(5453), pp. 637-640

Yu MF, Yakobson BI, and Ruoff RS. (2000c), *Controlled sliding and pullout of nested shells in individual multiwalled carbon nanotubes*, Journal of Physical Chemistry B, Vol. 104(37), pp. 8764-8767

Zhang P, Huang Y, Geubelle PH, Klein PA, Hwang KC. (2002), *The elastic modulus of single-walled carbon nanotubes: a continuum analysis incorporating interatomic potentials*, Int. J Solids Struct., Vol. 39, pp. 3893-3906

Zhao, Y. H. and G. J. Weng (1996), *Influence of random bridging on the elastic and elastoplastic properties of fiber reinforced composites*, Acta Mechanica, Vol. 116, pp. 29-44